DEVELOPMENT OF HIGH PERFORMANCE AND RADIATION SHIELDING CONCRETE UTILIZING INDIGENOUS INDUSTRIAL WASTE MATERIALS

BY

MUKHTAR OLUWASEUN AZEEZ

A Thesis Presented to the

DEANSHIP OF GRADUATE STUDIES

KING FAHD UNIVERSITY OF PETROLEUM & MINERALS

DHAHRAN, SAUDI ARABIA

In Partial Fulfillment of the
Requirements for the Degree of

MASTER OF SCIENCE

In

CIVIL ENGINEERING

MAY 2015

KING FAHD UNIVERSITY OF PETROLEUM & MINERALS

DHAHRAN- 31261, SAUDI ARABIA

DEANSHIP OF GRADUATE STUDIES

This thesis, written by **MUKHTAR OLUWASEUN AZEEZ** under the direction of his thesis advisor and approved by his thesis committee, has been presented and accepted by the Dean of Graduate Studies, in partial fulfillment of the requirements for the degree of

MASTER OF SCIENCE IN CIVIL ENGINEERING.

Dr. Salah U. Al-Dulaijan
(Advisor)

Dr. Omar A. Al-Swailem
Department Chairman (A)

Dr. Mohammed Maslehuddin
(Co-Advisor)

Dr. Salam A. Zummo
Dean of Graduate Studies

Dr. Akhtar A. Naqvi
(Member)

10/6/15
Date

Dr. Omar S. Al-Amoudi
(Member)

Dr. Shamshad Ahmad
(Member)

This work is dedicated to my dear parents, my wonderful siblings, my lovely wife, and my adorable son.

ACKNOWLEDGMENTS

All praise and adoration is due to Almighty Allaah, SubhaanaHu wa ta'aala for granting me the respite, wisdom, knowledge, patience, strength and sound health to complete this study successfully. May His peace and blessings be upon the noblest of mankind, Muhammad Ibn 'Abdillaah (SallaLLaahu 'alayhi wa sallam), his households, his companions and those who follow the path of guidance till the day of judgement.

I appreciate my dear parents for their immense moral and educational support, my siblings for their prayers and encouragement, and my mother's un-quenching prayers, which has seen me through the thick and thin of life till this very moment. I seek Allah's mercy and forgiveness on my father's soul, who by His will, left us at a time we needed him most. I also appreciate the great support, encouragement, trust, and understanding of my loving and caring wife (Kifayah Moromokemi) and the patience of my adorable son, Fawzaan Damilare, both of whom have endured my absence throughout the course of my MS degree. I also thank my relatives and in-laws for their prayers and words of encouragement.

I am indebted to the Ministry of Higher Education, Saudi Arabia, for the scholarship grant to purse my MS degree in KFUPM and the King Fahd University of Petroleum & Minerals through Civil & Environmental Engineering department and Research Institute for the support and necessary resources given to carry out this research work.

I acknowledge, with deep sense of gratitude and appreciation, the support and assistance given to me by my thesis advisor, Dr. Salah Al-Dulaijan. Thereafter, I am deeply indebted and grateful to my co-advisor, Dr. Mohammed Maslehuddin for his inspiration,

patience, encouragement, remarkable assistance and significant support since my arrival in KFUPM till the completion of this research. I also appreciate the assistance and direct involvement of Dr. Akhtar Naqvi in the conduct of this research. This appreciation will not be complete without acknowledging my other committee members, Dr. Shamsad Ahmad and Dr. omar Al-Amoudi for their guidance, support and constructive suggestions during this research.

This research would not have been possible without the support of Engr. Ibrahim and Engr. Barry, who assisted me right from the material selection stage till the completion of this work. I must also acknowledge Engr. Shameem and Engr. Rizwan for their words of encouragement and assistance throughout the course of this research.

I owe an unreserved gratitude to a brother and mentor, Engr. Saheed Kolawole Adekunle for his mentorship and support in every way since my arrival in KFUPM. I pray Allah reward him abundantly. I must also salute the companionship of my friend, Shina Adewumi, the support of a brother from another mother, Dahood Adegbite and the encouragement of my friends in different parts of the world, whose names I would not be able to mention here. May Allah bless everyone of them (Amin).

Finally, my deep sense of appreciation goes to the Nigerian Community in KFUPM (NCUPM) for their regular moral and spiritual supports throughout my stay in this campus. May Allaah in his infinite mercy continue to be with each and everyone of them (Aamin).

TABLE OF CONTENTS

LIST OF TABLES

LIST OF FIGURES

ABSTRACT

Full Name : [AZEEZ, MUKHTAR OLUWASEUN]

Thesis Title : [DEVELOPMENT OF HIGH PERFORMANCE AND RADIATION SHIELDING CONCRETE UTILIZING INDIGENOUS INDUSTRIAL WASTE MATERIALS]

Major Field : [CIVIL ENGINEERING (STRUCTURES)]

Date of Degree : [MAY 2015]

Heavyweight concrete (HWC) is generally utilized for radiation shielding, for both medical and nuclear purposes. Since the unit weight of normal concrete is less than that required for radiation shielding, heavyweight aggregates or metallic components, such as lead, copper, barites, magnetite etc., are utilized. The density achieved will depend on the type of aggregate used. Many a time, steel shot or iron ore are utilized to produce HWC. However, these materials are not readily available in the Kingdom of Saudi Arabia and are imported from other regions, thereby increasing their cost. However, certain industrial byproducts, such as steel slag aggregate together with locally available raw materials can be utilized to produce high performance and heavyweight concrete.

In this study, high performance and heavyweight concrete mixtures were developed utilizing local industrial byproducts. Steel slag, which is a major byproduct from steel production, locally available limestone aggregate and conventional imported raw materials (steel shot and iron ore aggregates) were used to developed the HWC mixtures. The mechanical, durability and radiation shielding properties of the HWC mixtures were investigated, and comprehensive analysis of the experimental results was carried out.

The mechanical properties (compressive, split tensile and modulus of elasticity) of the developed HWC mixtures were more than the minimum limit specified by ACI code of practice for conventional concrete. All the mixtures had high electrical resistivity and moderate chloride diffusion. Many of the blends had high radiation shielding resistance, which was comparable to the mixture produced with conventional iron ore aggregate.

ABSTRACT (ARABIC)

ملخص الرسالة

الاسم الكامل: مختار أولوسيون عزيز

عنوان الرسالة: تطوير خرسانة ذات كفاءة عالية مقاومة للاشعاعات باستخدام النفايات الصناعية

التخصص: هندسة مدنية (انشاءات)

تاريخ الدرجة العلمية: شعبان ١٤٣٦هـ

تستخدم الخرسانة الثقيلة لمقاومة الاشعاعات في مجالي الطب والصناعات النووية. حيث ان كثافة الخرسانة العادية اقل من الوزن المطلوب لمقاومة الاشعاعات. الحصى ذات الكثافة العالية او المكونات المعدنية مثل الرصاص والنحاس والباريت، المغنتيت تستخدم في تحضير الخرسانة ذات الكثافة العالية حيث ان الكثافة تعتمد على نوع الحصى المستخدمة. في كثير من الأحيان تستخدم قطع الحديد او الصلب لانتاج الخرسانة الثقيلة. هذه الخامات غير متوفرة دائما في المملكة العربية السعودية ويتم استيرادها من اماكن اخرى الذي يؤدي الى زيادة التكلفة. لكن انواع محددة من المنتوجات الثانوية الصناعية مثل خبث الصلب يمكن استخدامها مع مواد خام متوفرة محليا لانتاج خرسانة ذات كفاءة عالية مقاومة للاشعاعات.

في هذه الدراسة، تم تطوير خرسانة ذات كفاءة عالية مقاومة للاشعاعات مواد خام صناعية متوفرة محليا. خبث الصلب والذي يعتبر اهم نفايات صناعة الحديد. حصى الحجر الجيري المتوفر محليا مع مواد مستوردة مثل الرصاص الصلب وخام الحديد استخدمت لانتاج خلطات الخرسانة الثقيلة. الخصائص الميكانيكية، الديمومة، ومقاومة الاشعاعات االخرسانة الثقيلة تم فحصها بالاضافة الى تحليل شامل للنتائج.

الخصائص الميكانيكية (قوة الضغط، الشد، معامل المرونة) لخلطات الخرسانة الثقيلة كانت أكثر من الحد الادنى المحدد من قبل معهد الخرسانة الامريكية للخرسانة العادية. جميع الخلطات ابدت مقاومة عالية للتيار الكهربائي وانتشار متوسط للكلوريد. الكثير من الخلطات ابدت مقاومة عالية للاشعاعات مقارنة بالخلطات التي تم انتاجها من خامات الحديد التقليدية.

CHAPTER 1

INTRODUCTION

1.1 BACKROUND TO STUDY

The choice of materials for radiation shielding is usually a function of the type of radiation being emitted, the dose rate and the radioactive source. However, the choice of shielding materials could also be based on some other factors, such as the material weight and fabrication cost [1]. Another crucial factor in selection of materials used for radiation shielding purpose is availability of the materials in a particular country. Therefore, studies on the radiation absorption by materials that are available locally have become a significant area of research and, hence, it is necessary to have the knowledge of the materials that are effective for gamma ray and neutron shielding.

Series of researches have been carried out to ascertain the importance of concrete for radiation shielding and it has been established that concrete is among the most widely used materials for radiation shielding purposes in various facilities, which include medical hospitals containing radioactive sources, particle accelerators, and nuclear power stations [1]. Concrete is also being used for storing radioactive waste [2].

Aggregate composition in concrete plays an important role in its radiation shielding properties and this property may vary depending on the aggregate types used [3]. Another important constituent of concrete is the additives which play an essential role in

modifying primarily two properties; its structural strength [4] and its radiation shielding capacity [5].

While normal concrete produced with conventional coarse aggregates have found its usage in many applications, such as residential and commercial buildings, high rise structures, school buildings, etc., its usage is still limited in the case of those structures that are of critical importance, such as hospital, nuclear power station, etc., because of its poor radiation shielding capability. In this regard, radiation shielding requires the modification of normal concrete constituents in order to improve its shielding capability.

In general, the material that is usually utilized for radiation shielding purposes in medical and nuclear facilities is heavyweight concrete. Concrete having unit weight of more than 2,600 kg/m^3 (higher than normal weight concrete of 2400 kg/m^3) can be referred to as heavyweight concrete while aggregates having specific gravities of 3,000 kg/m^3 and above are called heavyweight aggregates [6]. Various high specific gravity aggregates such as barite, magnetite, hematite, and colemanite have been reportedly used in the literature by researchers to either partially or entirely replace the constituents of normal weight concrete (sand, gravel or crushed limestone) in order to produce heavyweight concrete for radiation shielding [6–11]. The resulting density of heavyweight concrete usually depends on the aggregate type used for the concrete. Typically, the use of barites could increase concrete density to as much as 3,500 kg/m^3, which is greater than the weight of normal concrete by 45%, while the use of magnetite could double concrete density to 5,000 kg/m^3, which is 100% greater than normal concrete [12]. Increasing the density of concrete by the use of high specific gravity aggregates have been shown to greatly improve its radiation shielding properties [12].

Metal ores or steel shots are commonly utilized to increase the weight of normal concrete in the Kingdom of Saudi Arabia. However, of late, there is an increasing trend of using industrial by-products, particularly the waste materials, for the production of heavyweight radiation shielding concrete.

In the proposed study, heavyweight and high performance radiation shielding concrete was developed utilizing locally-produced industrial waste material. Since such a concrete will utilize the local industrial waste products thus solving their disposal and environmental problems. Also, the dependence on the foreign source of constituents for heavyweight concrete will be reduced.

1.2 NEED FOR THIS RESEARCH

As stated earlier, heavyweight concrete for radiation shielding purposes is being produced in the Kingdom utilizing steel shots or iron ore, which are expensive as a result of their non-availability locally. The use of locally available limestone aggregate and industrial by-product, such as steel slag aggregate, in combination with conventional radiation shielding materials could be adopted to produce high performance and heavyweight concrete. If these materials produce fruitful results for heavyweight concrete in terms of their radiation shielding capability, mechanical and durability properties, it will lead to a significant saving in the production cost, as steel slag aggregate and limestone aggregates are cheaper than steel shots or iron ore, and environmental and disposal problem of the industrial waste products will also be solved.

1.3 OBJECTIVES

The overall objective of the proposed study was to develop a high performance and heavyweight concrete that could be utilized for radiation and nuclear shielding. The specific objectives were the following:

1. Investigate the possibility of utilizing the local industrial by-products to produce high performance and heavyweight radiation shielding concrete,
2. Evaluate mechanical properties, durability characteristics and radiation shielding properties of the developed concrete,
3. Assess the cost benefits of the developed heavyweight concrete compared with the conventional radiation shielding concrete,
4. Develop models relating the properties of the developed concrete, and
5. Provide recommendations on the avenues of application of the developed radiation shielding concrete.

1.4 RESEARCH BLUEPRINT

This research work was conducted in six different phases. Figure 1.1 shows the diagrammatical flow of the different phases of this work. In the first phase, detailed and comprehensive literature survey was performed to examine the existing information relating to the study.

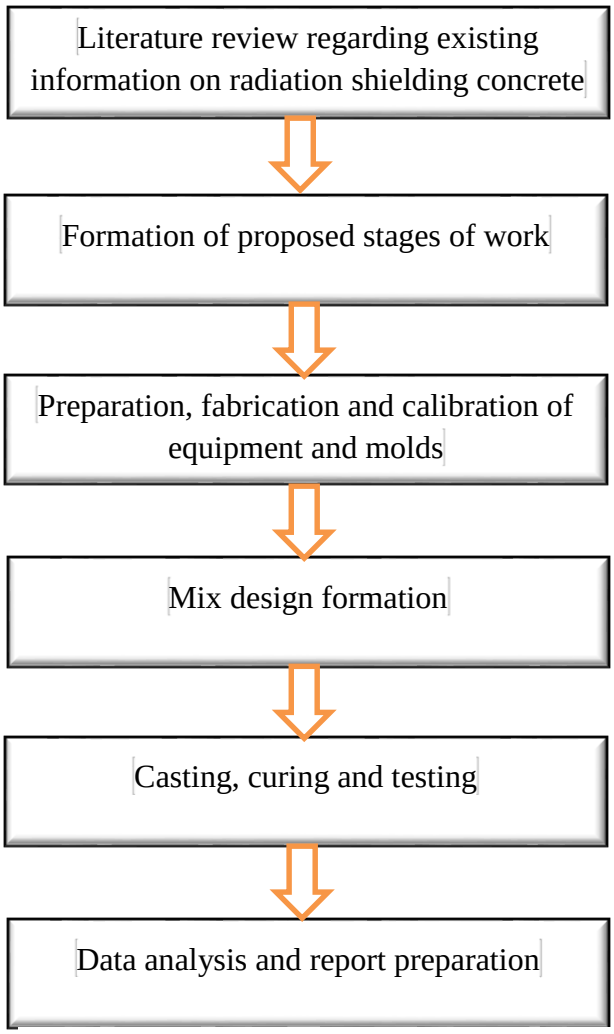

Figure 1.1 Phases of research work

The information collected in phase one together with the objectives of the research led to adequate formation of various stages of the research program to ensure timely and successful completion of the work. This was done as part of phase two of the research.

Preparation of test specimens moulds, fabrication and calibration of weighing scales and testing equipment were part of the work done in the third phase. Also, in phase three, the proposed materials to be used were acquired which included chemical admixture, fine aggregates, limestone aggregate and heavy weight aggregates which are iron ore, steel slag and steel shot.

In the fourth phase, mix design and aggregate combination pattern was developed based on calculations that aimed at combining the aggregates to achieve high and optimum concrete density. Since the major objective of the research was to develop heavyweight concrete for radiation shielding, the major determinant for specimen preparation was density of the concrete samples that could be easily achieved through calculation, and hence, there was no need to perform separate trial mixtures.

The developed mix design and aggregate combination pattern was taken to the laboratory for casting of concrete specimens for the proposed radiation and other hardened properties in the fifth phase. Depending on the specific test requirements, the specimens were water-cured at the laboratory ambient temperature for different periods of 3, 7, 28 and 90 days. Investigations were then carried out on the specimens to ascertain some hardened properties and radiation shielding response.

Phase six, which was the final phase, involved the analysis of data and preparation of report covering the whole research work. Conclusions were drawn from the experimental results and recommendations were provided.

CHAPTER 2

LITERATURE REVIEW

2.1 BACKGROUND TO HEAVYWEIGHT CONCRETE

In many of the researches on the improvement of concrete properties for radiation and nuclear shielding, much emphasis has been on the development of heavyweight concrete with density more than 2600 kg/m^3 utilizing different high specific gravity aggregates. While normal weight concrete with density in the neighbourhood of 2400 kg/m^3 has found most usage worldwide for different infrastructures, such as residential and office buildings, high rise structures, etc., its usage in buildings of critical importance in terms of radiation protection, such as medical facilities and nuclear power stations is limited because of its poor radiation shielding capability.

Regardless of the known poor performance of normal concrete in radiation shielding, some researchers have tried to improve its properties to suit radiation shielding requirements. They mostly concentrate on reducing the water contents, using other cementitious materials or the addition of some lightweight aggregate such as zeolite.

In the work of Kharita et al. [13], the effect of water cement ratio on shielding properties of ordinary concrete was investigated in which the experiment was performed with w/c ratio in the range between 0.43 to 0.63 and the gamma linear attenuation coefficient was

measured. It was reported that there was no significant effect of changes in water cement ratio on shielding properties of ordinary concretes.

Yilmaz et al. [14] investigated the neutron and gamma-ray shielding properties of some concrete materials. In their experiments, the neutrons and gamma-ray shielding by 12 concrete samples with and without mineral additives was studied. The mineral additives used were fly ash, silica fume and blast furnace slag as partial replacement for Portland cement in various percentages while normal aggregates were kept constant in all the mixtures. The results showed that the concrete sample with 100% Portland cement is slightly more effective for photon attenuation at 59.5keV energy and no significant difference between different samples was observed at 661keV. From the point of radiation shielding, the use of fly ash, silica fume and to some extent blast furnace slag as supplementary cementitious materials in concrete leads to only slight variation.

In another research by Türkmen et al. [15], silica fume added cement concrete has the highest photon attenuation coefficient in the energy range of 1.8-3.6keV as compared with the effects of blast furnace slag and zeolite addition. It was however discovered that in the energy range (4–10keV), the addition of silica fume, blast furnace slag and zeolite decreased the radiation attenuation and that the materials without cement have inferior properties than cement with respect to photon attenuation in this energy range. This shows that the addition of mineral admixture to normal concrete does not really improve its shielding properties because they are only effective at low energy range.

In an effort to justify the use of normal weight and lightweight concrete for radiation shielding, Akkurt et al. [16] used zeolite (clinoptilolite), a natural volcanic porous tuff

composed of hydrated alumina silicates as an aggregate in lightweight concrete. The linear attenuation coefficient of specimens prepared with combination of normal aggregates and zeolite in different concentration (0%, 10%, 30% and 50%) was measured. Conclusion was drawn that the addition of zeolite as an aggregate in concrete is not an alternative option to be utilized for the purposes of radiation shielding. This was because increasing zeolite concentration decreased the linear attenuation coefficient measured with four concrete blocks.

The shielding characteristics of concrete using natural local aggregates obtainable in Syria was studied by Kharita et al. [3]. Six types of concrete specimens were prepared using aggregates from various sources with one of the specimens containing 100% hematite as aggregate while another contained mixture of hematite and black coastal sand. The shielding properties of these six types were studied for gamma ray (from Cs-137 and Co-60 sources) and for neutrons (from Am-Be source). It was observed that the best specimens for neutron and gamma shielding were specimens prepared with hematite and mixture of hematite with black coastal sand, even though some of the other specimens too showed some good results. The distinct radiation shielding characteristics of hematite concrete was attributed to its high density for gamma shielding and presence of high content of iron and iron hydroxide for neutron shielding.

Many other studies have been carried out by different researchers on the use of high specific gravity aggregates in concrete, which in turn produces heavyweight concrete for radiation shielding.

Akkurt et al. [17] investigated the linear attenuation coefficients for concrete specimens prepared with 0%, 5%, 10%, 15%, 20% and 25% marble aggregates. The measurements were performed using a gamma-ray spectrometer that contains a NaI(Tl) detector and Multi-Channel-Analyzer (MCA) connected to a PC. Three different gamma-ray energies were used at 662, 1173 and 1332 keV from 137Cs and 60Co sources. The measured results were compared with the calculations obtained using computer code of XCOM for 1 keV-1 GeV gamma energies.

Akkurt et al. [18] evaluated the half-value layer thickness of concrete containing limonite, siderite and barite at different ratios. Measurements were taken by a collimated beam of gamma-ray from 60Co sources. The total linear attenuation coefficient and half-value layer thickness were evaluated.

Pomaro et al. [19] studied the change in properties of concrete exposed to nuclear radiation. The development of the damage front in a concrete shielding wall was analyzed under neutron radiation and results within the wall thickness were reported for long-term radiation spans and several concrete mixtures in order to discuss the resulting shielding properties. Experimental data on the decay of the elastic modulus of concrete were utilized to develop a 3D finite element research code, which accounts for the coupling among moisture, heat transfer and the mechanical field in concrete treated as a fully coupled porous medium. It was reported that the numerical model allows for assessing the durability of concrete exposed to a radioactive environment.

Gencel et al. [20] carried out experimental measurements and Monte Carlo simulations to obtain neutron and gamma attenuation characteristics for concrete with hematite-loaded

concrete. The mechanical strength of hematite specimens was also studied. The outcome suggested that hematite inclusion does not have significant effect on the neutron absorption capability. However, the mechanical strength and the gamma-ray attenuation capability both increased with increasing hematite content.

The extent of photoneutron production by heavyweight concrete in radiation therapy was investigated by Mesbahi et al. [21] using Monte Carlo simulations. Neutron and photon spectra of an 18 MeV photon beam of the Varian linac head were used for all simulations. The simulations were carried out on ordinary and five high density concretes prepared with high density elements, such as Datolite-Galena, Magnetite, Magnetite-Steel, Serpentine and Limonite-Steel. It was reported that photoneutron production strongly depends on their composition. However, the authors recommend further studies on the effect of concrete composition on photoneutrons in radiation therapy rooms [21].

Basyigit [22] investigated the radiation shielding properties of heavyweight concrete mixtures produced using heavyweight aggregates of different mineral origin. The results showed that the heavyweight concrete prepared with heavyweight aggregates of different mineral origin are useful radiation absorbents [22].

Gencel [23] investigated the properties of hematite aggregate concrete. Concrete specimens with 0% (control), 15%, 30%, 45% and 60% of conventional aggregate replaced by hematite aggregate were fabricated with 300, 350, 400 and 450 kg/m^3 cement contents. The water-cement ratio was kept constant at 0.40. Physical and mechanical experiments were carried out on the concrete produced. It was reported that slump and

compressive strength, like other mechanical properties, increased as the hematite aggregate replacement volume increased [23].

The radiation shielding and mechanical properties of lead-concrete was studied by Ochbelagh et al. [24]. The effect of gamma radiation on the compressive strength of concrete during solidification was studied. It was reported that the strength of gamma-radiated concrete was high and the dense structure was confirmed by scanning electron microscopy. The gamma-ray shielding properties of concrete mixed with different percentages of lead were also studied. Concrete with 90% lead powder and 10% cement was reported to have maximum strength and gamma-ray shielding properties [24].

A high performance and high strength heavyweight concrete for radiation shielding structures was developed by Peng and Hwang [25]. The natural aggregates in concrete were replaced with round steel balls. The diameters of the steel balls were 0.5 and 1 cm, and their density was 7.8 kg/m^3. Dense packing mixture methods were used to produce heavyweight concrete with densities of 3,500 and 5,000 kg/m^3. It was reported that the slump of the concrete specimen was 260-280 mm and its slump flow was 610-710 mm. More importantly, its compressive strength was 88.48 MPa.

Gencel et al. [7] studied the physical and mechanical properties of concrete prepared with different concentrations of hematite (10 to 50 volume % at 10% intervals). The concrete specimens were prepared with a water-to-cement ratio of 0.42 and cement content of 400 kg/m^3. It was reported that the addition of hematite increased the unit weight so that a smaller thickness of concrete was required to provide radiation shielding. The loss in compressive strength, after 30 freeze-thaw cycles was 21.3% while the composite

containing 10% hematite lost only 7.8% of the strength. The drying shrinkage of hematite concrete was lower than that of plain concrete.

Gencel et al. [8] evaluated the radiation shielding of concrete prepared with varying proportions of colemanite. The physical and mechanical properties, such as slump, air content, compressive strength, split tensile strength, Schmidt hardness, modulus of elasticity, freeze-thaw durability, unit weight and pulse velocity of that concrete were also studied. It was reported that the properties of concrete were affected by the quantity of colemanite. Up to 30% colemanite was recommended to be used as a replacement of aggregate.

Gallego et al. [26] presented the results of tests conducted on a high-density magnetite concrete commercially available under the trade name Hormirad as a neutron shielding material. The purpose of the reported study was to characterize the investigated material's behavior against neutrons, as well as to test different mixings, including boron compounds in an effort to improve the neutron shielding efficiency of the investigated material. Slabs of different thicknesses were prepared and exposed to a 241Am-Be neutron source under controlled conditions. The original mix, which included a high fraction of magnetite, was then modified by adding different proportions of anhydrous borax ($Na_2B_40_7$). For comparison purposes, the same experiments were repeated with slabs of ordinary concrete (HA-25). In parallel to the experiments, Monte Carlo calculations were performed utilizing code MCNP5. The results showed an advantageous behavior of the Hormirad compared with ordinary concrete. The borated concretes exhibited a small improvement in the neutron attenuation compared with Hormirad alone.

Okuno et al. [27] investigated the properties of a novel neutron shielding concrete using colemanite rock and peridotite rock. Its shielding performance was evaluated through the transmission experiments by using 252 Cf spontaneous fission source and calculations was made with MCNP5 code. It was reported that a neutron 1/100 attenuation length of the neutron concrete shield with a typical colemanite content of 10 wt% is shorter by a factor of 1.7 than that of normal concrete. It was reported that the shielding performance becomes better when the thickness is thicker and the incident neutron spectrum is softer. The colemanite-peridotite concrete (neutron shielding concrete) was applied to biological shields of the Versatile High Intensity Total Diffractometer on the Japan Proton Accelerator Research Complex. Using this concrete permitted a reduction in the thickness of the shielding wall by a maximum of 25 cm compared to the normal concrete and a reduction of the iron in the beam dump.

Sharma et al. [28] studied the mechanical and radiation shielding properties of fiber reinforced concrete with steel fibers, lead fibers and a combination of the two (hybrid fibers). Compressive strength, split tensile strength and flexural toughness were among the mechanical properties investigated and radiation shielding of gamma-rays was investigated by comparing the attenuation provided by different types of concrete against each other and against blank readings without attenuation. It was reported that the hybrid fibers showed a significant enhancement in both mechanical and radiation shielding properties.

Kharita et al. [29] studied the effect of carbon powder addition on the properties of hematite radiation shielding concrete. Carbon powder was added to shielding concrete made of hematite aggregates to investigate its effects on shielding properties. The powder

was added in different percentages, and the mechanical and radiation attenuation properties of the prepared concretes were determined. It was reported that, the addition of 6% (by wt.) carbon powder of the concrete increased its strength by about 15%. The shielding effectiveness decreased for both gamma and neutrons with increasing carbon powder percentage. But the loss in shielding effectiveness for both gamma rays and neutrons were within measurement error range for carbon powder addition of 6%. Simulation for the experimental measurements was carried out using Monte Carlo MCNP code, to understand the effect of carbon powder on the shielding effectiveness against neutrons. The authors [29] reported a good agreement between the simulation and experimental results.

Awadallah and Imran [30] studied the gamma radiation attenuation capacity of aggregates in Jordan. The attenuation coefficients of limestone, bricks and concrete were measured utilizing HPGe-spectrometer with a multiple gamma radiation source of different energy lines. It was reported that the variations in the attenuation coefficients, at the same energy line, were within the experimental uncertainties. An empirical formula was proposed to calculate attenuation at various incident energies. Limestone of average thickness of 7 cm was found to stop 75% of a 662 keV energy gamma beam while a brick of the same thickness was effective in stopping 60% of the same beam. The total attenuation coefficient of concrete calculated at 1333 keV was reported to be 11.2 m^{-1}, which was less than that of limestone and bricks.

Akkurt et al. [31] investigated the radiation shielding of concrete prepared with different quantities of barite and normal aggregates. The linear attenuation coefficients were calculated using XCOM at photon energies of 1 keV to 100 GeV. The obtained results

were compared with the measurements at the photon energies of 0.66 MeV and 1.33 MeV. It was reported that the type of aggregates is more important than their quantity.

Akkurt et al. [10] investigated the gamma-ray shielding properties of concrete produced with barite ($BaSO_4$). Different volumes of barite aggregates were used to prepare the concrete specimens, and thus each concrete had different density. The mass attenuation coefficients were calculated using XCOM at photon energies of 1 keV to 100 GeV. The results were compared with the measurements made at 0.66 and 1.25 MeV.

Mahdy et al. [32] studied the shielding properties of heavyweight and high strength concrete. Twelve mixtures that achieved a slump of above 100 mm and strength of up to 140 MPa at 180 days were selected from 41 trial mixtures. The concrete mixtures were prepared with w/c ratio of 0.24 and superplasticizer content of 3.5%, three levels of silica fume (0, 10%, 20% by weight of cement), two coarse aggregate proportions of total aggregate (0.48, 0.65 by volume of magnetite and natural sand fine aggregates). The compressive strength and shielding properties of the investigated mixtures indicated clear benefits from the use of silica fume as a mineral admixture and from using magnetite as fine as well as coarse aggregates [32].

El-Sayed et al. [33] studied the attenuation properties of barite concrete as a biological shield for nuclear power plants, particle accelerators, research reactors, laboratory hot cells and different radiation sources. Investigation has been performed by measuring the transmitted fast neutron and gamma-ray spectra through cylindrical barite concrete specimens (3.49 $g \cdot cm^{-3}$). A reactor-collimated beam and neutron-gamma spectrometer with stilbene scintillator were used during measurements. A pulse shape discriminating

technique based on zero cross over method was used to discriminate between neutron and gamma pulses. Also, slow neutron fluxes were measured using a collimated reactor beam and BF3 counter, where the macroscopic cross section was evaluated using the attenuation relation. The measured and calculated results were compared and a reasonable agreement was reported [33].

Maslehuddin et al. [34] studied the radiation shielding properties of concrete prepared with electric arc furnace slag aggregates (EAFSAs) and steel shots. It was reported that concrete mixed with 50% EAFSA and 50% steel shots meets the weight, compressive strength and radiation shielding requirements and, the use of 50% EAFSA results in substantial cost reduction and conservation of useful material such as iron ore.

Even though some work has been done on the radiation shielding of concrete, the bulk of the work has been on radiation shielding properties with few investigation on mechanical and durability properties of the same concrete developed. It is worthy of note that structural application of radiation shielding concrete requires the structure to be able to withstand load and environmental effects, such as corrosion. In this regard, there is a need to develop high performance and heavyweight concrete utilizing industrial byproducts for radiation shielding. The utilization of the industrial byproducts will lead to a saving in the quantity of cement thereby decreasing the weak carbon foot print of the construction industry.

2.2 HARDENED PROPERTIES

Majority of previous researchers have concentrated on the mechanical and durability properties of normal and lightweight concrete. Few studies have been done on the mechanical and durability properties of heavyweight concrete. This is not surprising as heavyweight concrete is a special concrete utilized for only specialized purposes including radiation shielding.

2.2.1 Compressive, Tensile Strength and Modulus of Elasticity

Beushausen and Dittmer [35] investigated the influence of two common South Africa aggregate (Andesite and Granite) on the compressive strength, flexural and split tensile, and elastic modulus of high strength concrete. The aggregates were used to produce concrete strength between 30 MPa and 120 MPa range. It was reported that concrete produced with granite has the higher compressive strength than Andesite concrete. However, the stiffer Andesite aggregate produced concrete with a significantly higher elastic modulus.

Hong et al. [36] studied the effect of aggregate surface roughness on mechanical properties of interface between coarse aggregates and mortar and on the subsequent failure processes of concrete. By testing the interfacial bond strength, it was found that the tensile and shear bond strengths of the interface increased and tended to be constant as the roughness of the aggregate surface increased. Maximum tensile and shear bond strength of the interface was achieved with quartzite concrete, followed by limestone and then basalt.

Cetin and Carrasquillo [37] also investigated the influence of coarse aggregate on the mechanical properties of high performance concrete. Crushed river gravel, trap rock, dolomitic limestone, and calcitic limestone were used in the study. It was observed that differences in mineralogical characteristics of coarse aggregate, as well as the aggregate shape, surface texture, and hardness appear to be responsible for the differences in the performance of the high performance concrete.

Wu et al. [38] investigated the influence of aggregate size distribution on mechanical properties of concrete by acoustic emission technique. The acoustic technique is a dynamic nondestructive test method for concrete testing. An increase in fracture energy of concrete was observed with increment of maximum aggregate size.

Meddah et al. [39] studied the effect of content and particle size distribution on the compressive strength of concrete. Their result showed that mixtures without chemical admixture made with a ternary combination of granular fraction and having a maximum size of 25mm, that assures a continuous granular size distribution, have shown the highest compressive strength.

Devi and Gnanavel [40] examined the properties of concrete produced using steel slag as partial replacement of fine and coarse aggregate. Compressive strength, tensile strength, flexural strength and some durability tests were investigated. It was found that steel slag replacement in normal concrete improves the compressive, tensile and flexural strength.

Zhou et al. [41] carried out an experimental study to investigate the modulus of elasticity at 7, 28 and 91 days of high performance concrete mixes, of low water/cement ratio and fixed mortar composition, containing six different types of aggregates of constant volume

fraction. Their results showed that, apart from the aggregates of very low and very high modulus, concrete modulus at 28 days can be predicted quite well by well-known models. Increase in modulus thereafter is slight. Compressive strength (about 90 N/mm^2 at 28 days with normal aggregates) is drastically reduced by the weaker aggregates and is also reduced (by about 9%) by the stiffer (steel) aggregates.

2.2.2 Resistivity and Chloride Diffusion

Reinforcement corrosion is a major durability problem in reinforced concrete structures exposed to marine environment or to repeated applications of de-icing salts because of the aggressive nature of chloride ions [42]. The early occurrence and high rate of corrosion of reinforcement is a problem that has been of interest for many decades [43]–[45]. For a routine quality control requirement, measurement of chloride diffusivity can be time consuming and elaborate, and thus, a rapid and reliable method for quick assessment is usually sought after. The rate at which corrosion can occur in a rebar embedded inside concrete can be assessed by measurement of the flow rate of ions through concrete between the anodic and cathodic region of the rebar. The electrical resistivity of concrete has a significant effect on this flow rate [46] and measuring it can be used to depict the possibility of occurrence of corrosion in reinforcement [47], [48].

The effect of chloride and sulphate contamination on the electrical resistivity of concrete was investigated by Saleem et al. [49]. Their results indicate that both moisture, chloride and sulphate contamination influence the electrical resistivity of concrete. At higher salt concentrations, moisture content has very little influence on electrical resistivity. This

indicates that in near dry concrete, high salt concentrations could sustain reinforcement corrosion.

Presuel-Moreno et al. [50] investigated the evolution of resistivity vs. time of concrete prepared with three different compositions and subjected to various curing regimes for an extended period of time. Two of the curing regimes consisted of immersing the specimens in either tap water or 3.5% NaCl solution. The other three curing regimes consisted of exposure to fog room, high humidity and laboratory humidity. The measured resistivity values were used to estimate the aging factor. It was found that the aging factor is time dependent for concrete with mineral admixtures and the curing exposure affects the magnitude of the aging factor.

Jingwei et al. [51] investigated the effects of recycled coarse aggregate (RCA) distribution on chloride diffusion from four modelled recycled aggregate concrete (RAC) with different RCA replacement ratios (R_{RA}). A rapid chloride migration (RCM) equipment was used to investigate the chloride diffusivities of each type of the modelled RAC and the diffusivities were also simulated by a finite element method (FEM). They reported that the chloride diffusivities of the modelled RAC generally increase with the increase of R_{RA}; while for the same R_{RA}, the chloride diffusivities and the chloride concentration distribution in the modelled RAC are still different due to the effect of different aggregate arrangements.

Dousti et al. [52] examined the effect of exposure temperature ranging from 22 °C to 50 °C on chloride diffusion in concretes containing different percentages of silica fume or natural zeolite. It was found that concrete diffusivity and chloride penetration depth

increase with exposure temperature, which is in agreement with the Arrhenius theory. They also reported that resistance of concrete mixtures against chloride diffusion was improved with the use of silica fume and zeolite.

Farahani et al. [53] carried out a prediction model study of chloride diffusion coefficient for silica fume concrete under long-term exposure to a durability site located in the southern region of Iran. The study was carried out on 16 concrete mixtures containing silica fume with variable water/ binder ratios exposed to seawater for a maximum period of 60 months and the empirical model was developed by applying regression analysis based on Fick's second law on the experimental results. They reported that adding the silica fume up to a dosage of 10% and reducing the water/binder ratio reduces the chloride diffusion coefficient in concrete. Their study also confirms that the chloride diffusion coefficient increases with temperature and decreases over time.

Hobbs [54] attempted to predict the probable effect of the aggregate on chloride ion diffusion into saturated concrete. It was discovered that variations in the concrete chloride ion diffusion coefficient of up to 10:1 could be induced if the chloride ion diffusion coefficient of an aggregate ranges from 0.2 to 10 times that of the cement paste matrix. Such a variation is equivalent to a change in free water-cement ratio from 0.77 to 0.45.

An experimental study to assess the effect of cumulative lightweight aggregate (LWA) content (including lightweight sand) in concrete on its water absorption, water permeability, and resistance to chloride-ion penetration was carried out by Liu et al. [55]. Comparison was made between the results and those of cement paste and a control

normal weight aggregate concrete (NWAC) with the same w/c. Their results indicate that although the total charge passed, migration coefficient, and diffusion coefficient of the LWAC were not significantly different from those of NWAC with the same w/c, resistance of the LWAC to chloride penetration decreased with increase in the cumulative LWA content in the concretes.

CHAPTER 3

EXPERIMENTAL PROGRAM

The materials characterization and experimental procedures adopted during the course of this study are addressed in this chapter. In accordance with the objectives of this research which is to develop high performance and heavyweight concrete (HWC) for radiation shielding, three different aggregates (which are steel slag, steel shots and iron ore) with high specific gravities were sourced locally and their characteristics was analyzed. Limestone aggregate and dune sand were also procured. Locally produced cement was used as filler while superplasticizer was adopted as chemical admixture to achieve a suitable workability for all the mixtures.

The research work was divided into three different stages. Stage one involved procurement of materials for the HWC as stated above. In the second stage, mix design was done by combining the aggregates in different proportions with a view to achieving high density and specimens were cast based on the developed mix deign. Three different aggregate combination groups were considered where each group consisted of 5 mixtures, together with another 4 mixtures containing 100% of each of the 4 aggregate types making a total of 19 mixtures. The third stage involved the testing of the specimens to ascertain their mechanical, durability and radiation shielding properties.

The subsequent sections of this chapter serves to discuss the experimental programs in detail.

3.1 MATERIALS

3.1.1 Cement

ASTM C 150 Type I known as Ordinary Portland Cement (OPC), was used in all the concrete mixtures. The specific gravity of the cement is 3.15 and it is commonly used for concrete production in the Kingdom. In order to achieve relatively high performance concrete, especially in terms of compressive strength, high cement content of 400 kg/m^3 was used with a water-cement ratio of 0.4 for all the specimens. The chemical composition of the cement is presented in Table 3.1.

Table 3.1: Chemical constituent of the cement.

Constituent	Weight %
SiO_2	20.52
Al_2O_3	5.64
CaO	64.40
K_2O	0.36
Fe_2O_3	3.80
MgO	2.11
Na_2O	0.19
SO_3	2.10
Alkalis	0.43
Loss on ignition	0.70
C_2S	19.00
C_3S	55.00
C_3A	10.00
C_4AF	7.00

3.1.2 Fine Aggregates

Locally available dune sand was utilized as fine aggregate in all the mixtures. The specific gravity of the sand was 2.53 while its water absorption was 0.6%. The fine aggregate grading is presented in Table 3.2.

Table 3.2: Fine aggregate grading.

Sieve opening	Percent passing
4.75 mm	100
2.36 mm	100
1.18 mm	100
600 µm	76
300 µm	10
150 µm	4

3.1.3 Coarse Aggregates

Natural limestone and heavyweight aggregates obtained from different local sources were used as coarse aggregates. Grading of the aggregates was carried out in the laboratory as well as the analysis for water absorption and specific gravity. The aggregate grading conformed to ASTM C 33 while the specific gravity and absorption determination conformed to ASTM C 127, respectively. Each of the aggregates used are described in the following sections.

(i) Crushed limestone

Crushed limestone obtained locally was one of the coarse aggregates used in this study to produce heavyweight concrete. The maximum aggregate size of the limestone aggregate was 19 mm. The absorption capacity and specific gravity of the limestone aggregate were 1.1% and 2.6, respectively. The coarse aggregate grading is presented in Table 3.3.

Table 3.3: Crushed limestone grading.

Sieve opening (mm)	Percent passing
19.0	100
12.5	60
9.5	40
4.75	10
2.36	0

(ii) Steel slag

Steel slag aggregate was obtained from SABIC steel plant, Saudi Arabia. It is a major locally available industrial waste used in this study. The aggregate, being a heavyweight aggregate with specific gravity of 3.47, was used in combination with other heavyweight aggregates. The maximum size of the aggregate was 19 mm and its water absorption was 1.5%. Table 3.4 shows the grading of steel slag aggregate.

Table 3.4: Steel slag grading.

Sieve opening (mm)	Percent passing
19.0	100
12.5	70
9.5	40
4.75	5
2.36	0

(iii) Iron ore

The second heavyweight aggregate used was iron ore with a specific gravity of 4.4 and water absorption of 1.4%. Iron ore is not readily available locally because it is imported from outside the Kingdom. The iron ore aggregate used consisted of just two size ranges of 4.75 mm with 40% retained and 2.36 mm with 60% retained.

(iv) Steel shot

Steel shot is another imported material but its usage was considered because of its high specific gravity. It is the heaviest aggregate used in this study with specific gravity of 7.85 and its water absorption is 0%. The water absorption was zero because steel shot is basically steel balls with no pores in the surface, hence, possibility of water absorption is zero.

Table 3.5 shows the summary of the specific gravity and water absorption for all the aggregates used in this study.

Table 3.5: Specific gravity and water absorption of the aggregates.

Aggregate	Specific gravity	Water absorption (%)
Steel shot	7.85	0
Iron ore	4.4	1.4
Steel slag	3.47	1.5
Limestone	2.6	1.1
Sand	2.53	0.6

3.1.4 Chemical Admixture

A superplasticizer (SP) was utilized as to enhance the concrete workability without increasing the water-cement ratio. The superplasticizer used was termed SP 430 and it was obtained locally from a supplier in the Eastern province of Saudi Arabia. The proportions of superplasticizer used in all the mixtures to achieve a workability of 100 ± 25 mm varied from 1.5% to 2.3% by weight of cement. The technical details of SP 430 as obtained from the manufacturer is given in Table 3.6.

Table 3.6: SP 430 technical data.

Specific gravity @ 20^{o}C	1.2 ± 0.01
Chloride content	Nil
Alkali content	< 72.0 g of Na_2O
Appearance	Brown liquid

3.1.5 Water

Portable water obtained from the laboratory was used throughout for the preparation of all the concrete mixtures.

3.2 MIX PROPORTIONS

Nineteen (19) mixtures were prepared with different proportions of the coarse aggregates. Four groups were formed containing combinations of the coarse aggregates in different proportions. The groups contain mixtures with 100% coarse aggregates, mixtures with combination of steel slag and iron ore aggregates, mixtures with combination of steel slag and steel shot aggregates, and mixtures with limestone and steel shot aggregates. Absolute volume design method was used to get the quantities of each constituent of the mix proportions such as fine aggregates, coarse aggregates, cement, water and superplasticizer. The absolute volume method is given by equation (1) shown below:

$$V_{TA} + \sum V_i = 1 \quad (1)$$

Where V_{TA} is the volume of the total aggregate including fine and coarse aggregates that has to be solved for in the equation above. V_i is the volume of other constituents including cement, water, superplasticizer and entrapped air. Since the water/cement ratio and volume of superplasticizer to achieve adequate workability are known, as stated in the preceding sections, also, allowable percentage of entrapped air is known (based on ACI 211.1-91 recommendation); the only unknown is the volume of total aggregate.

Re-writing equation (1) in terms of mass-specific gravity ratio, we have:

$$V_{TA} = 1 - \sum \frac{m_i}{\rho_i} \tag{2}$$

And

$$V_{TA} = \frac{m_{sand}}{\rho_{sand}} + \frac{m_{stones}}{\rho_{stones}} \tag{3}$$

Where m is the mass of each constituent and ρ is the specific gravity of each constituent.

Representing the ratio of sand/TA (total aggregate) by f, we have:

$$f = \frac{m_{sand}}{m_{sand} + m_{stones}} \tag{4}$$

Therefore, we can obtain m_{stones} in terms of m_{sand} as

$$m_{stones} = \frac{(1-f)}{f} X\ m_{sand} \tag{5}$$

The mass of sand can be obtained by substituting for m_{stones} in (3) as given below,

$$m_{sand} = \frac{V_{TA}\ X\ \rho_{sand}\ X\ \rho_{stone}\ X\ f}{\rho_{stone}\ X\ f + \rho_{sand}\ X\ (1-f)} \tag{6}$$

At this stage, m_{stone} can be obtained by substituting the value of m_{sand} in (5). The value of sand/TA ratio that was used was 0.38.

The individual components of each coarse aggregates can then be obtained using the percentage distribution given in the preceding sections. Volume of mixing water used was adjusted for by incorporating the absorption capacities of the aggregates.

Since the mix proportions consisted of 19 mixtures as stated earlier, the mass of total aggregate obtained in the equations above constituted of one or two combinations of the coarse aggregate types in different percentages.

Tables 3.7 through 3.10 show the weights of each constituents (in kg per cubic meter of concrete) of the mixture. The percentage combinations of each aggregate types were chosen to achieve relatively high concrete density. The percentage of entrapped air allowed for was 2% as recommended by ACI 211.1-91. A convenient naming scheme was chosen for the mixtures and were used as the IDs in the tables. SA stands for steel slag aggregate, SS stands for steel shot aggregate, IO stands for iron ore aggregate while LSA stands for limestone aggregate. For example, SA65-IO35 implies a mixture containing 65% of steel slag aggregate and 35% of iron ore aggregate, making up the total coarse aggregate in that mixture. In all the mixtures, 400 kg/m^3 cement content was used and the water/cement ratio was also kept constant at 0.4. The SP varied from 1.5% to 2.3% of the total cement content for all the mixtures to achieve a slump value between 80 to 100 mm.

Table 3.7: Weights of the constituent materials (Steel slag + Iron ore).

MATERIALS	(SA80-IO20)	(SA65-IO35)	(SA50-IO50)	(SA35-IO65)	(SA20-IO80)
Cement, kg/m^3	400	400	400	400	400
w/c ratio	0.4	0.4	0.4	0.4	0.4
Water, kg/m^3	185	185	186	186	186
Iron Ore, kg/m^3	273	485	706	935	1173
Steel slag, kg/m^3	1090	902	706	503	293
Sand, kg/m^3	835	850	866	881	899
SP (% of cement)	1.7	1.7	1.7	1.8	1.8
SP, kg/m^3	6.8	6.8	6.8	7.2	7.2
Theoretical Density (kg/m^3)	2790	2829	2871	2912	2958

Table 3.8: Weights of the constituent materials (Steel slag + steel shot).

MATERIALS	(SA80-SS20)	(SA65-SS35)	(SA50-SS50)	(SA35-SS65)	(SA20-SS80)
Cement, kg/m^3	400	400	400	400	400
w/c ratio	0.4	0.4	0.4	0.4	0.4
Water, kg/m^3	182	180	178	175	172
Steel shot, kg/m^3	283	521	784	1075	1402
Steel slag, kg/m^3	1133	968	784	579	351
Sand	868	912	961	1014	1074
SP (% of cement)	1.8	1.8	1.9	2.1	2.2
SP, kg/m^3	7.2	7.2	7.6	8.4	8.8
Theoretical Density (kg/m^3)	2874	2988	3113	3251	3407

Table 3.9: Weights of the constituent materials (Steel shot + limestone aggregate).

MATERIALS	(SS80-LSA20)	(SS65-LSA35)	(SS50-LSA50)	(SS35-LSA65)	(SS20-LSA80)
Cement, kg/m^3	400	400	400	400	400
w/c ratio	0.4	0.4	0.4	0.4	0.4
Water, kg/m^3	170	172	173	174	175
Limestone, kg/m^3	335	537	707	854	981
Steel shot, kg/m^3	1338	997	707	460	245
Sand, kg/m^3	1025	940	867	805	752
SP (% of cement)	2.1	2.0	2.0	1.9	1.8
SP, kg/m^3	8.4	8.0	8.0	7.6	7.2
Theoretical Density (kg/m^3)	3277	3053	2863	2701	2561

Table 3.10: Weights of the constituent materials (100% aggregates).

MATERIALS	(SA100)	(SS100)	(IO100)	(LSA100)
Cement, kg/m^3	400	400	400	400
w/c ratio	0.4	0.4	0.4	0.4
Water, kg/m^3	185	167	187	177
Steel slag, kg/m^3	1331	0	0	0
Steel shot, kg/m^3	0	1904	0	0
Iron Ore, kg/m^3	0	0	1503	0
Limestone, kg/m^3	0	0	0	1128
Sand, kg/m^3	816	1167	921	691
SP (% of cement)	1.7	2.3	1.8	1.5
SP, kg/m^3	6.8	9.2	7.2	6.0
Theoretical Density (kg/m^3)	2738	3647	3020	2400

3.3 PREPARATION AND CURING OF SPECIMEN

Preparation and curing of the heavyweight concrete specimens to be used for various tests in this study were done in the controlled laboratory environment. Appropriate weights of each of the concrete constituents were measured and mixed in an electric mixer of 1.7 m^3 capacity. The dry aggregates together with cement were first mixed for about a minute in the mixer to achieve adequate mixing before adding about 50% of the required water with the mixer still rotating. Measured quantity of SP was mixed with the remaining water and added gradually to the mixture while the mixer was still in operation. The whole constituents were then thoroughly mixed in the rotating mixer for about 15 ± 5 minutes to achieve homogenous concrete. After mixing, the concrete mixture was poured to the moulds of required shapes and sizes. The moulds were then vibrated until adequate consolidation was achieved.

After casting, the specimens were covered with plastic sheets to prevent moisture lost and they were left for 24 hrs in the laboratory before being de-moulded. The specimens were placed in the curing tank fully submerged in sweet water for the required number of days before experimental investigation was carried out.

Table 3.10 shows the types, dimension and numbers of specimen prepared for the evaluation of mechanical, durability and radiation shielding properties of the heavyweight mixtures. The table also includes the test standards adopted in this study.

Table 3.11: Details of specimens prepared for investigation.

S/N	TEST	TEST STANDARD	SPECIMEN	TEST AGE, DAYS	NUMBER OF SPECIMENS
1	Unit weight	ASTM C 642	100 mm cube	28	12
2	Compressive strength	ASTM C 39	100 mm cube	3, 7, 28 & 90	
3	Tensile strength (Split)	ASTM C 496	75 X 150 mm cylinder	28	3
4	Modulus of elasticity	ASTM C 469	75 X 150 mm cylinder	28	3
5	Drying Shrinkage	ASTM C 157	50 X 50 X 250 mm prisms	Up to 180	3
6	Chloride diffusion	ASTM C 1556	75 X 150 mm cylinder	180	3
7	Electrical resistivity	2-electrode method	75 X 150 mm cylinder	28	3
8	Radiation shielding	KFUPM PGNAA technique	100 mm cube	28	3
	Number of specimens per mix				**30**
	Total number of specimens				**570**

3.4 PROPERTIES

3.4.1 Unit Weight

Aside from the theoretical unit weights calculated during preparation of mix proportion, the actual unit weight of the mixtures was determined to ascertain the density of the heavyweight concrete (HWC). Unit weight of specimens was tested after 28 days of water curing. The procedure was carried out by measuring the actual dimensions of the 100 mm cube together with the actual weight of each specimen. Automatic weighing balance was used to measure the weight while the dimensions were measured with the aid of a Vernier caliper, as shown in Figure 3.1. Unit weight was then determined by dividing the actual weight by the actual dimensions as given in the equation below.

$$Unit\ weight, \rho\ \left(\frac{kg}{m^3}\right) = \frac{Actual\ weight\ (kg)}{Actual\ cube\ volume\ (m^3)} \tag{7}$$

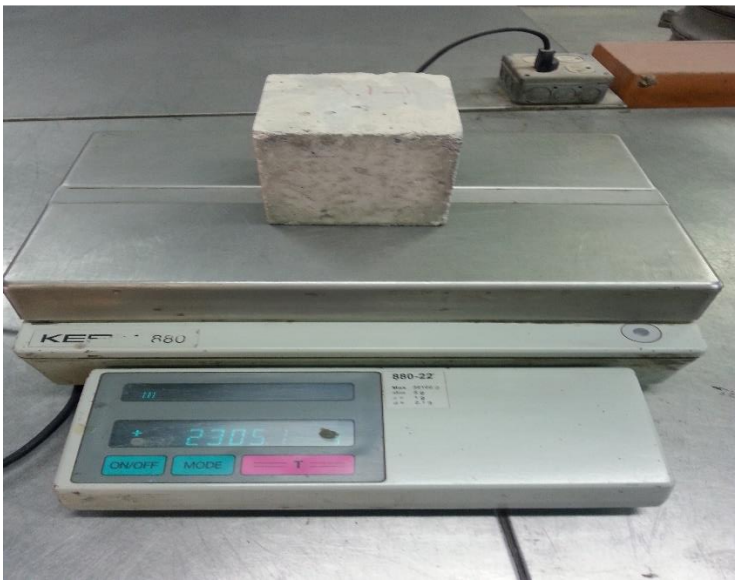

Figure 3.1: Weighing balance for unit weight measurement.

3.4.2 Compressive Strength

The compressive test specimens which were 100 mm cubes were tested according to ASTM C 39 after 3, 7, 28 and 90 days of water curing. The specimens were tested under the application of constant compressive force of 1.5 kN/s using automatic hydraulic type compressive testing machine, as shown in Figure 3.2. The specimens were loaded continuously until failure and the failure (maximum) load was noted. Three (3) specimens were tested for each of the mixtures. Figure 3.3 shows the specimens after failure in compression. The compressive strength was determined by dividing the maximum load by the cross-sectional area of the cube.

$$\sigma = \frac{P}{A} \tag{8}$$

Where:

σ = compressive strength, MPa,

P = Maximum applied compressive load, N, and

A = cross-sectional arear of specimen, mm^2

Figure 3.2: Matest® hydraulic type compressive testing machine.

Figure 3.3: Compressive strength specimens after failure in compression.

3.4.3 Splitting Tensile Strength

The 75 x 150 mm cylindrical specimens for split tensile strength were tested according to ASTM C 496 after 28 days of water curing. The specimens were tested under the application of constant compressive loading of 0.4 kN/s through a bearing strip. The automatic hydraulic type compressive testing machine shown in Figure 3.4 was used for the test. After the specimens were loaded until failure, achieved by splitting of the specimens, the failure load was recorded. Figure 3.5 shows the tensile strength specimens before and after splitting.

The split tensile strength was determined according to the formula below as given in ASTM C 496.

$$T = \frac{2P}{\pi l d} \tag{9}$$

Where:

T = splitting tensile strength, MPa

P = maximum applied load, N

l = specimen length, mm

d = specimen diameter, mm

Figure 3.4: Split tensile test arrangement.

Figure 3.5: (a) Tensile test specimens before testing (b) Specimens after splitting.

3.4.4 Modulus of Elasticity

Modulus of elasticity test specimens were 75 x 150 mm cylinder. Test was carried out according to the specifications of ASTM C 469 on three 28-day water cured specimens, Strain gauge was used to record the deformation as the specimens were being loaded. The specimens were Sulphur capped on the rough surface while the other smooth surface were left uncapped. After capping, the curved surfaces of the specimens were properly cleaned and two strain gauges were attached at opposite sides as shown in Figure 3.6.

Figure 3.6: Modulus of elasticity test specimen with connection to data logger.

The same automatic testing machine used for compressive and tensile strengths was used to apply compressive loading to the specimens via a load cell at constant rate of 0.5 kN/s until failure. Figure 3.7 shows the test arrangement while figure 3.8 shows a sample after failure. In the arrangement, wires from the strain gauges were connected to data logger to capture the direct strain. The load cell was also connected to the data logger to capture load changes at the chosen constant interval of 0.5 kN.

The recorded data was copied from data logger for plots of stress-strain curves and subsequent calculation of modulus of elasticity. The formula from Section 7.1 of ASTM C469 given below was used for the calculation.

$$E = \frac{S_2 - S_1}{\epsilon_2 - 0.000050} \quad (10)$$

Where:

E = chord modulus of elasticity, MPa

S_2 = stress corresponding to 40% of ultimate load, MPa

S_1 = stress corresponding to a longitudinal strain, ϵ_1, of 50millionths, MPa and

ϵ_2 = Longitudinal strain produced by S_2

Figure 3.7: Test arrangement for modulus of elasticity.

Figure 3.8: Sample after failure in compression.

3.4.5 Drying Shrinkage

Shrinkage measurement was taken according to the provisions of ASTM C 157 on 50 x 50 x 250 mm prism specimens with 3 specimens from each mixture. It involved measuring changes in length of each specimen with time. The measurement, which was taken at regular intervals for a total period of 120 days, started after 3-days of water curing. A setup consisting of a stand fitted with LVDT connected to a data logger was used, as shown in Figure 3.9.

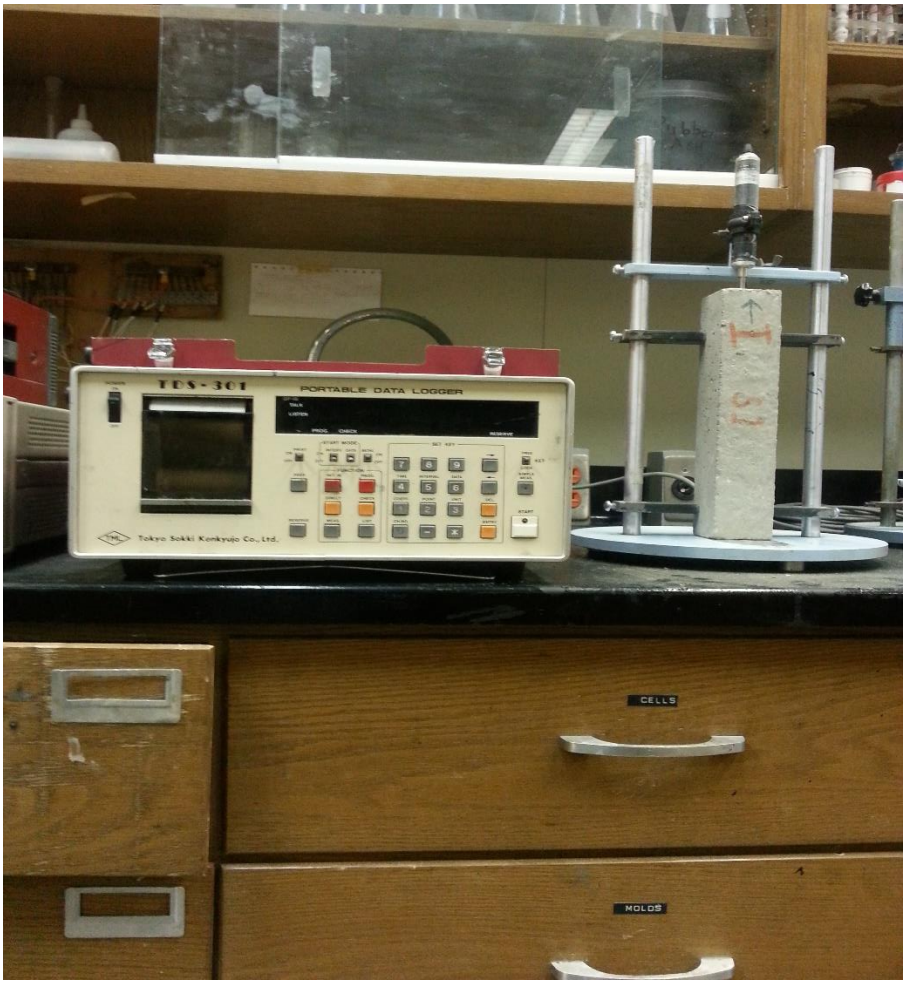

Figure 3.9: Shrinkage measurement setup.

3.4.6 Chloride Diffusion

Chloride diffusion was evaluated on 75 x 150 mm cylindrical specimens in order to determine the coefficient of chloride diffusion. The test was carried out according to the specifications of ASTM C 1556. After 28 days of water curing the samples, they were left to dry for another 7 days before being coated. Epoxy coating was applied to the curved surface and one circular face, leaving the finished surface uncoated to ensure unidirectional flow of chloride ions in the concrete specimens. 5% Sodium Chloride (NaCl) solution was prepared and the specimens were immersed in the solution for six months. At the end of the exposure period, 5mm thick concrete discs were cut at intervals for chloride analysis. Table 3.12 shows the location of each disc along the depth of the cylindrical specimens. Figure 3.10 shows a typical concrete disc after cutting. The discs were then pulverized until they were fine enough to pass through sieve #100 as shown in Figure 3.11.

Table 3.12: Size and location of discs along specimen depth

Disc No	Depth, mm	Average Depth, mm
1	0-5	2.5
2	10-15	12.5
3	20-25	22.5
4	45-50	47.5
5	75-80	77.5
6	95-100	97.5

Figure 3.10: 5 mm thick concrete disc.

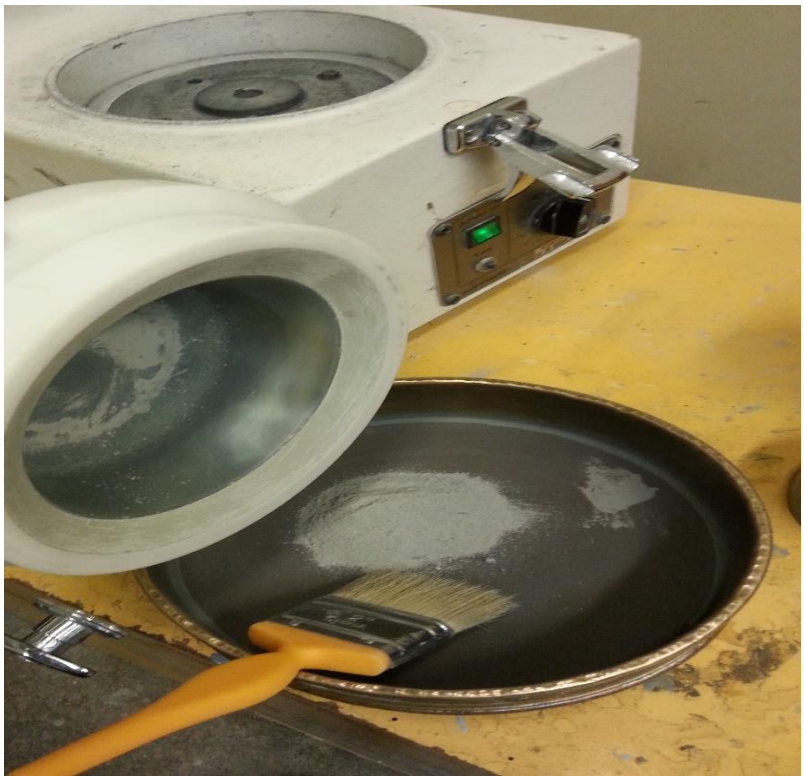

Figure 3.11: Pulverized sample being passed through sieve #100.

After pulverizing, the samples were analyzed for water soluble free chloride concentration, which is a measure of the quantity of chloride ion that may influence rebar corrosion. The detailed procedure is given below:

1. 5 grams of powder was taken from each sample into the beaker.
2. 50 ml of hot distilled water was added and the mixture thoroughly stirred and left for 24 hours for proper digestion of chloride ion.
3. The solution was filtered into the flask and the filtrate was made 100 ml by adding distilled water.
4. 0.2 ml of the solution was taken and 9.8 ml of distilled water was added to it to make it 10 ml.
5. 2 ml each of 0.25 M ferric ammonium sulphate and mercury thiocyanate was then added into the 10 ml solution.
6. Solution was gently shaken to ensure adequate mixing and was taken into a test tube.
7. The test tube was placed inside a spectro-photometer (set at 460 nm wavelength) and the absorbance value was recorded.
8. The free chloride concentration was then calculated using chloride calibration curve.

Figure 3.12 shows the test arrangement relating to the procedures described above.

(a) Test samples during chloride digestion (b) Test samples during filtration

(c) Spectro-photometer for absorbance measurement

Figure 3.12: Test setup for chloride concentration measurement.

Chloride concentration was plotted against the depth and the coefficient of chloride diffusion was determined by fitting the equation given in Section 10.1.1 of ASTM C 1556 (reproduced below) into the curve.

$$C(x,t) = C_s - (C_s - C_i).erf\left(\frac{x}{2\sqrt{D_e\, t}}\right) \quad (11)$$

Where:

$C(x,t)$ = chloride concentration at depth x, mass %,

C_s = chloride concentration at the surface, mass %,

C_i = initial chloride concentration prior to submersion in NaCl solution, mass %,

x = depth below exposed surface, cm,

t = exposure time, s, and

D_e = effective chloride diffusion coefficient, cm^2/s.

3.4.7 Electrical Resistivity

The electrical resistivity of a concrete also plays an important role in deducing the likelihood of corrosion in concrete members. Three (3) 75 x 150 mm cylindrical specimens were accessed in each mixture for electrical resistivity. The resistance through the specimens was measured by passing current to the specimens through probes that were connected from a multimeter to spongy terminals. The terminals were kept moist for each measurement to ensure good electrical contacts on the ends of the concrete

specimens. Figure 3.13 shows the setup for electrical resistivity measurement where a concrete specimen was tightly secured between the two ends of the mechanical device.

The formula below was used to calculate the resistivity of each specimen by converting the measured resistance to electrical resistivity.

$$\rho = R\frac{A}{l} \tag{12}$$

Where:

ρ = Electrical resistivity, kΩ-cm

R = Measured resistance, Ω

A = Cross-sectional area of specimen, cm^2 and

l = Specimen length, cm

Figure 3.13: Electrical resistivity setup.

3.4.8 Radiation Shielding

Concrete cube specimens of 100 mm dimension were used to evaluate the radiation shielding response of the heavyweight concrete. The specimens were irradiated by ^{137}Cs source using the experimental setup shown in figure 3.14. The setup consisted of a ^{137}Cs gamma-ray source, lead collimator and a 4 x 4 inches BGO detector placed inside a lead shield. Gamma-ray source of 662 keV energy was used to irradiate the specimens. The gamma-ray spectrum was first acquired without any concrete specimen by capturing the radiation from the Cs source using a PC based multichannel analyzer, as shown in figure 3.15. Concrete specimens were then placed between the source and detector and the gamma-ray spectrum was acquired with the specimen in place.

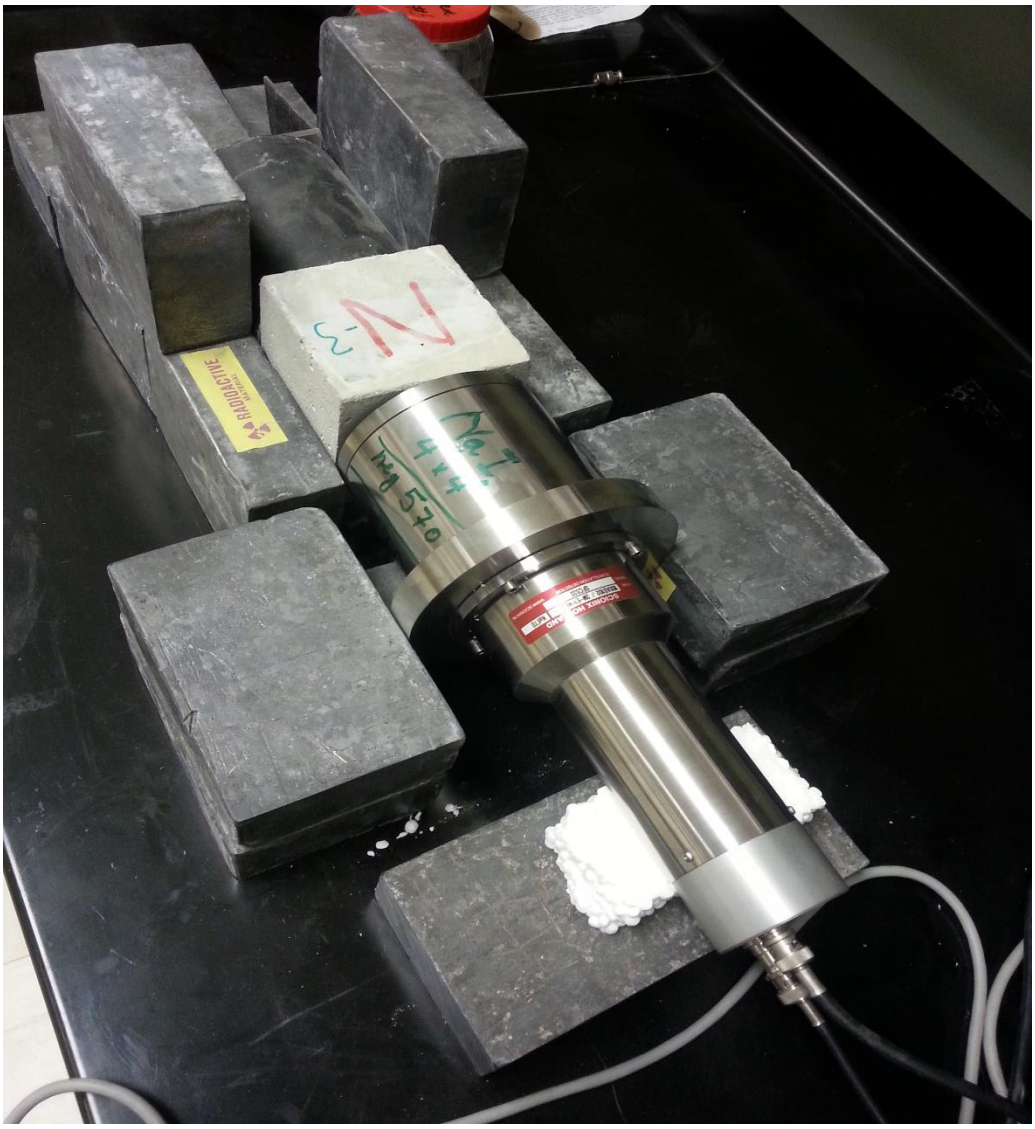

Figure 3.14: Setup for gamma-ray intensity measurement.

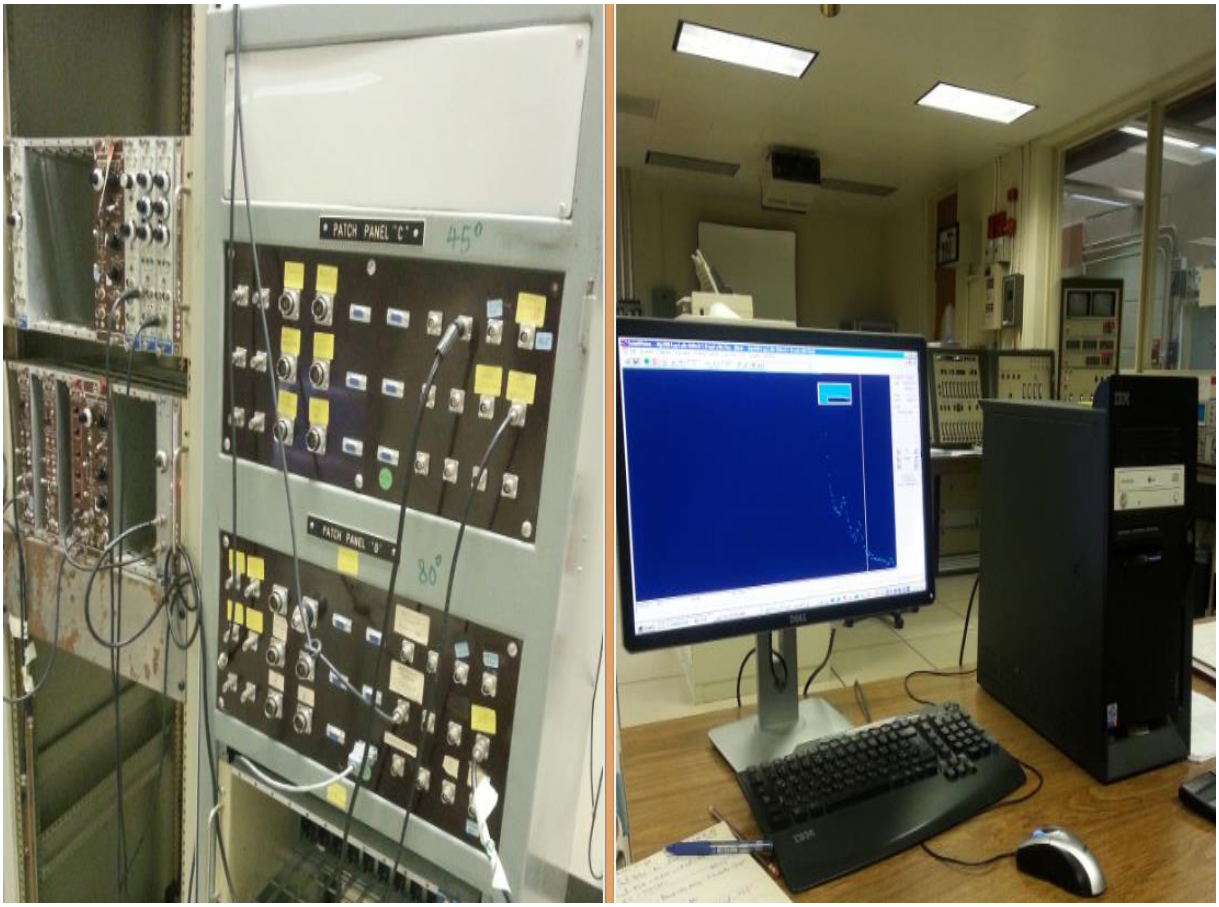

Figure 3.15: PC based multichannel analyzer.

The gamma-ray spectrum contained a single peak for each measurement and sufficient time was considered in order to obtain good statistics in the area under the peak. The total intensity under the peaks was obtained by summing the pulse height intensity contained within the area in the photo peaks.

The effective linear attenuation coefficient μ,eff was calculated from the following relation, as given by L'Annunziata [56].

$$I_x = B\, I_o\, e^{-\mu t} \tag{13}$$

Where:

μ = effective linear attenuation coefficient, mm^{-1}

I_x = gamma-ray attenuated intensity

I_o = gamma-ray un-attenuated intensity

B = build up factor, taken as 1 for good geometry

t = thickness of specimen, mm

CHAPTER 4

RESULTS AND DISCUSSION

4.1 UNIT WEIGHT

Table 4.1 shows the average 28-day unit weight of all the 19 HWC mixtures. Although, limestone aggregate concrete is not considered as heavyweight concrete because of its relatively low unit weight, it is still included in this study to serve as a baseline for comparison since, in addition to its widely usage as coarse aggregate, many researchers have done lots of work on limestone aggregate concrete. Based on what is obtainable in the literature, concrete specimen having unit weight above 2600 kg/m^3 is generally taken as heavyweight concrete. However, this is not a limiting requirement, especially in this study, where the eventual radiation shielding performance of the developed mixtures is the main objective, and hence, mixtures with slightly lower density than 2600 kg/m^3 will not be disregarded.

Table 4.1: Unit weight of HWC specimens

Mix ID	Unit weight, kg/m^3
LSA100	2435
SA100	2790
SS100	3563
IO100	3029
SA80-IO20	2783
SA65-IO35	2827
SA50-IO50	2859
SA35-IO65	2935
SA20-IO80	2999
SA80-SS20	2866
SA65-SS35	2981
SA50-SS50	3029
SA35-SS65	3185
SA20-SS80	3358
LSA80-SS20	2576
LSA65-SS35	2734
LSA50-SS50	2787
LSA35-SS65	3008
LSA20-SS80	3231

4.1.1 Mixtures with 100% coarse aggregate types

Figure 4.1 shows the average 28-day unit weight of HWC mixtures prepared with 100% coarse aggregate types. The figure shows that limestone aggregate mixture is the lightest with unit weight less than the specified 2600 kg/m^3 while steel shot aggregate mixture is the heaviest in this group. From Section 3.1.3, it has been reported that limestone aggregate has a specific gravity of 2.6 while steel slag, iron ore and steel shot aggregates have specific gravities of 3.47, 4.4 and 7.85 respectively. The specific gravities of the coarse aggregates directly influence the unit weight of the resulting concrete since other constituents remain constant.

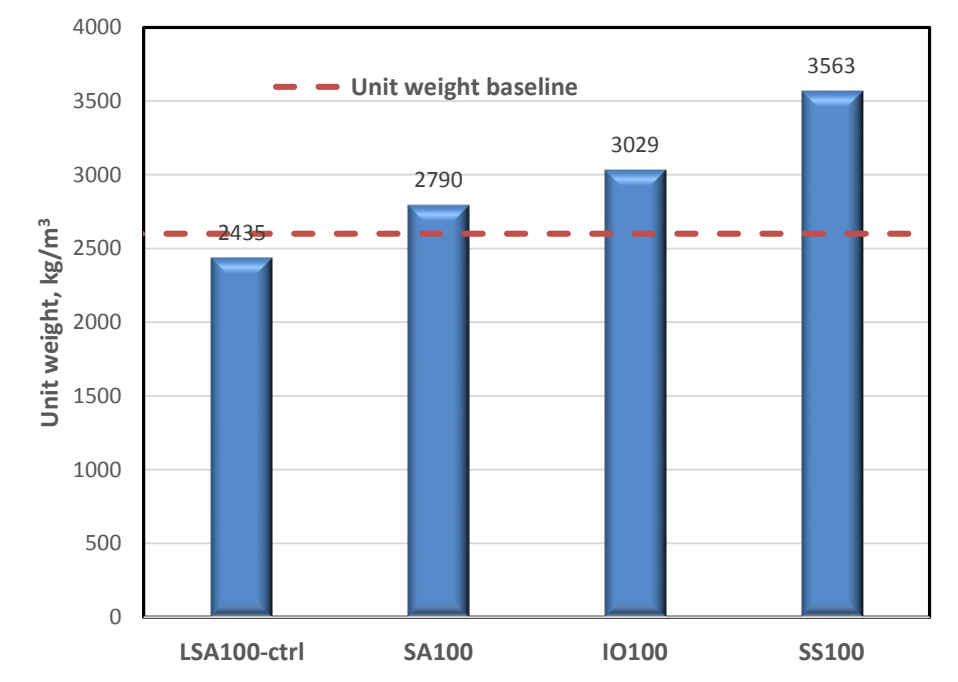

Figure 4.1: Unit weight of HWC with 100% coarse aggregate types.

4.1.2 Mixtures with steel slag and iron ore as coarse aggregate

Figure 4.2 shows the average 28-day unit weight of HWC mixtures prepared with combination of steel slag and iron ore aggregates in varying proportions. As expected, the unit weight increases as the percentage of iron ore aggregate increases. The unit weight of the mixtures in this group ranges from 2783 kg/m^3 to 2999 kg/m^3, which is more than the specified 2600 kg/m^3.

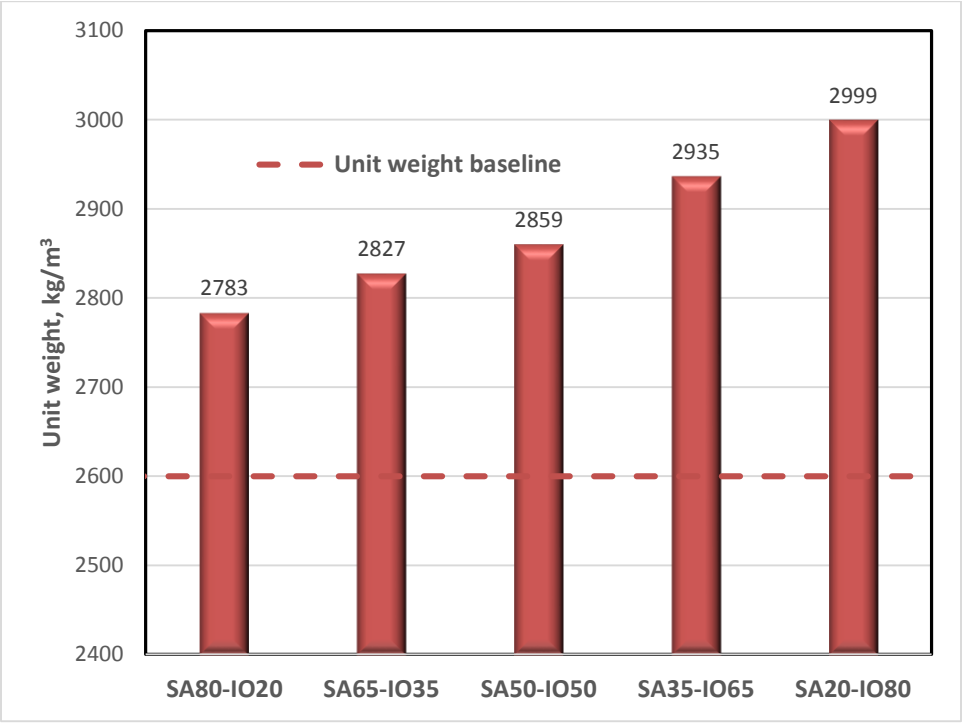

Figure 4.2: Unit weight of HWC with steel slag and iron ore aggregates.

4.1.3 Mixtures with steel slag and steel shot as coarse aggregate

Figure 4.3 shows the average 28-day unit weight of HWC mixtures prepared with combination of steel slag and steel shot aggregates in varying proportions. As expected, the unit weight increases as the percentage of steel shot aggregate increases. All the mixtures in this group have unit weight more than the specified 2600 kg/m^3.

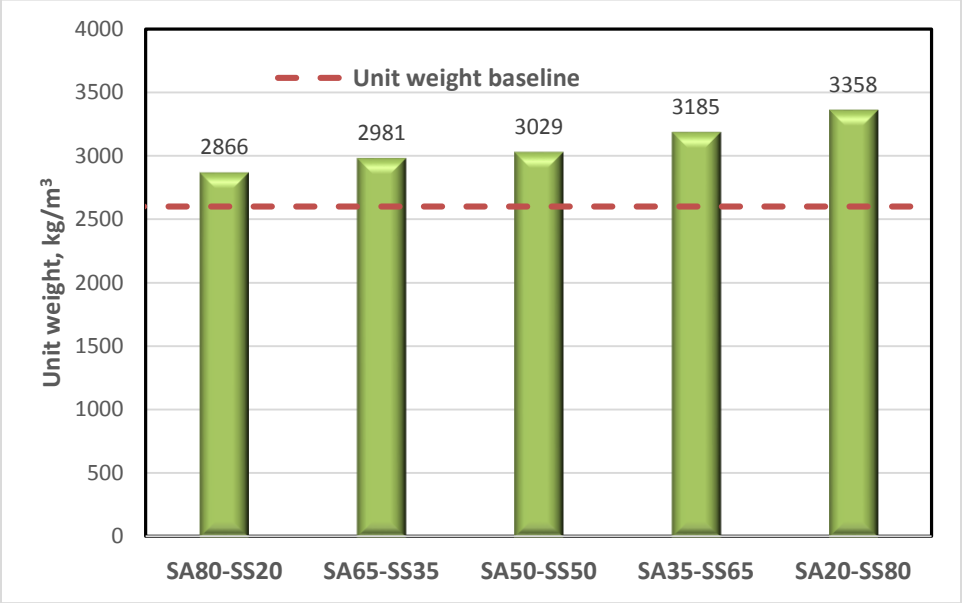

Figure 4.3: Unit weight of HWC with steel slag and steel shot aggregates.

4.1.4 Mixtures with limestone and steel shot as coarse aggregate

Figure 4.4 shows the average 28-day unit weight of HWC mixtures prepared with combination of limestone and steel shot aggregates in varying proportions. The figure shows a gradual increase of unit weight from 2576 kg/m^3 to 3231 kg/m^3 as the percentage of steel shot aggregates increases. Only LSA20-SS80 has lower unit weight below the specified 2600 kg/m^3.

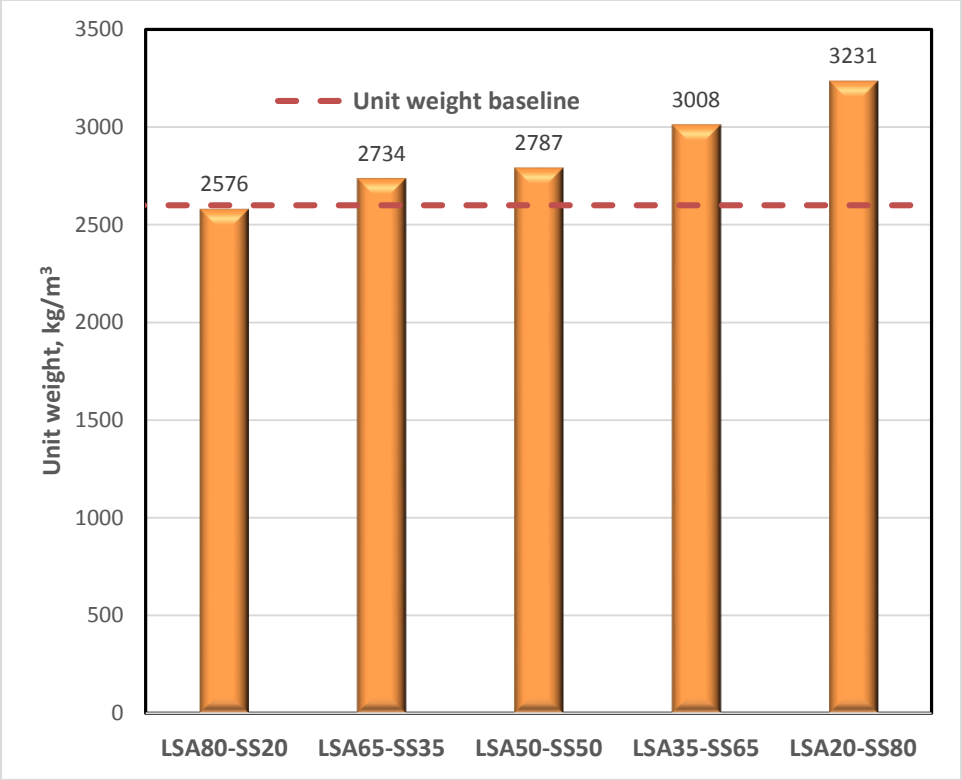

Figure 4.4: Unit weight of HWC with limestone and steel shot aggregates.

4.2 COMPRESSIVE STRENGTH

The compressive strength result for all the 19 HWC mixtures is summarized in Table 4.2. The compressive strength values at ages 3, 7, 28 and 90 days of curing are shown in the table. The reported values in this table are the averages of three specimens prepared from each mix. As stated earlier in Section 3.2, all the 19 mixtures have been grouped into four categories with three of the four consisting of two aggregate combination while the fourth group consist of 100% each of the aggregates used.

Table 4.2: Compressive strength of HWC specimens

Mix ID	Compressive Strength (MPa)			
	3 days	7 days	28 days	90 days
LSA100	28.0	34.5	42.0	52.0
SA100	31.7	38.3	45.3	55.7
SS100	20.4	23.5	29.6	36.1
IO100	28.7	31.0	40.3	45.5
SA80-IO20	29.0	35.0	44.0	52.0
SA65-IO35	31.5	32.3	39.0	47.6
SA50-IO50	30.0	32.0	38.4	45.2
SA35-IO65	27.6	31.7	37.7	44.0
SA20-IO80	27.0	30.0	39.0	44.0
SA80-SS20	31.6	31.6	39.6	49.9
SA65-SS35	28.5	32.0	39.3	50.0
SA50-SS50	27.7	28.8	37.0	47.6
SA35-SS65	21.6	29.0	34.0	42.0
SA20-SS80	23.2	29.5	32.0	39.3
LSA80-SS20	27.5	33.0	41.0	49.3
LSA65-SS35	27.4	33.0	40.3	46.9
LSA50-SS50	27.2	32.8	38.6	45.8
LSA35-SS65	28.7	30.6	32.3	40.1
LSA20-SS80	19.0	22.7	26.0	32.2

4.2.1 Mixtures with 100% coarse aggregate types

The plot of compressive strength evolution with time for the first group is shown in Figure 4.5. This group consist of 100% of each types of the coarse aggregates which are LSA100, SA100, SS100 and IO100 consisting of 100% limestone aggregate, steel slag aggregate, steel shot aggregate and iron ore aggregate respectively. Figure 4.6 shows the 28-day strength of each mixture as percentage of 28-day strength of limestone aggregate mixture.

In this group and subsequent groups, LSA100 would be taken as the control mix because limestone is usually the conventional aggregate for concrete production especially in the Kingdom of Saudi Arabia and its impact on concrete properties has been widely researched.

As seen in figure 4.5, all mixtures in this category except SA100 have compressive strengths at all ages lower than that of the control mix except SA100. The varying compressive strength values exhibited by the four mixtures is because of the different composition and properties of the coarse aggregates, since paste quality is the same for all mixtures. It has been widely reported that concrete properties can be influenced by both paste quality and aggregate properties [37], [41], [57], [58].

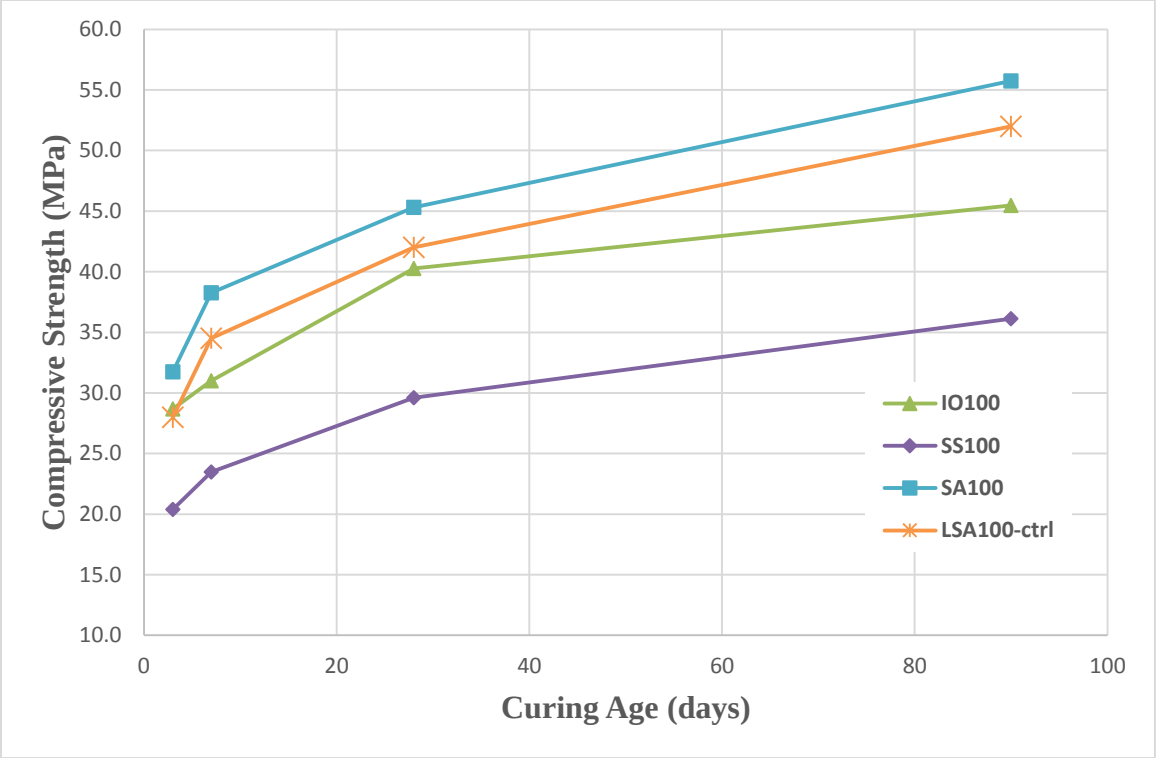

Figure 4.5: Compressive strength of HWC with 100% coarse aggregate types.

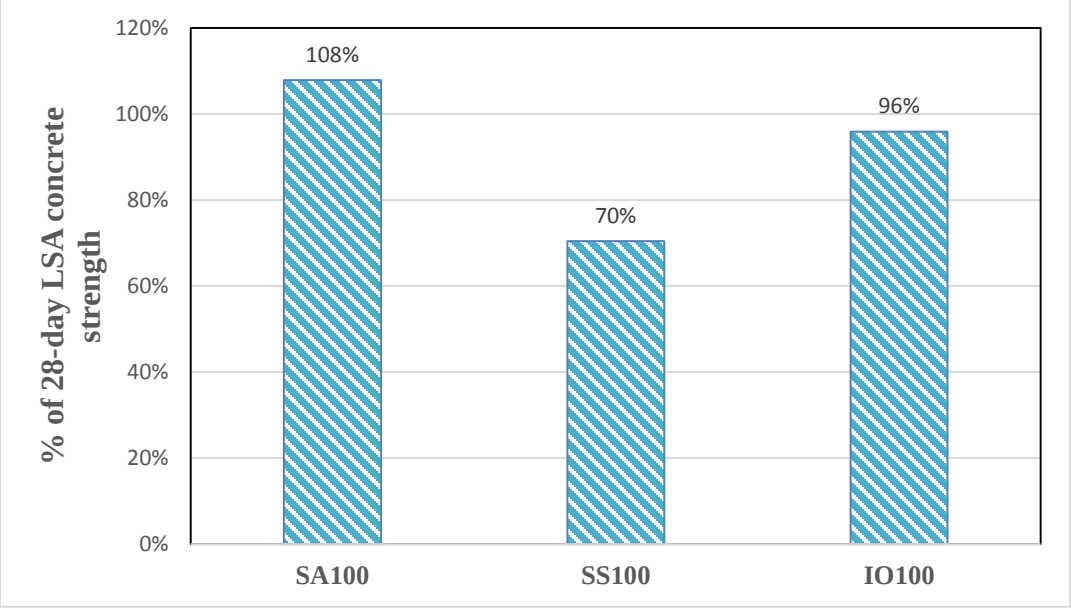

Figure 4.6: HWC with 100% aggregate types - 28-day strength as percentage of 28-day LSA concrete strength.

The compressive strength of steel slag aggregate at all ages are higher than that of limestone aggregate as seen in figure 4.5 and 4.6. Although, sleet slag is not widely used as coarse aggregate in concrete production, its use in special cases may be of demand and it has been reported to have better compressive strength than limestone aggregate concrete in some literature as evidenced by Maslehuddin et al [59] and Devi et al [40].

The compressive strength of LSA100 mixture is very close to that of SA100. The good performance of limestone aggregate concrete is not surprising as it has been reported to give good quality concrete giving rise to its widely usage for concrete production [60]–[62].

The compressive strength obtained with the use of 100% iron ore (IO100) is lower than that of LSA100 and SA100. This lower value can be as a result of the effect of particle size distribution and maximum aggregate size on concrete properties [38], [39], [63]. The maximum aggregate size of the iron ore aggregate is 4.75 mm and its distribution consisted of only 2 size ranges, that is, 4.75 mm with 40% retained and 2.36 mm with 60% retained. Whereas, both limestone and steel slag aggregate have well graded particle size distribution with maximum aggregate size of 19 mm. The lower aggregate size of the iron ore aggregate implies higher surface area, which will require more volume of paste for adequate bonding. Since the w/c ratio and cement content were kept constant for all mixtures, this explains the fact that IO100 may not be develop similar compressive strength value with SA100 and LSA100 because it theoretically requires more volume of paste.

Specimens produced with 100% steel shots gave the lowest compressive strength at all ages as can be seen in Figure 4.5. From Figure 4.6, it can be seen that the compressive strength of SS100 at 28-day is 62% of the corresponding strength of the LSA100 specimen. The poor performance could be due to the shape and size of steel shot aggregate. In the first instance, steel shot is spherically shaped and has smooth surface that automatically reduces the bond between paste and aggregate, and hence, reducing the compressive strength. The surface roughness plays an important role in enhancing interfacial bond between aggregate and paste [36], [64]–[66]. In addition, because of the small size of steel shot aggregate, there would be need for high paste volume to lubricate its higher surface area. This effect is similar to what was explained above for iron ore.

4.2.2 Mixtures with steel slag and iron ore as coarse aggregate

In this group, steel slag and iron ore aggregates were combined in varying percentages from lowest of 20% to highest of 80% as given in table 4.2. The compressive strength development with curing time plotted from values in table 4.2 is shown in figure 4.7. Figure 4.8 shows the 28-day strength of each mixture as percentage of 28-day strength of limestone aggregate mixture. It can be seen in figure 4.7 that all the mixtures in this group except SA80-IO20 have compressive strength at all ages lower than that of the control mix. From figure 4.8, SA65-IO35 developed 93% of the control mix compressive strength, while SA35-IO65 developed 90%.

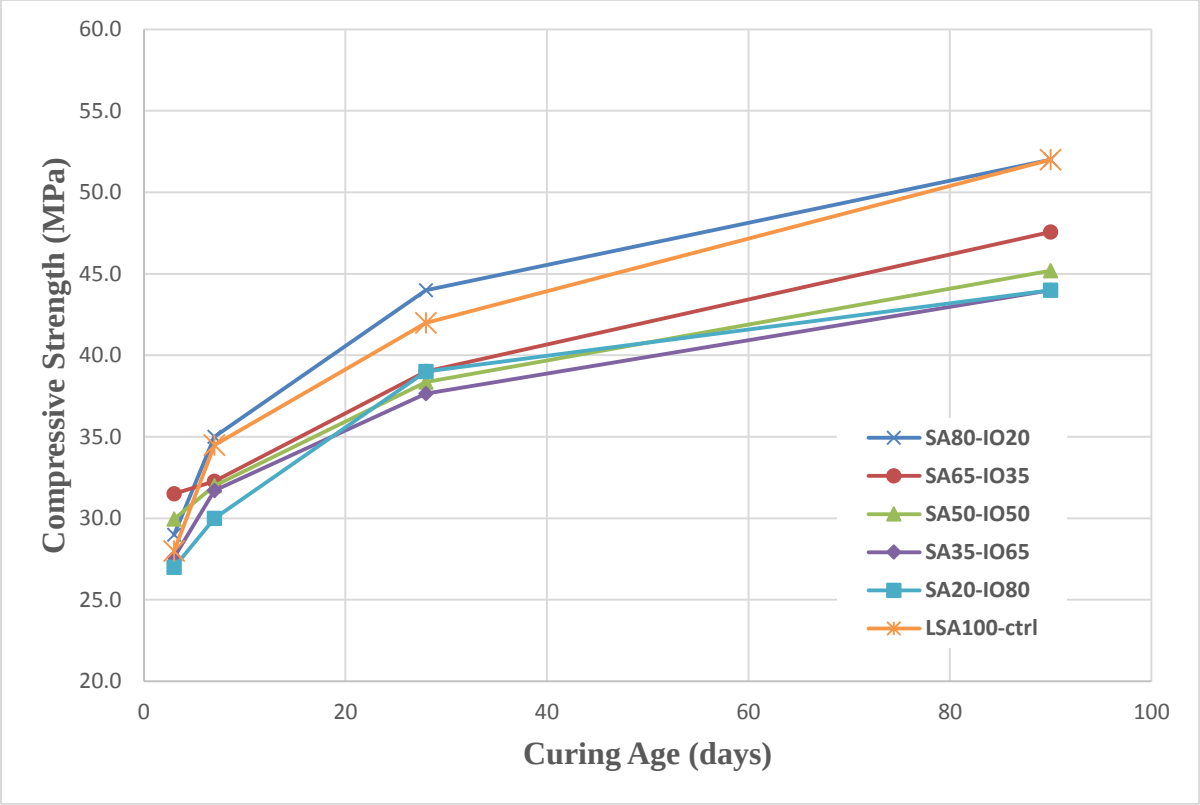

Figure 4.7: Compressive strength of HWC with steel slag and iron ore aggregates.

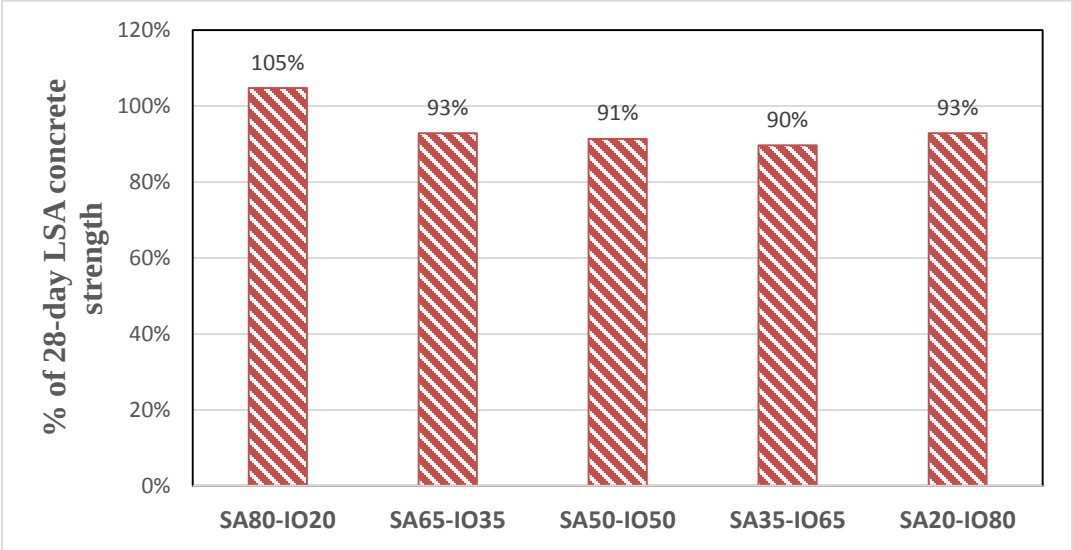

Figure 4.8: HWC with steel slag and iron ore aggregate - 28-day strength as percentage of 28-day LSA concrete strength.

4.2.3 Mixtures with steel slag and steel shot as coarse aggregate

Figure 4.9 shows the graph of compressive strength evolution with curing time for mixtures prepared with varying percentages of steel slag and steel shot aggregates. The 28-day strength of the mixtures as percentage of 28-day strength of control mix is shown in figure 4.10.

From figure 4.9, all the mixtures in this group have compressive strength at all ages lower than that of the control mix. Figure 4.10 shows that increasing the steel shot percentage reduces the compressive strength of the mixtures. The reduction here is more than what was observed in the case of steel slag and iron ore combination. This can be easily attributed to the spherical and smooth surface characteristics of steel shot aggregate.

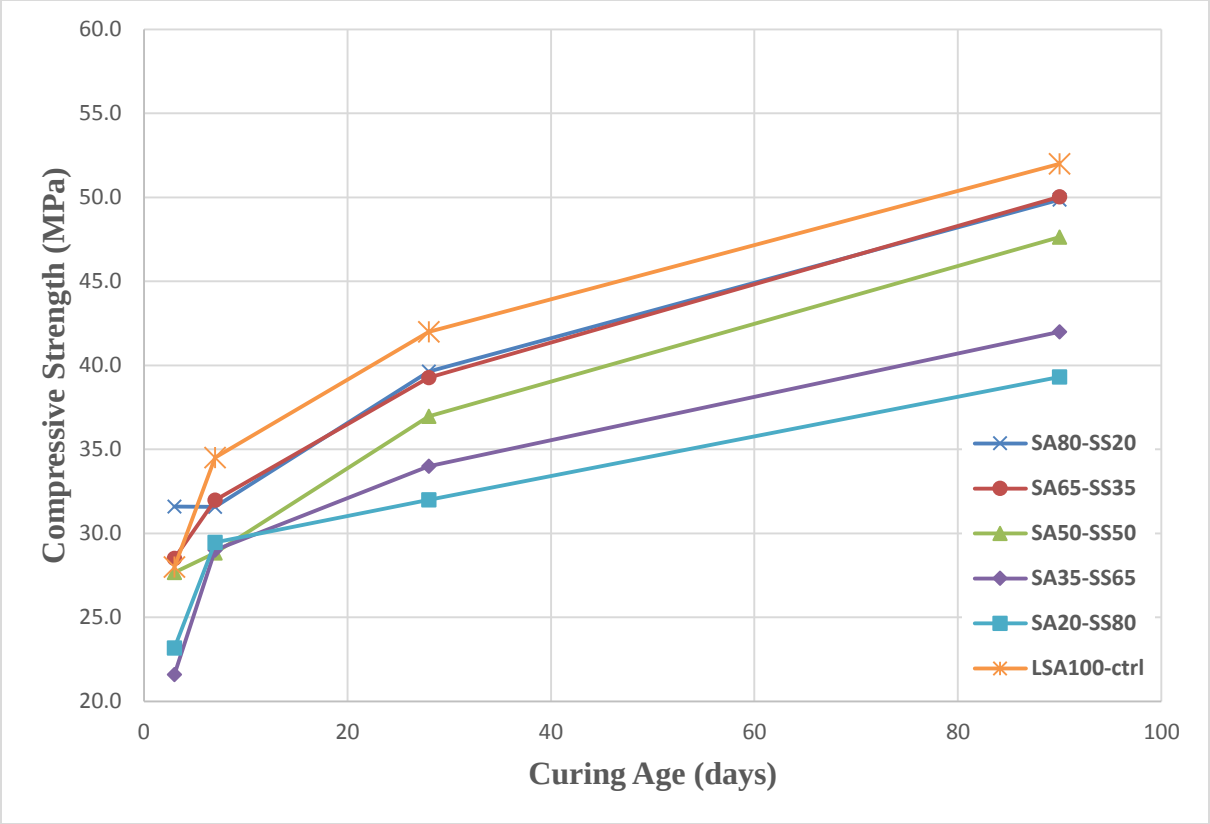

Figure 4.9: Compressive strength of HWC with steel slag and steel shot aggregates.

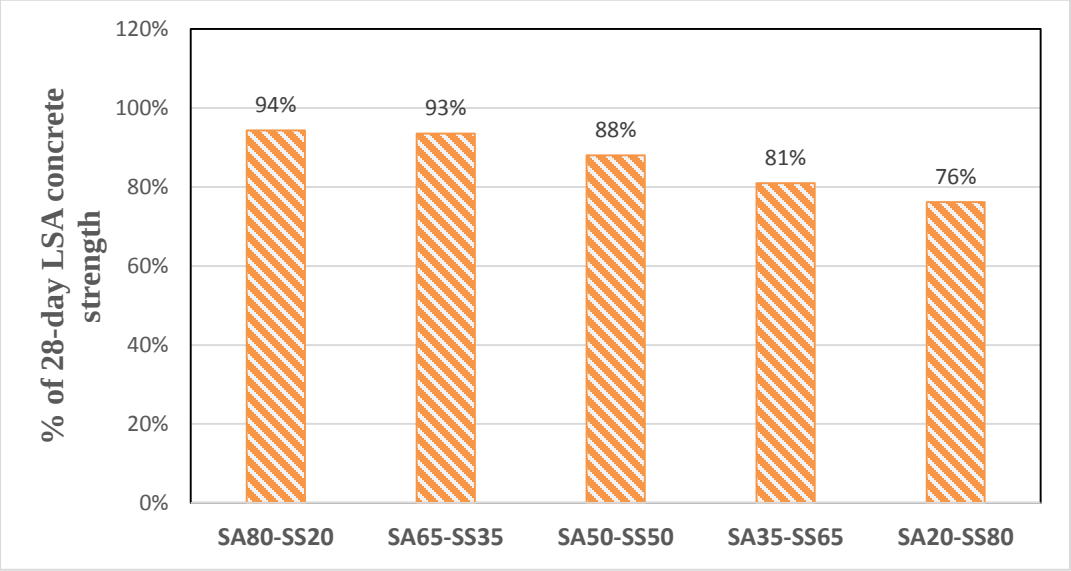

Figure 4.10: HWC with steel slag and steel shot aggregate - 28-day strength as percentage of 28-day LSA concrete strength.

4.2.4 Mixtures with limestone and steel shot as coarse aggregate

Figure 4.11 shows the graph of compressive strength evolution with curing times for mixtures prepared with varying percentages of limestone and steel shot aggregates. The 28-day strength of the mixtures as percentage of 28-day strength of control mix is shown in figure 4.12.

Figure 4.11 shows that all the mixtures in this group have lesser compressive strength than control mix at all ages. It can be seen from figure 4.12 that the 28-day compressive strengths was reducing as the percentage replacement of steel shot aggregates increases. LSA20-SS80 has the lowest compressive strength, which is 62% of LSA100 strength. This behavior is similar to what was observed in the case of steel slag and steel shot aggregates combination, and it is because of the particle shape and roughness of steel shot aggregates.

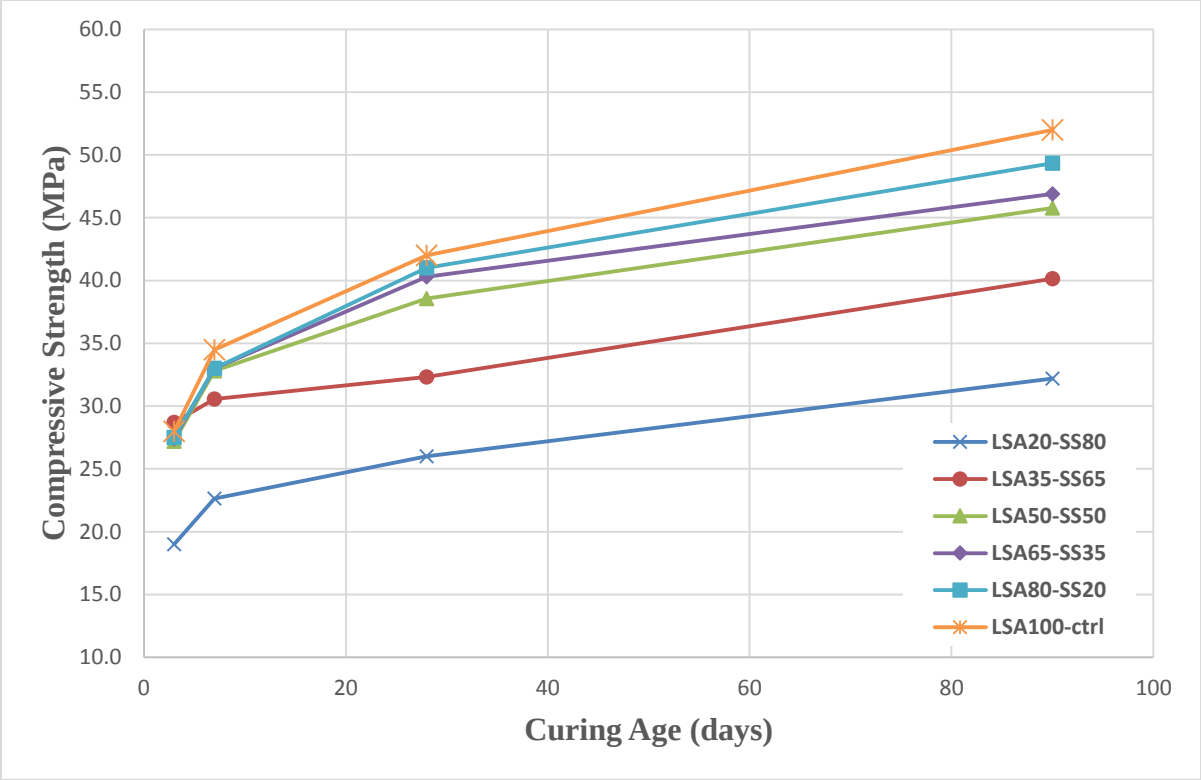

Figure 4.11: Compressive strength of HWC with limestone and steel shot aggregates

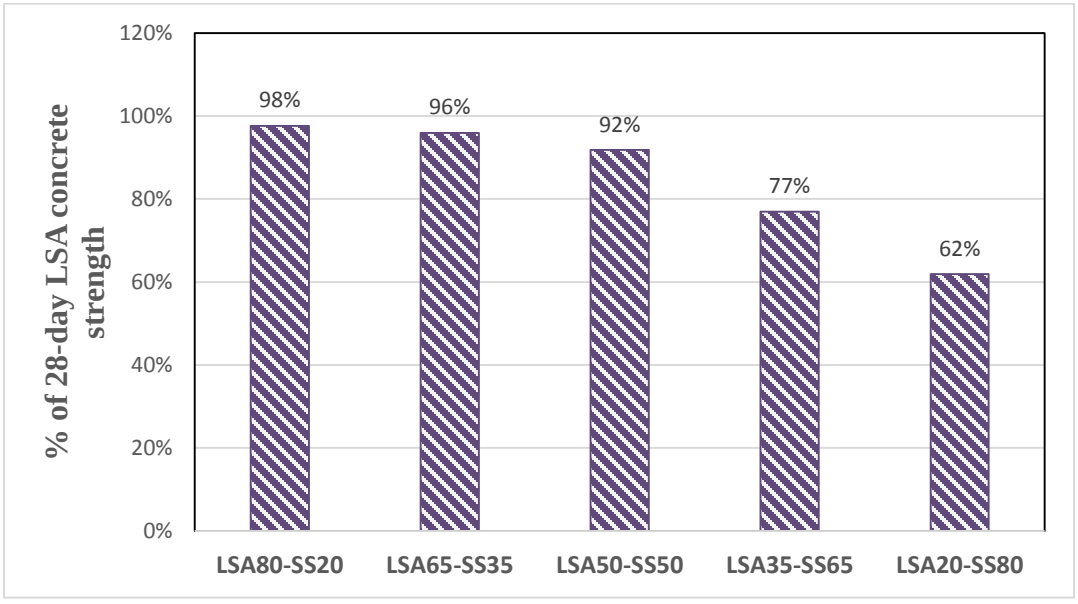

Figure 4.12: HWC with limestone and steel shot aggregate – 28-day strength as percentage of 28-day LSA concrete strength.

4.3 SPLIT TENSILE STRENGTH

Split tensile strength of concrete is one of the mechanical properties of concrete that predicts the tensile behavior of concrete when subjected to tensile stresses. According to ACI code and other codes of practice, this property of concrete can be determined directly from compressive strength value in the absence of experimental results.

The 28-day splitting tensile strengths, f_{ct} of the 19 HWC mixtures are presented in table 4.3. Also shown in the table are the corresponding 28-day compressive strength for the mixtures. The splitting tensile values ranges from 3.0 – 5.5 MPa corresponding to compressive strength of 26.0 – 52.0 MPa. In general, mixtures prepared with steel slag aggregate have the highest splitting tensile strength, followed by those prepared with limestone aggregate, iron ore aggregate and steel shot aggregate, in decreasing order.

Table 4.3: Splitting tensile strength of HWC specimens.

Mix ID	f_{ct}, MPa	f_c', MPa
LSA100	4.7	42.0
SA100	5.5	45.3
SS100	3	29.6
IO100	4	40.3
SA80-IO20	5.1	44.0
SA65-IO35	4.7	39.0
SA50-IO50	4.2	38.4
SA35-IO65	4.6	37.7
SA20-IO80	4.6	39.0
SA80-SS20	4.5	39.6
SA65-SS35	4.1	39.3
SA50-SS50	4.1	37.0
SA35-SS65	3.8	34.0
SA20-SS80	3.6	32.0
LSA80-SS20	4.7	41.0
LSA65-SS35	4.5	40.3
LSA50-SS50	3.9	38.6
LSA35-SS65	3.6	32.3
LSA20-SS80	3.2	26.0

4.3.1 Mixtures with 100% coarse aggregate types

The 28-day average splitting tensile strengths of mixtures prepared with 100% aggregate types are presented in figure 4.13. SA100 possess the highest splitting tensile strength of 5.5 MPa among the four mixtures. This value is 17% higher than that of LSA100, as can be seen in Figure 4.13. Beshr et al. [67] reported a similar result, where steel slag aggregate concrete has the highest split tensile strength among the various aggregate types used in their study. As can be seen in figure 4.13, the splitting tensile strength for IO100 and SS100 was found to be 4 MPa and 3 MPa respectively. These results show that aggregate type and properties influence the splitting tensile strength of concrete, since the quality of paste is the same for all the mixtures. Also, the values show that there is direct relationship between compressive strength and splitting tensile strength, because all the mixtures had the same behavior in terms of compressive strength.

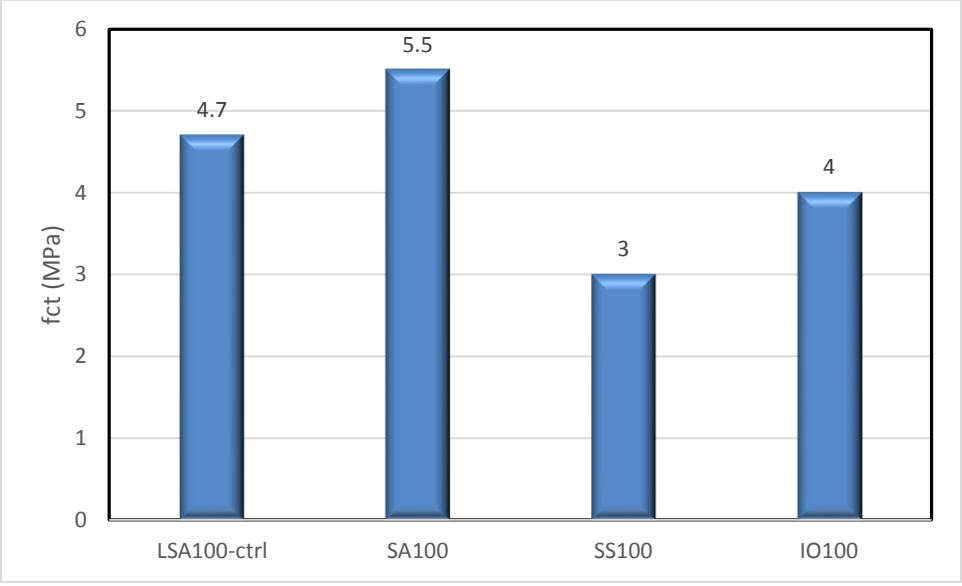

Figure 4.13: 28-day average split tensile strength (f_{ct}) of HWC with 100% coarse aggregate types.

4.3.2 Mixtures with steel slag and iron ore as coarse aggregate

Figure 4.14 shows the average splitting tensile strength of HWC mixtures prepared with combination of steel slag aggregate and iron ore aggregate in varying proportions. The graph shows that increasing the percentages of iron ore aggregate resulted in a decrease the splitting tensile strengths up to 50% iron ore, before equilibrium was attained at 65% and 80% iron ore. This behavior is similar to what was recorded for compressive strength in Section 4.1.2, and it shows that splitting tensile strength is proportional to compressive strengths. Only SA80-IO20 has higher splitting tensile strength than control mix.

Figure 4.14: 28-day average split tensile strength (fct) of HWC with steel slag and iron ore aggregates.

4.3.3 Mixtures with steel slag and steel shot as coarse aggregate

The 28-day average splitting tensile strengths of mixtures prepared with combination of steel slag aggregate and steel shot aggregates in varying proportions are shown in figure 4.15. Increasing the percentage of steel shot aggregate gave rise to a decrease in splitting tensile strength of the mixtures in this group, except for SA50-SS50 that exhibited a shift in the series. In general, there is clear relationship between the splitting tensile strength and compressive strength for this group also.

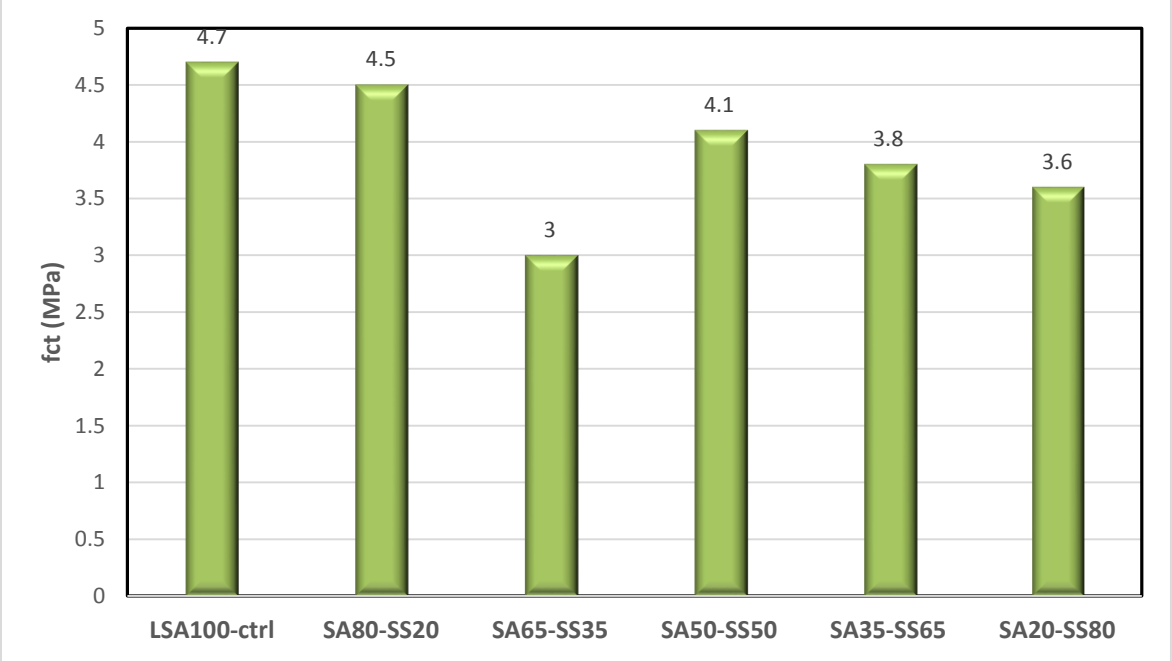

Figure 4.15: 28-day average split tensile strength (fct) of HWC with steel slag and steel shot aggregates.

4.3.4 Mixtures with limestone and steel shot as coarse aggregate

Figure 4.16 shows the average splitting tensile strength of HWC mixtures prepared with combination of limestone aggregate and steel shot aggregate in varying proportions. As expected, the use of steel shot aggregate gave rise to a reduction in splitting tensile strength of LSA100. However, LSA100 and LSA80-SS20 have the same splitting tensile strengths, which shows that using 20% steel shot does not have significant effect on the value of LSA100.

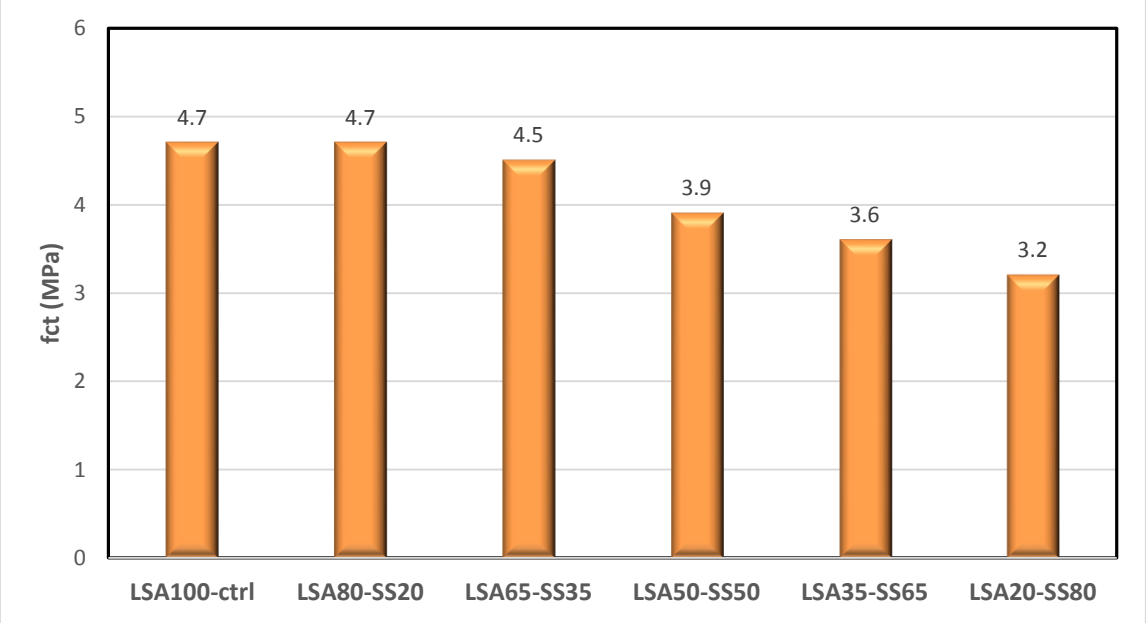

Figure 4.16: 28-day average split tensile strength (fct) of HWC with limestone and steel shot aggregates.

Figure 4.17 shows a plot relating the splitting tensile strength against compressive strength for the HWC mixtures. The figure also shows the upper limit model given by ACI 318-08, which relates splitting tensile strength with compressive strength of normal weight concrete. It can be seen from figure 4.17 that the splitting tensile strengths from

experimental results are higher than the upper limit specified by ACI for normal weight concrete, except for SS100 that falls below the model. This is expected as the ACI model is an upper limit that can be used in the absence of experimental results, on the basis that very low probability of the actual results falling below the model.

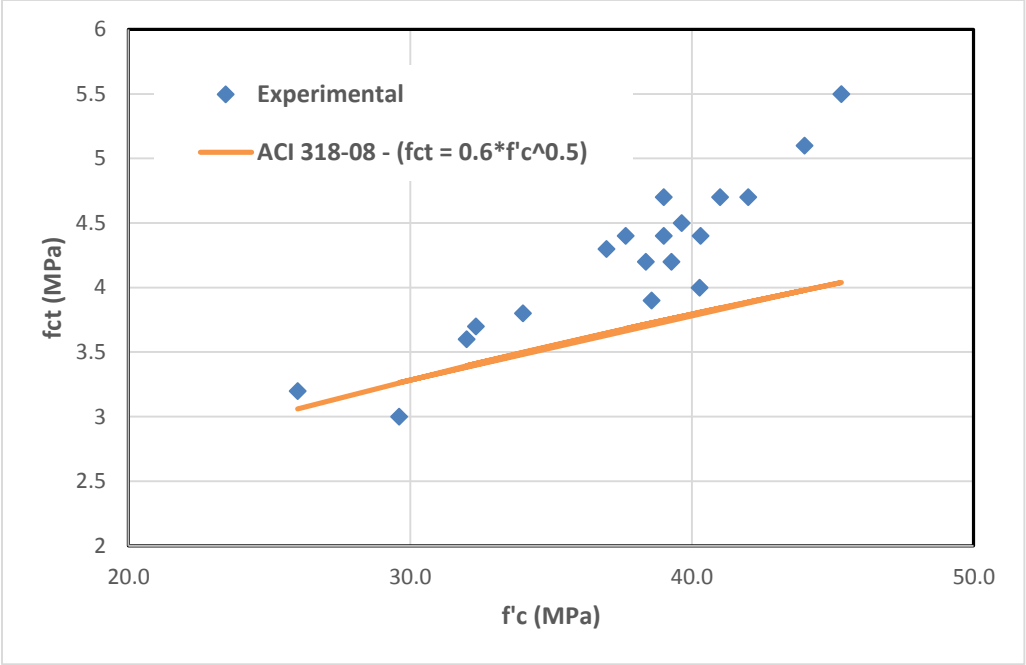

Figure 4.17: Splitting tensile strength against compressive strength of HWC mixtures.

4.4 ELASTIC MODULUS

Elastic modulus test was carried out on the HWC mixtures to determine their stiffness characteristics. The elastic modulus, E_c of the 19 HWC mixtures is presented in table 4.4. Also shown in the table are the corresponding 28-day compressive strengths for the mixtures. The elastic modulus values ranges from 33.0 – 43.9 GPa corresponding to compressive strength of 39.0 – 45.3 MPa.

Table 4.4: Elastic modulus of HWC specimens.

Mix ID	Ec, GPa	f_c', MPa
LSA100	36.7	42.0
SA100	43.9	45.3
SS100	42.2	29.6
IO100	34.0	40.3
SA80-IO20	42.9	44.0
SA65-IO35	36.0	39.0
SA50-IO50	35.2	38.4
SA35-IO65	33.2	37.7
SA20-IO80	33.0	39.0
SA80-SS20	33.6	39.6
SA65-SS35	35.4	39.3
SA50-SS50	38.9	37.0
SA35-SS65	37.6	34.0
SA20-SS80	40.0	32.0
LSA80-SS20	35.0	41.0
LSA65-SS35	36.3	40.3
LSA50-SS50	37.0	38.6
LSA35-SS65	36.1	32.3
LSA20-SS80	37.1	26.0

4.4.1 Mixtures with 100% coarse aggregate types

Figure 4.18 shows the elastic modulus of HWC mixtures prepared with 100% coarse aggregate types. From figure 4.18, it can be seen that SA100 and SS100 have higher elastic modulus than the control mix, LSA100, while IO100 has the lowest value of 34 GPa in this group. SA100, LSA100 and IO100 have elastic modulus in agreement with their compressive strengths while SS100 behaves differently. Even though SS100 has the lowest compressive strength in this group, the elastic modulus result implies that mixture prepared with steel shot aggregates may have higher resistance to deformation. This may be due to the high stiffness of steel shot aggregate as compared to other aggregate types in this group. Although, there is no data to ascertain the stiffness of each aggregate types. Beushausen [35] reported a similar behavior where it was concluded that aggregate with higher strength and stiffness results in high elastic modulus concrete.

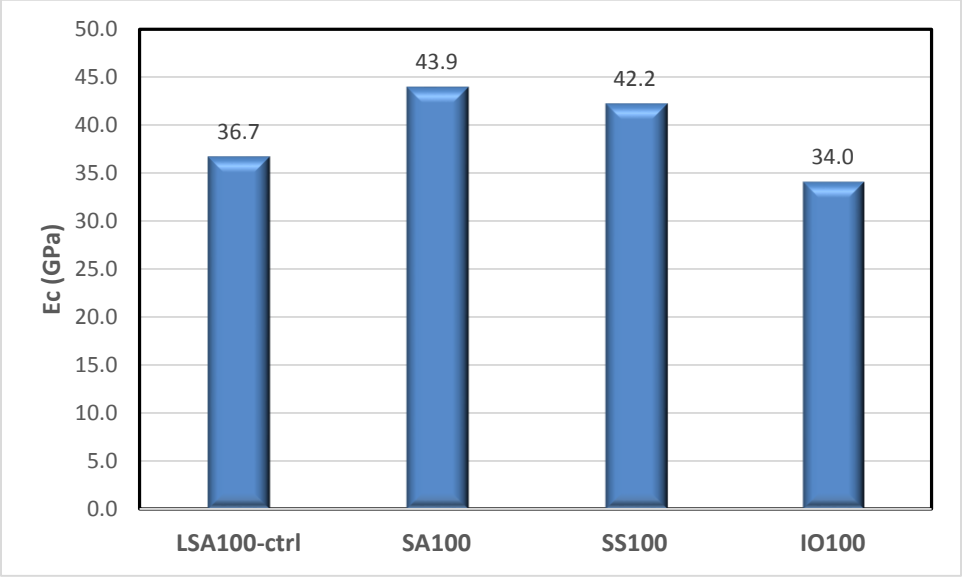

Figure 4.18: Elastic modulus of HWC with 100% coarse aggregate types

4.4.2 Mixtures with steel slag and iron ore as coarse aggregate

Figure 4.19 shows the elastic modulus of HWC mixtures prepared with combination of steel slag and iron ore aggregates. Figure 4.19 shows that only SA80-IO20 is stiffer than the control mix while the elastic modulus of other mixtures reduces as the percentage of iron ore aggregates increases. This observation stills shows that iron ore mixtures has overall lesser elastic modulus than limestone aggregate mixtures as described in previous section.

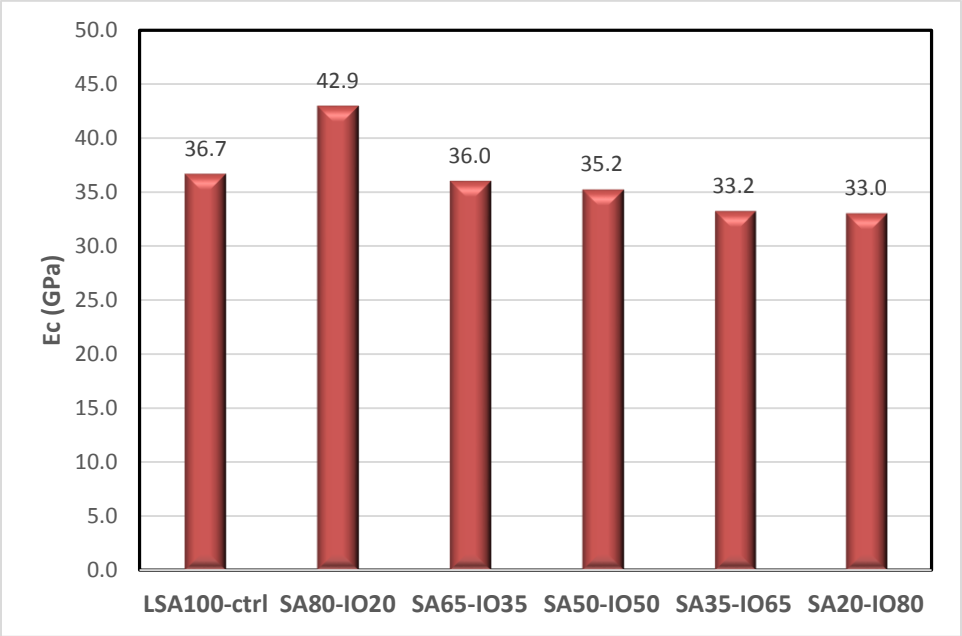

Figure 4.19: Elastic modulus of HWC with steel slag and iron ore aggregates.

4.4.3 Mixtures with steel slag and steel shot as coarse aggregate

Figure 4.20 shows the elastic modulus of HWC mixtures prepared with combination of steel slag and steel shot aggregates. The inclusion of 20% steel shot aggregate in mix

SA80-SS20 gave rise to elastic modulus of 33.6 GPa which is less than 43.9 GPa recorded for SA100 in the previous section. However, increasing the steel shot percentage gave rise to gradual increase in elastic modulus up to 40.0 GPa for SA20-SS80. Mixtures with 50% steel shot and above have higher elastic modulus than the control mix.

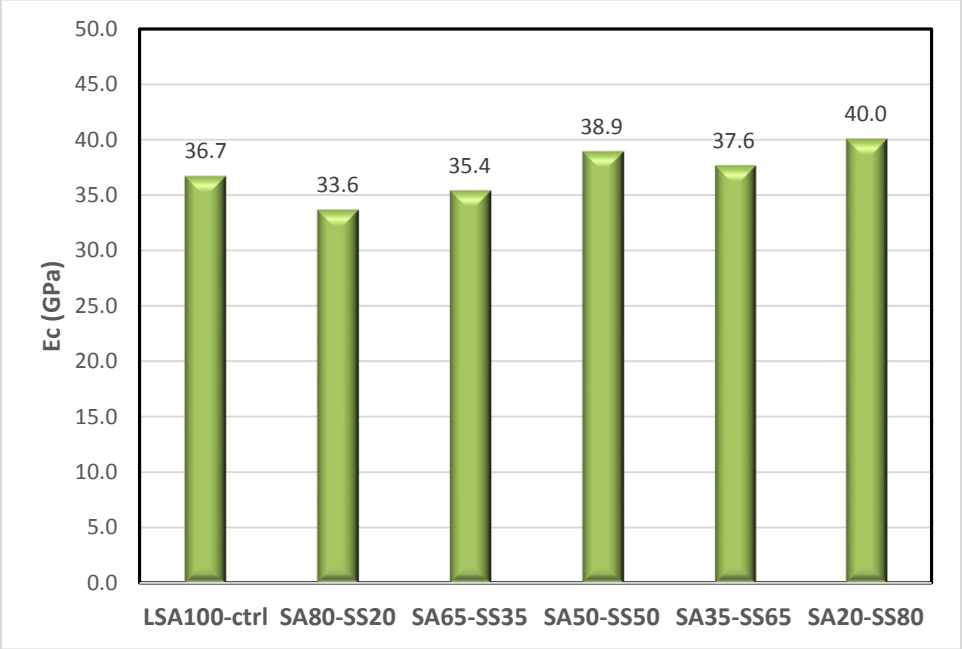

Figure 4.20: Elastic modulus of HWC with steel slag and steel shot aggregates.

4.4.4 Mixtures with limestone and steel shot as coarse aggregate

Figure 4.21 shows the elastic modulus of HWC mixtures prepared with combination of steel slag and steel shot aggregates. Figure 4.21 shows that all the mixtures in this group have elastic modulus values close to the control mix, except LSA20-SS80 with 39 GPa, which is close to 42.2 GPa that was recorded for SS100 in the preceding section.

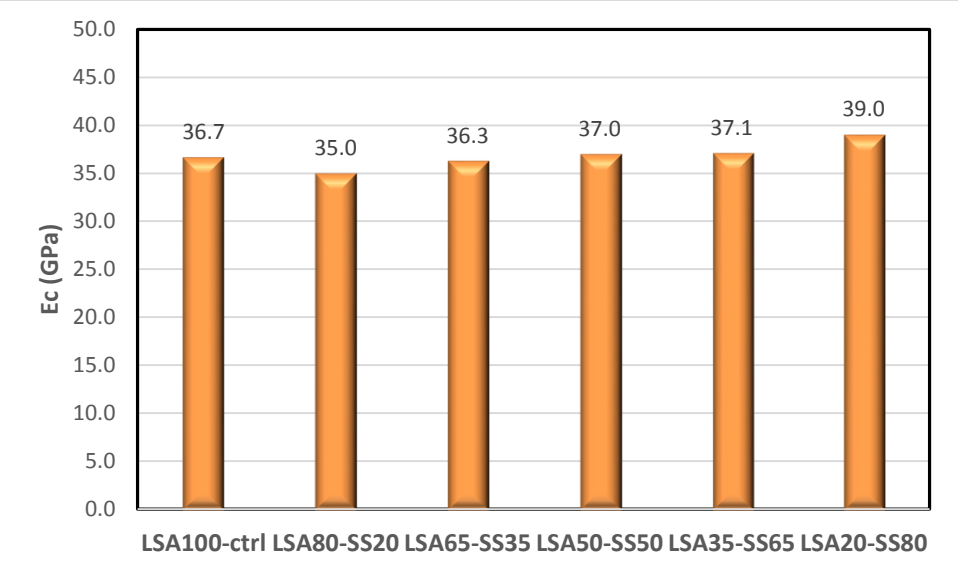

Figure 4.21: Elastic modulus of HWC with limestone and steel shot aggregates.

Figure 4.22 shows a plot relating the elastic modulus against compressive strength for the HWC mixtures. The figure also shows the upper limit model given by ACI 318-08, which relates elastic modulus with compressive strength of normal weight concrete. It can be seen from figure 4.18 that the elastic modulus from experimental results are higher than the upper limit specified by ACI for normal weight concrete. This is expected as the ACI model is an upper limit that can be used in the absence of experimental results.

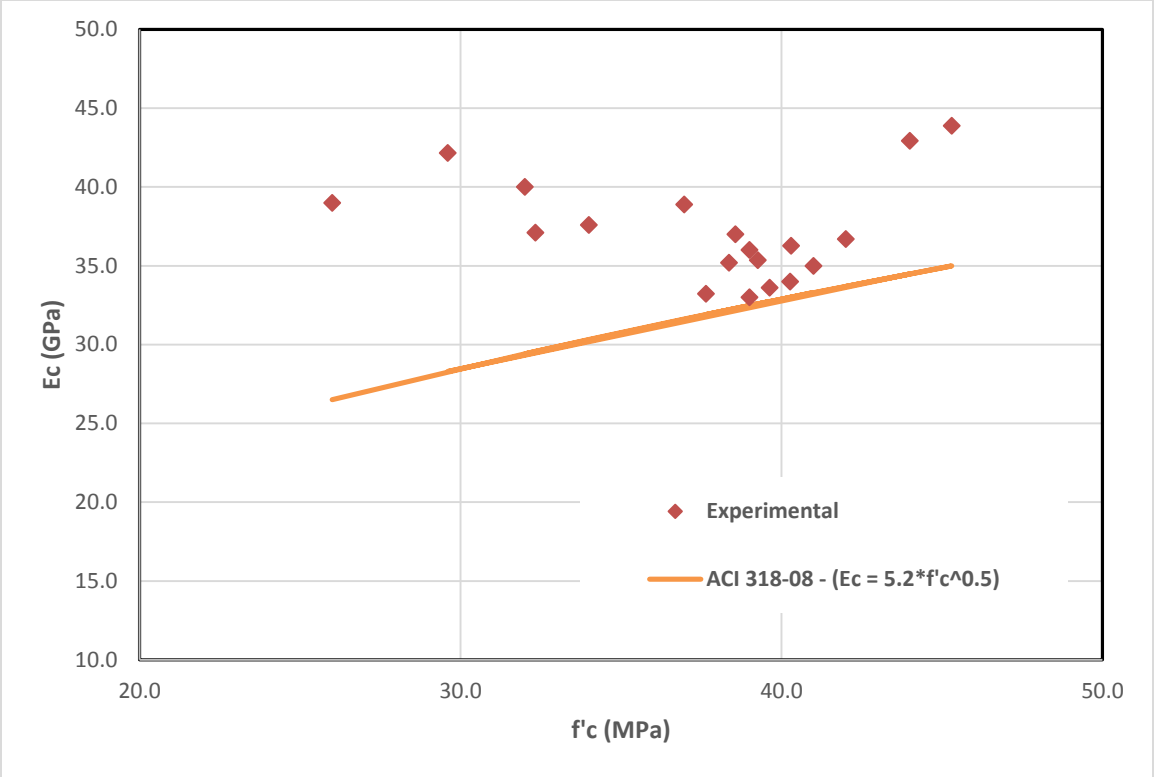

Figure 4.22: Elastic modulus against compressive strength of HWC mixtures

4.5 DRYING SHRINKAGE

Drying shrinkage was measured for HWC prism specimens of 50 x 50 x 250 mm for a period of 180 days. Table 4.5 shows the recorded strain at different periods after 14 days water curing for all the 19 mixtures. The reported values in this table are the averages of three specimens prepared for each mix. The ultimate drying shrinkage values at 180-day ranges from a low of 296 microns for SA35-SS65 to a high of 1000 microns for SA50-IO50.

Table 4.5: Average drying shrinkage strain of HWC mixtures.

	Exposure period, (days) / Shrinkage, microns									
Mix ID	**3**	**7**	**14**	**21**	**28**	**42**	**56**	**90**	**120**	**180**
LSA100	187	307	403	427	488	507	553	654	682	685
SA100	119	203	387	487	627	632	620	597	627	706
SS100	77	340	398	461	482	514	520	528	532	548
IO100	167	253	362	466	665	688	705	708	749	790
SA80-IO20	284	579	582	595	608	656	707	772	837	902
SA65-IO35	271	477	535	587	631	690	776	816	874	930
SA50-IO50	203	439	573	769	756	835	940	971	981	1000
SA35-IO65	188	247	294	406	435	473	503	552	571	577
SA20-IO80	187	491	499	515	517	530	582	619	663	681
SA80-SS20	65	166	244	572	786	834	863	910	940	968
SA65-SS35	49	255	299	319	512	517	527	538	577	642
SA50-SS50	29	73	112	146	342	351	361	372	387	393
SA35-SS65	23	151	200	265	286	287	289	289	291	296
SA20-SS80	96	168	224	323	359	395	402	423	428	434
LSA80-SS20	389	717	837	897	928	961	968	970	977	993
LSA65-SS35	147	315	451	585	604	664	689	732	812	852
LSA50-SS50	114	301	442	518	634	647	655	680	683	700
LSA35-SS65	261	330	414	498	567	609	641	668	700	703
LSA20-SS80	296	445	487	524	536	544	549	553	567	571

4.5.1 Mixtures with 100% coarse aggregate types

Figure 4.23 shows the plot of average drying shrinkage values against exposure period for specimens prepared with 100% coarse aggregate types. The slope of the lines depicted a rapid increase in drying shrinkage during the initial exposure period up till 28 days while maintaining gradual increase beyond this period till 180-day. IO100 exhibited the highest volume decrease while SS100 exhibited the lowest, as depicted by figure 4.23. SA100 and LSA100 however behave in a somewhat similar manner. Since the volume of paste is the same for all the specimens, the perceived difference in behavior can only be attributed to the quantity and characteristics of the aggregates. It has been reported in papers that shrinkage generally reduces with increment in aggregate quantity [68], [69]. With the same quantity, finer aggregate may result in higher shrinkage strains. The behavior of iron ore aggregate specimen is thus expected since it contains smaller diameter particles.

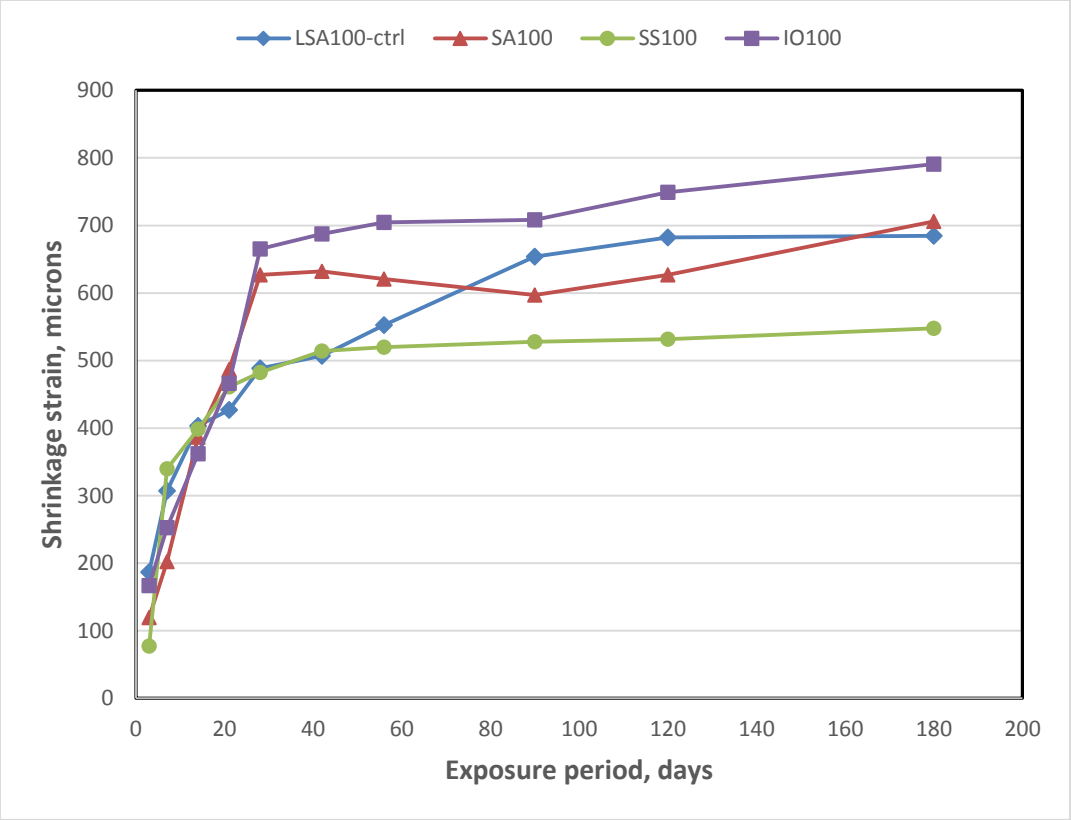

Figure 4.23: Average drying shrinkage of HWC with 100% coarse aggregate types.

4.5.2 Mixtures with steel slag and iron ore as coarse aggregate

The average drying shrinkage plot for specimens prepared with combination of steel slag and iron ore aggregates is shown in figure 4.24. The figure shows that SA20-IO80 exhibited the highest volume decrease (highest shrinkage strains) while SA80-IO20 exhibited the lowest volume decrease. There is rapid increase in drying shrinkage strain in the first 28 days of exposure.

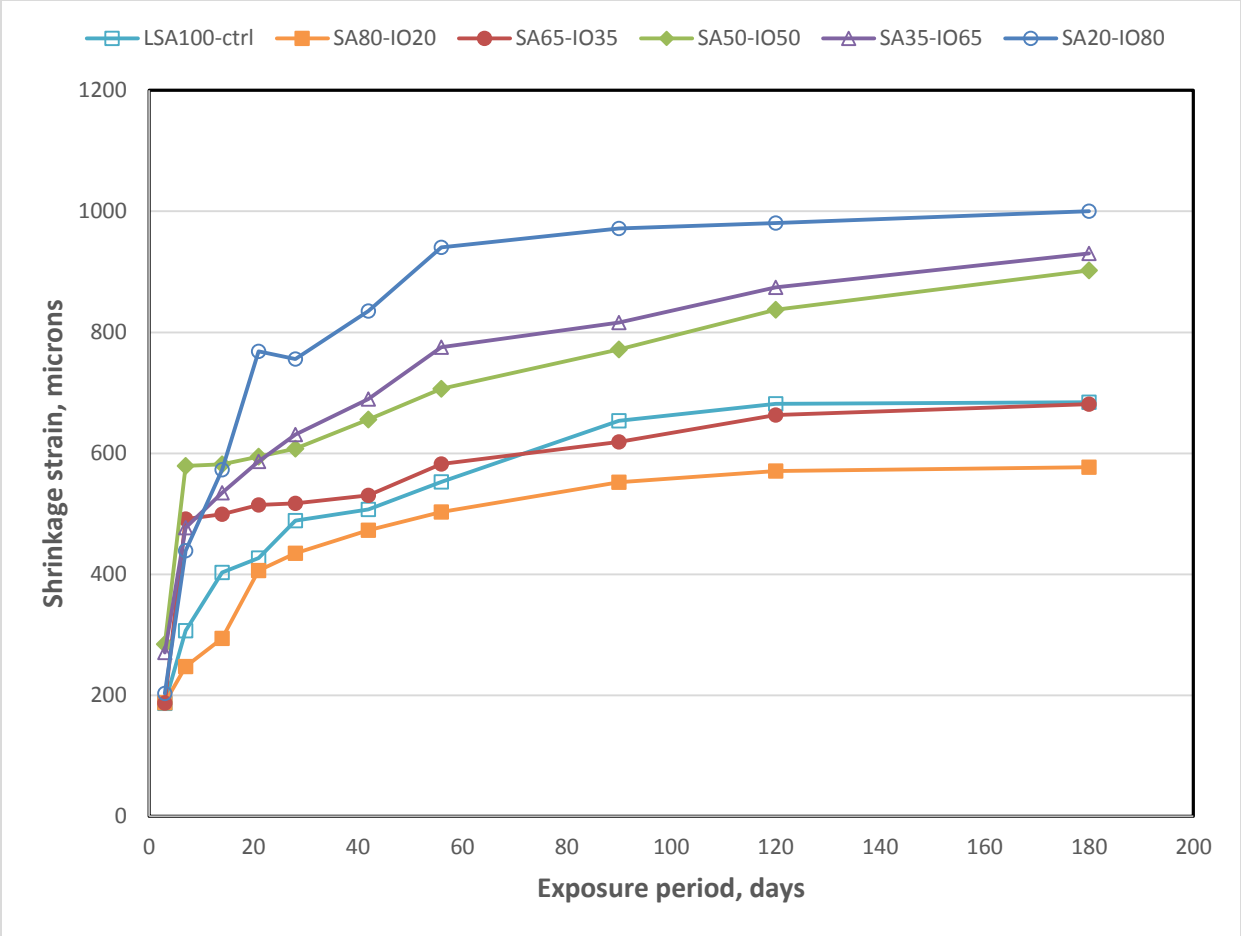

Figure 4.24: Average drying shrinkage of HWC with steel slag and iron ore aggregates.

4.5.3 Mixtures with steel slag and steel shot as coarse aggregate

Figure 4.25 shows the average drying shrinkage plot for specimens prepared with combination of steel slag and steel shot aggregates. SA80-SS20 has the highest shrinkage strain throughout the exposure period while SA20-SS80 has the lowest. It can also be observed from the slope of the graph that most of the specimens reached about 90% of their 180-day shrinkage strain at 42-day.

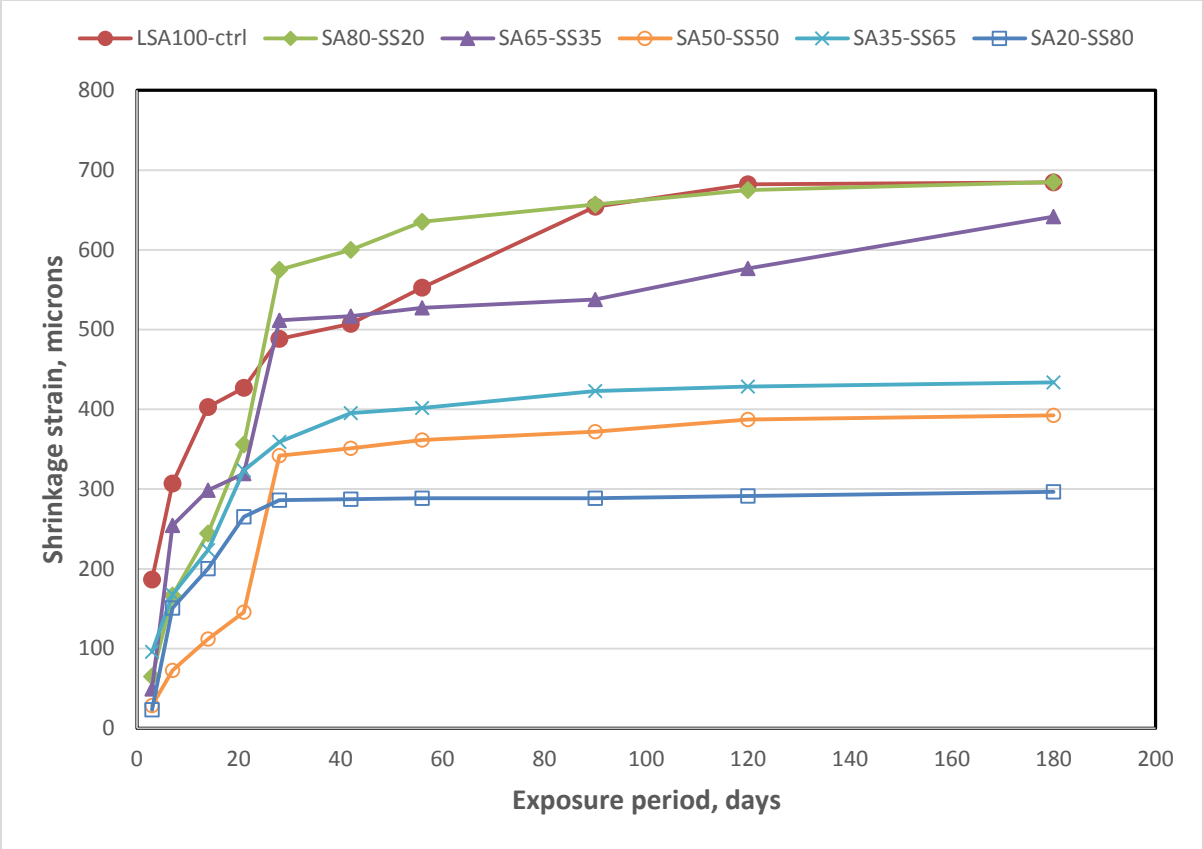

Figure 4.25: Average drying shrinkage of HWC with steel slag and steel shot aggregates.

4.5.4 Mixtures with limestone and steel shot as coarse aggregate

The average drying shrinkage plot for specimens prepared with combination of limestone and steel shot aggregates is shown in figure 4.26. The figure depicts a rapid initial increase in shrinkage strain during the first 28 days. As expected, specimens with 50% steel shot and above have lower shrinkage strains than specimens with higher limestone percentage. LSA80-SS20 has the highest shrinkage strain while LSA20-SS80 has the lowest.

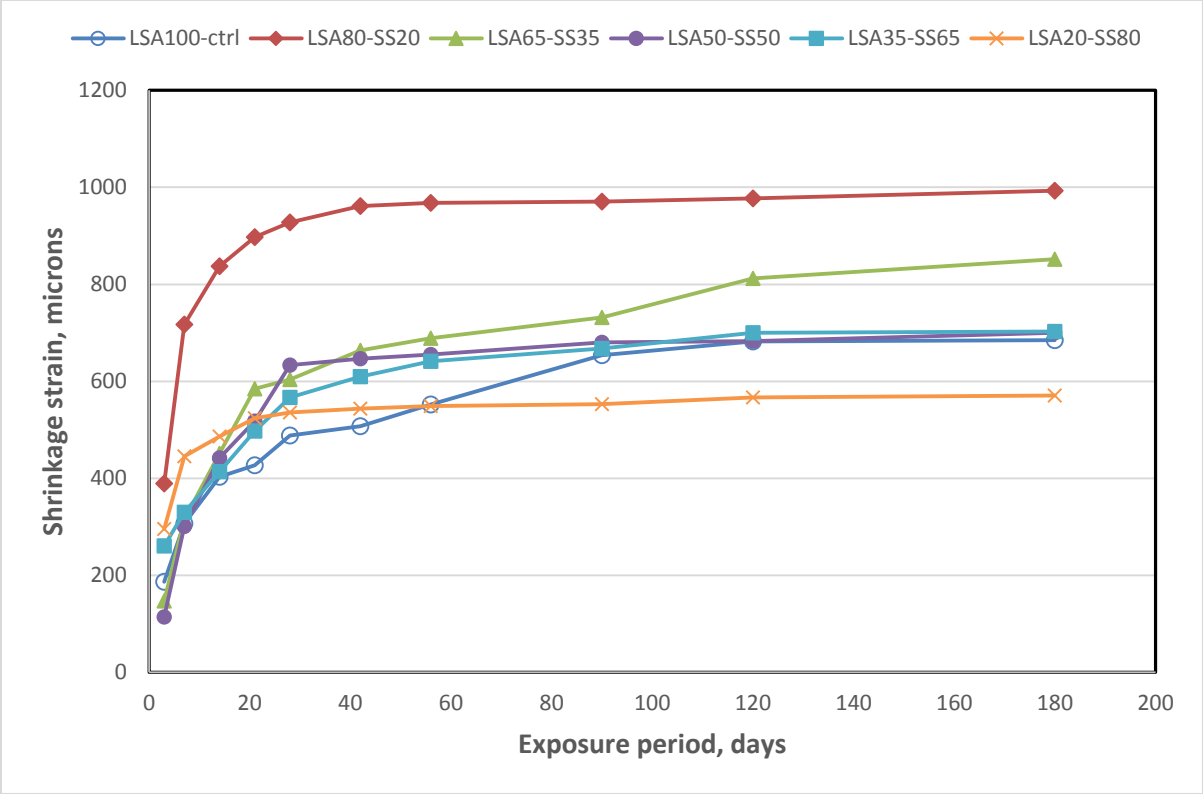

Figure 4.26: Average drying shrinkage of HWC with limestone and steel shot aggregates.

4.6 ELECTRICAL RESISTIVITY

The rate at which corrosion can occur in a rebar embedded inside concrete can be assessed by measurement of the flow rate of ions through concrete between the anodic and cathodic region of the rebar. The electrical resistivity of concrete has a significant effect on this flow rate [46] and measuring it can be used to depict the possibility of occurrence of corrosion [47]. An empirical indication of possibility of corrosion of a de-passivated rebar for various resistivity ranges is shown in table 4.6. The resistivity values in this table were taken at 3% moisture content.

Table 4.6: Empirical resistivity thresholds for de-passivated steel [46], [70]

Resistivity range	Likelihood of corrosion
$\rho < 5.0\ k\Omega.cm$	Very high
$\rho = 5.0 - 10.0\ k\Omega.cm$	High
$\rho = 10.0 - 20.0\ k\Omega.cm$	Low to moderate
$\rho > 20.0\ k\Omega.cm$	Low to negligible

In order to obtain the resistivity at 3%, measurements were taken at 7 different moisture contents for all the 19 HWC mixtures and a plot of electrical resistivity against moisture content was developed. The measured values were then correlated to obtain an exponential relationship of the form: $\rho = Be^{kx}$, which was found to give the best correlation. B and k are constant for each mixture and x is the moisture content. This correlation was used to obtain the electrical resistivity at 3% moisture content. The summary of the correlation parameters and corresponding electrical resistivity in kΩ.cm at 3% moisture content is presented in table 4.7.

The lowest resistivity, as shown in the table, is 21 kΩ.cm for SS100 while the highest is 46 kΩ.cm for SA100. Going by the criteria given in table 4.6, it can be seen that the chance of corrosion occurring in the rebar embedded in all the HWC concrete specimens is very low. However, mixtures with high percentage of steel shot aggregates have resistivity values close to 20 kΩ.cm, as against other specimens that have resistivity values above this threshold.

Table 4.7: Correlation parameters and electrical resistivity of HWC specimens

Mix ID	B	k	R^2	$\rho = Be^{kx}$, kΩ.cm
LSA100	290.5	-0.73	0.9359	36
SA100	780.1	-0.942	0.9087	46
SS100	521.5	-1.066	0.9545	21
IO100	743	-1.006	0.9836	36
SA80-IO20	685	-0.931	0.9376	42
SA65-IO35	396	-0.82	0.9189	34
SA50-IO50	753.4	-0.975	0.9463	40
SA35-IO65	633.5	-0.937	0.9842	38
SA20-IO80	1325	-1.192	0.954	37
SA80-SS20	960.8	-1.053	0.9543	41
SA65-SS35	977.4	-1.094	0.9598	37
SA50-SS50	893.2	-1.12	0.9659	31
SA35-SS65	625.5	-1.07	0.9357	25
SA20-SS80	836.3	-1.208	0.9591	22
LSA80-SS20	2008	-1.217	0.9497	36
LSA65-SS35	2267	-1.33	0.943	35
LSA50-SS50	1528	-1.282	0.9345	33
LSA35-SS65	1038.5	-1.178	0.9352	30
LSA20-SS80	894.6	-1.196	0.919	25

4.6.1 Mixtures with 100% coarse aggregate types

The electrical resistivity at 3% moisture content for specimens prepared with 100% coarse aggregate types is shown in figure 4.27. Figures 4.28-4.31 show the electrical resistivity plot against moisture content for the mixtures, from where the values in Figure 4.27 were determined. All the specimens in this group have resistivity above the limit for 'low to negligible' probability of corrosion initiation, according to the criteria in Table 4.6. SA100 has the highest resistivity of 46 kΩ.cm, which indicate that it is the most resistant to corrosion initiation in this group, while SS100 has the lowest value of 21 kΩ.cm making it the least resistant. This result is not surprising since steel shot is purely iron balls, making it more conductive and hence lower resistivity value.

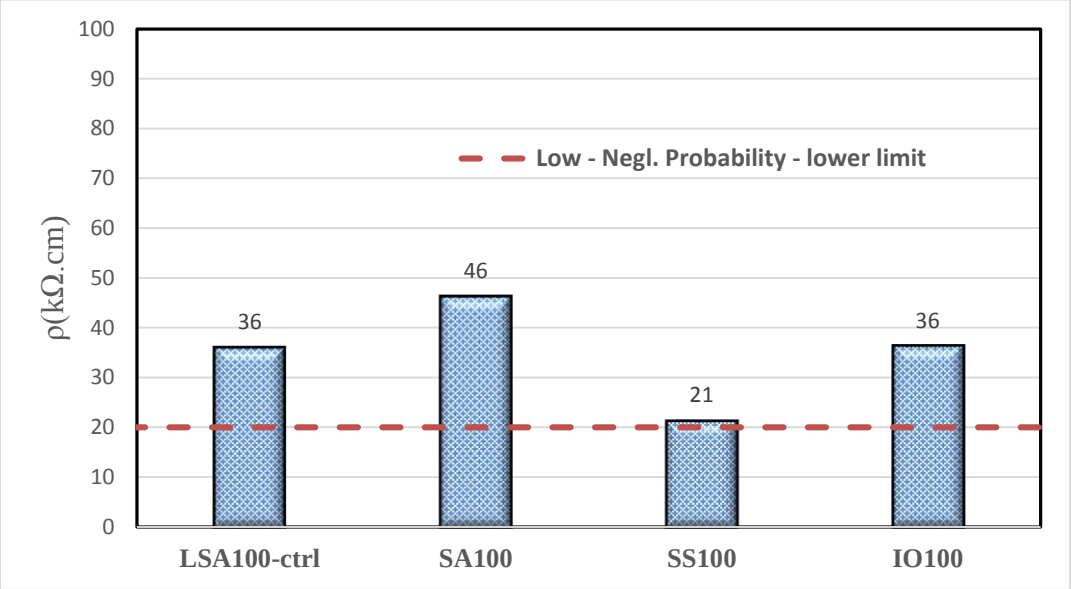

Figure 4.27: Electrical resistivity of HWC with 100% coarse aggregate types.

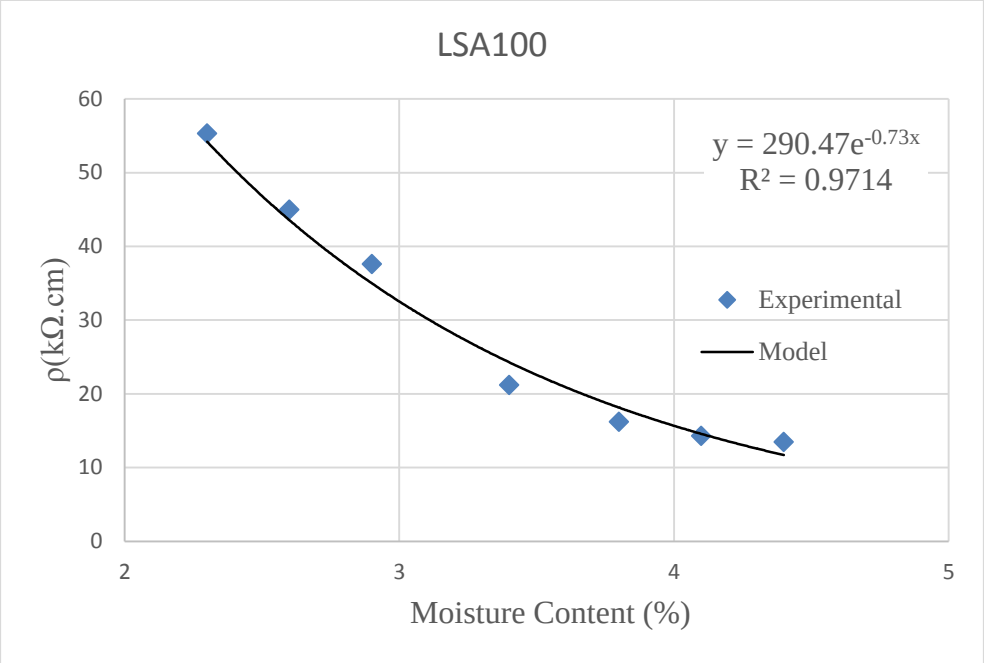

Figure 4.28: Electrical resistivity vs moisture content for LSA100.

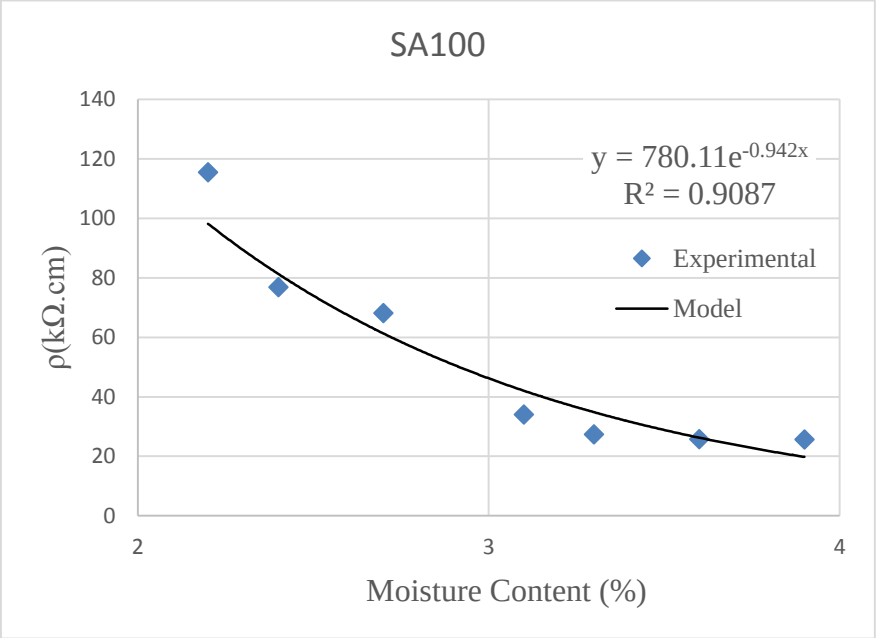

Figure 4.29: Electrical resistivity vs moisture content for SA100.

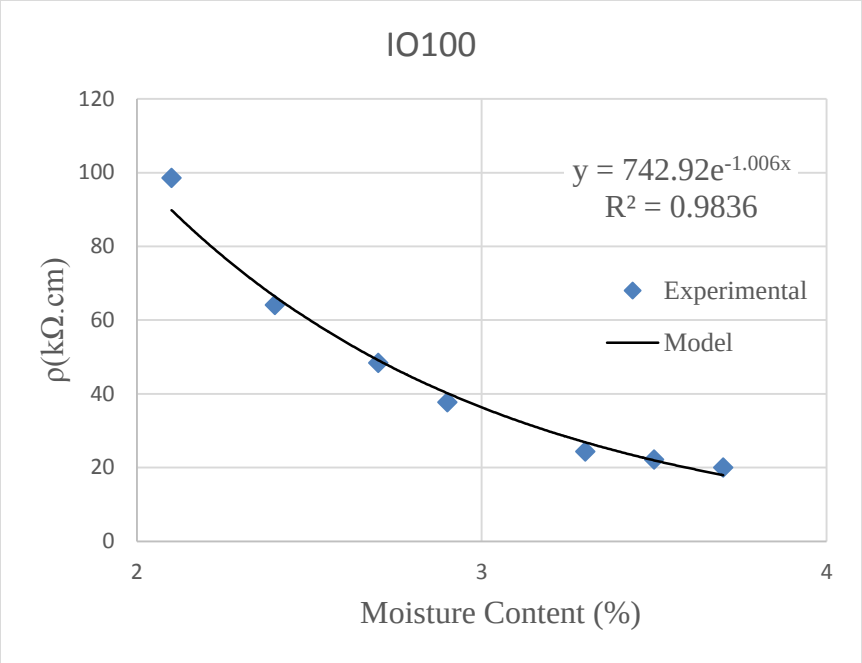

Figure 4.30: Electrical resistivity vs moisture content for IO100.

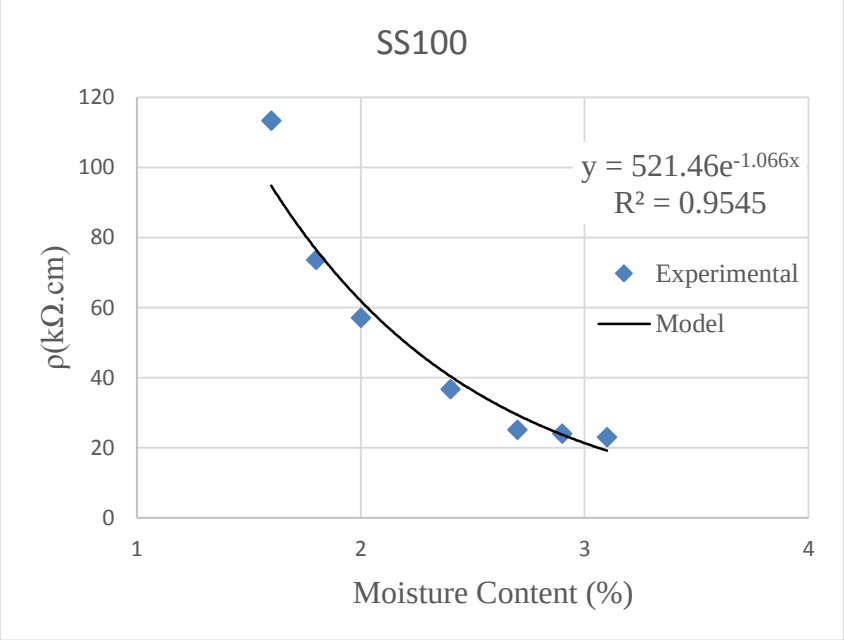

Figure 4.31: Electrical resistivity vs moisture content for SS100.

4.6.2 Mixtures with steel slag and iron ore as coarse aggregate

Figure 4.32 shows the electrical resistivity at 3% moisture content for specimens prepared with combination of steel slag and iron ore aggregates. Figures 4.33-4.37 show the electrical resistivity plot against moisture content for the mixtures. From Figure 4.36, it can be seen that all the specimens have resistivity values above the 'low to negligible' probability limit of corrosion initiation. Even though all the specimens have almost equal resistivity values, a distinction can still be observed, such that SA80-IO20 has the highest with SA65-IO35 being the lowest. However, no significant explanation can be made from the graph since there is no observable trend in the group.

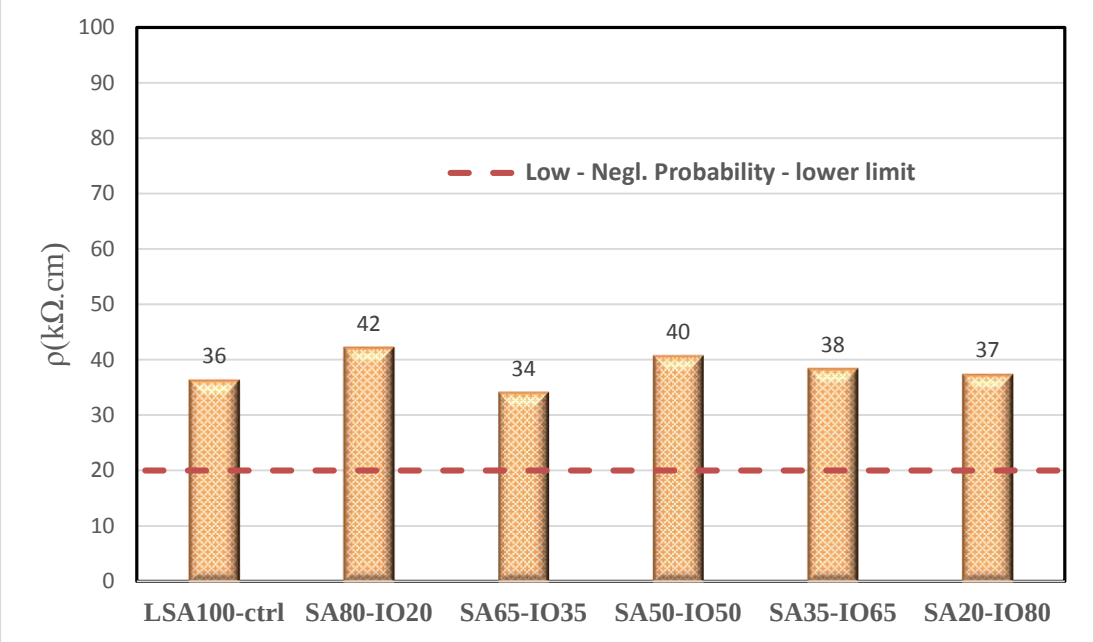

Figure 4.32: Electrical resistivity of HWC with steel slag and iron ore aggregates.

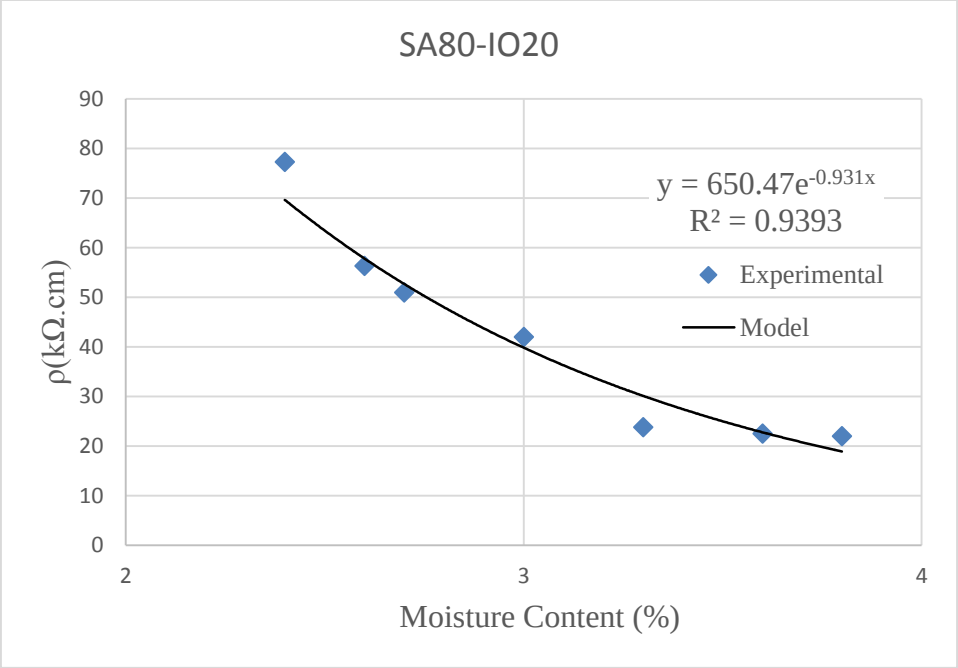

Figure 4.33: Electrical resistivity vs moisture content for SA80-IO20.

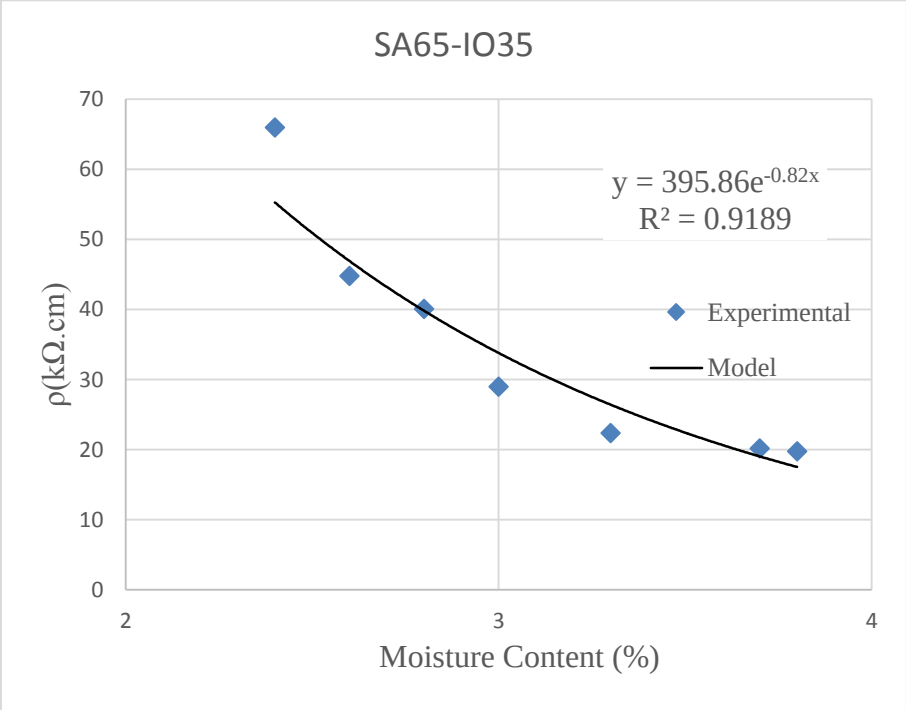

Figure 4.34: Electrical resistivity vs moisture content for SA65-IO35.

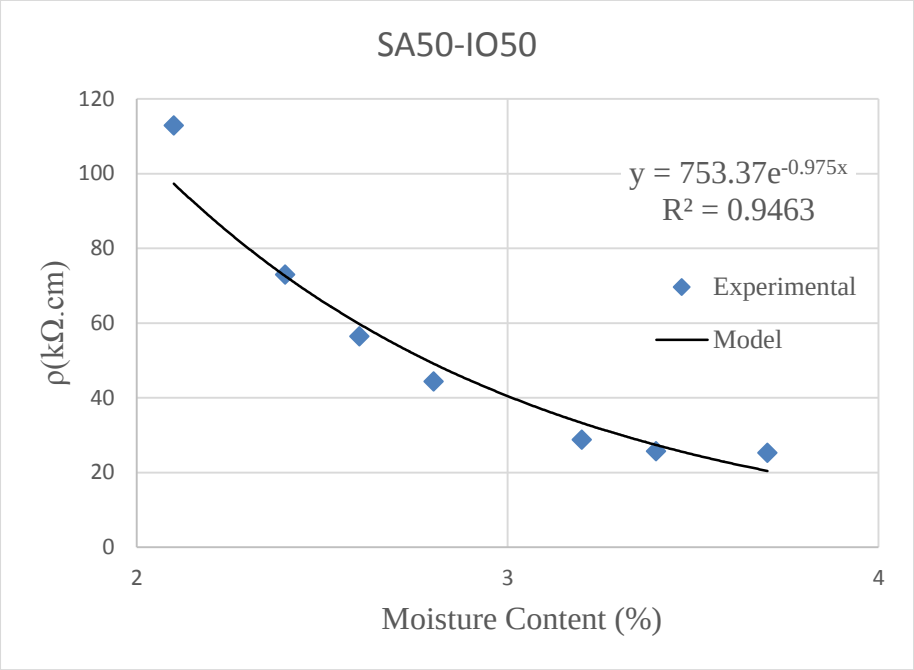

Figure 4.35: Electrical resistivity vs moisture content for SA50-IO50.

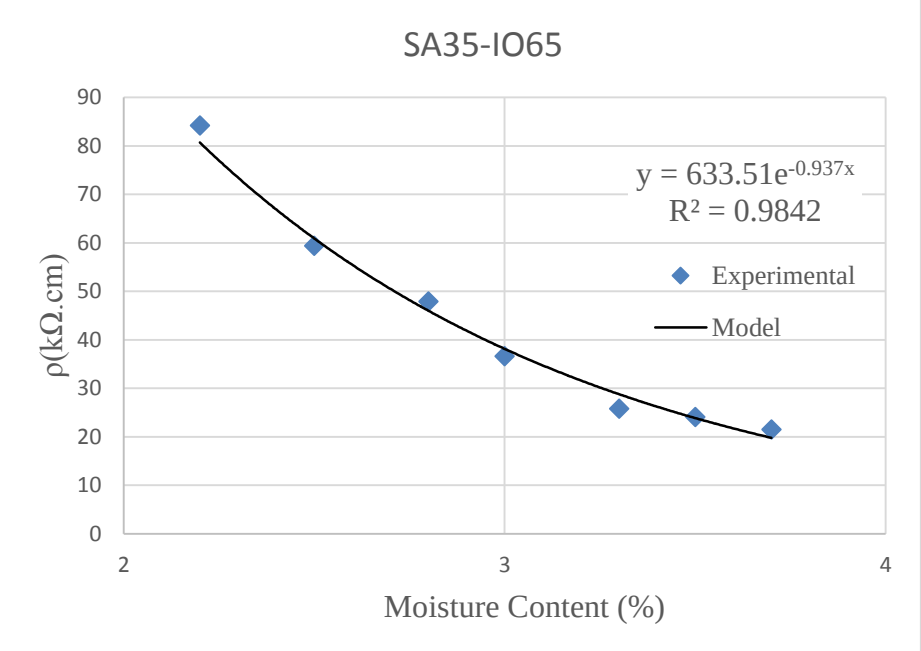

Figure 4.36: Electrical resistivity vs moisture content for SA35-IO65.

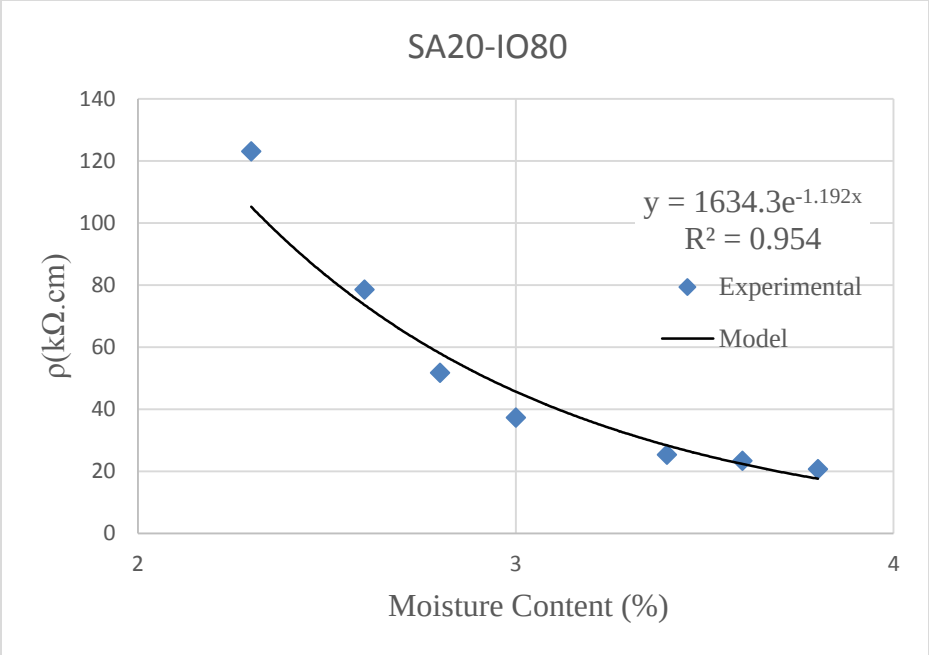

Figure 4.37: Electrical resistivity vs moisture content for SA20-IO80.

4.6.3 Mixtures with steel slag and steel shot as coarse aggregate

Figure 4.38 shows the electrical resistivity at 3% moisture content for specimens prepared with combination of steel slag and steel shot aggregates. Figures 4.39-4.43 show the electrical resistivity plot against moisture content for the mixtures. All the specimens in this group have resistivity values above the 'low to negligible' probability limit of corrosion initiation. SA80-SS20 has the highest electrical resistivity while SA20-SS80 has the least resistivity of 22 kΩ.cm.

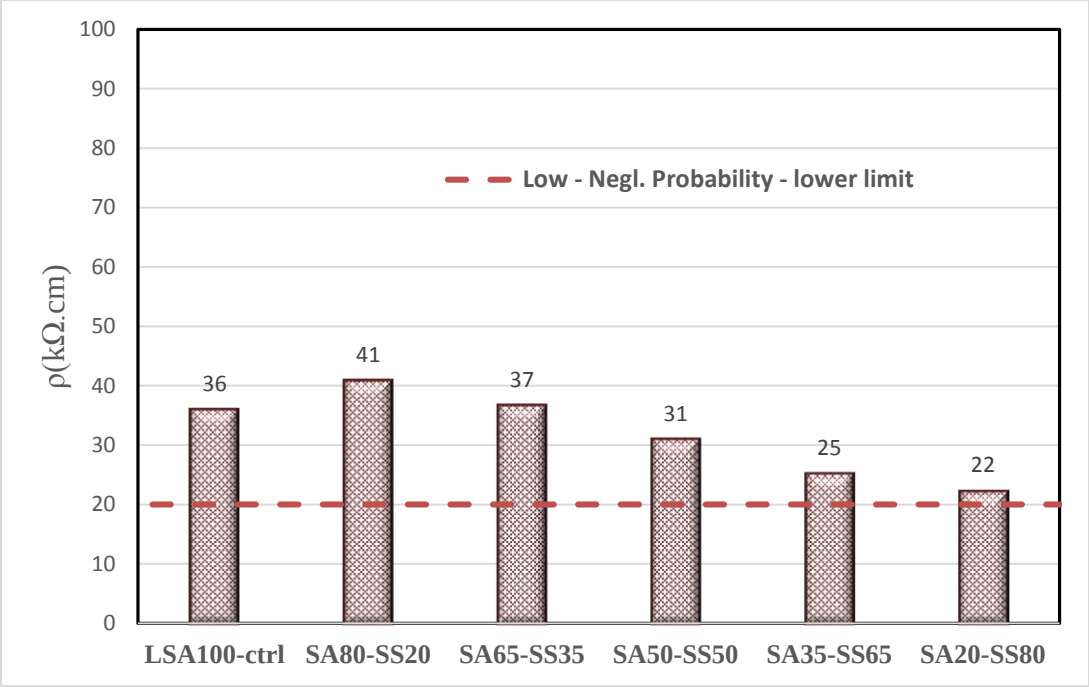

Figure 4.38: Electrical resistivity of HWC with steel slag and steel shot aggregates.

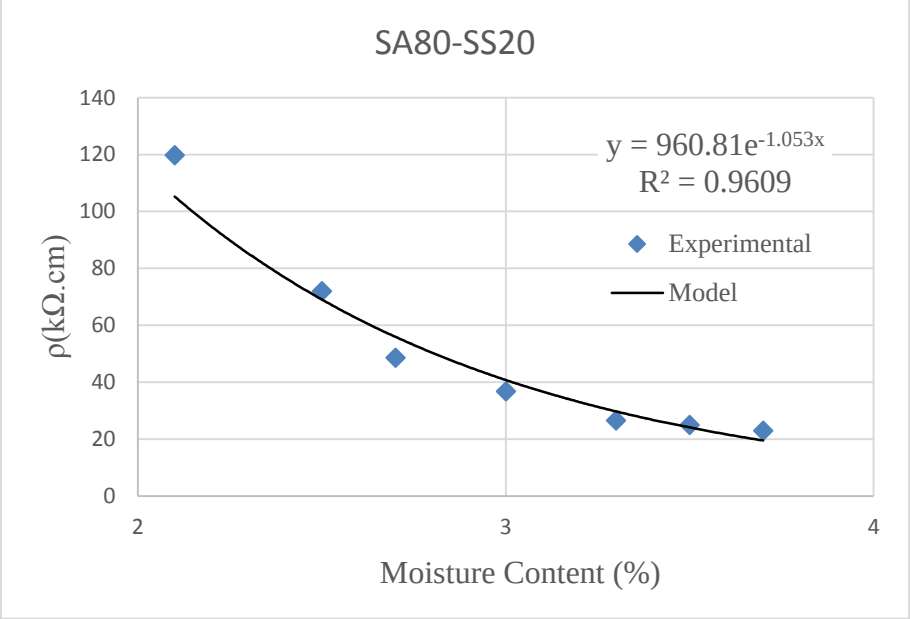

Figure 4.39: Electrical resistivity vs moisture content for SA80-SS20.

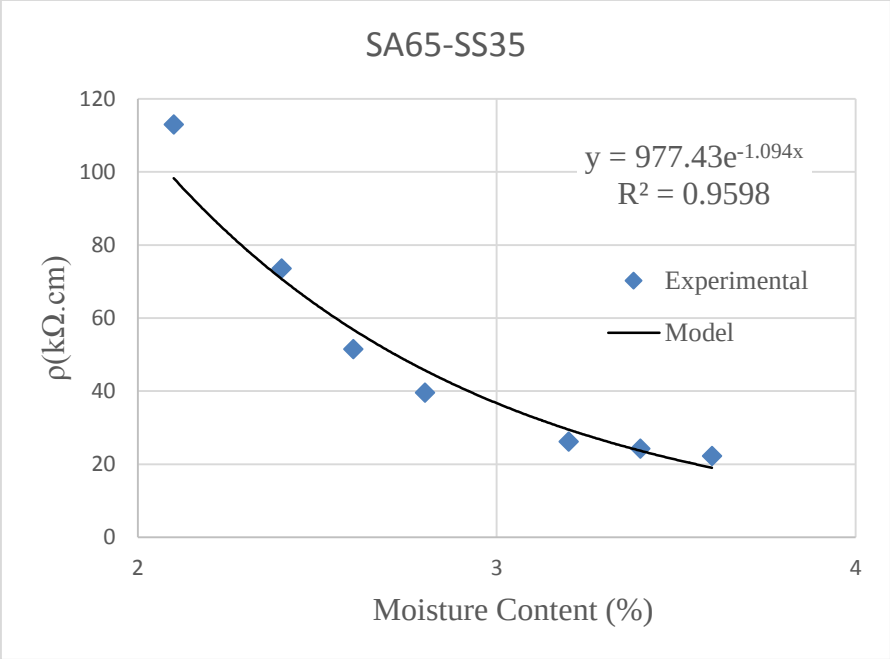

Figure 4.40: Electrical resistivity vs moisture content for SA65-SS35.

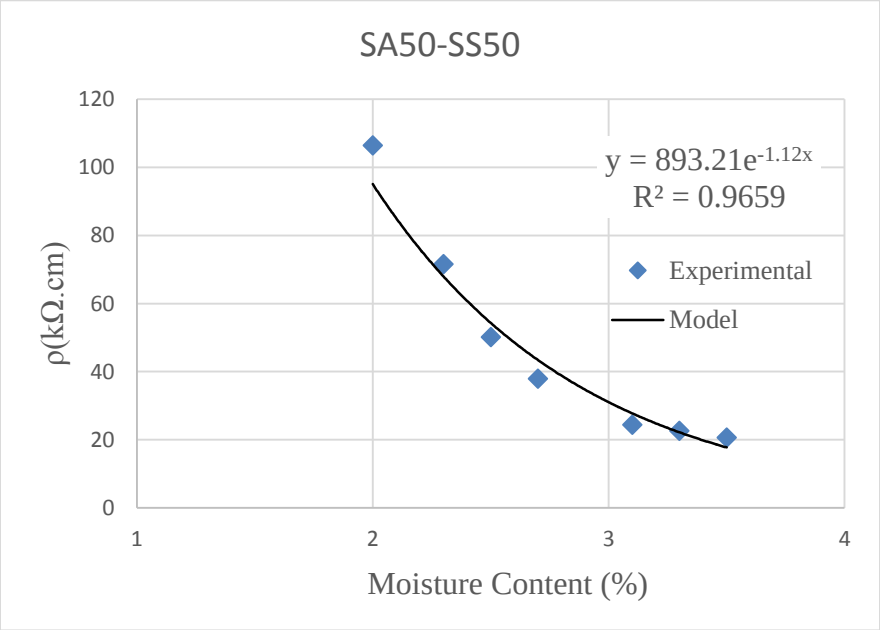

Figure 4.41: Electrical resistivity vs moisture content for SA50-SS50.

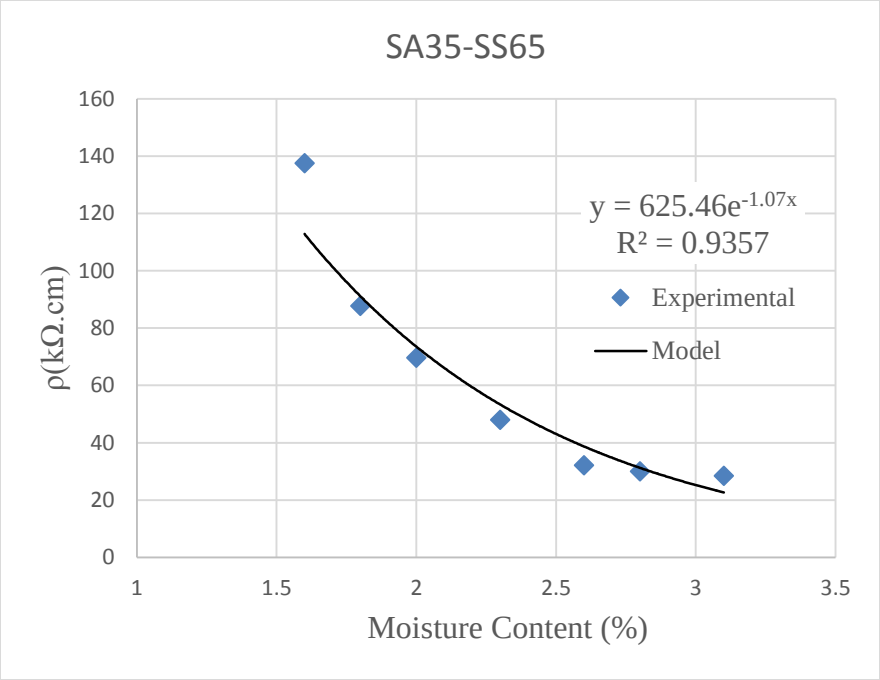

Figure 4.42: Electrical resistivity vs moisture content for SA35-SS65.

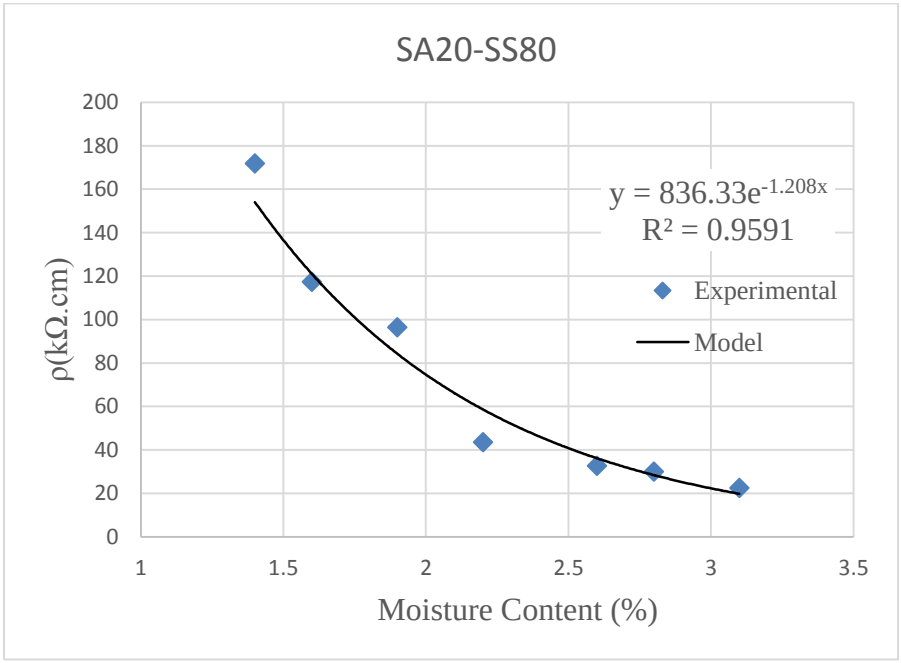

Figure 4.43: Electrical resistivity vs moisture content for SA20-SS80.

4.6.4 Mixtures with limestone and steel shot as coarse aggregate

The electrical resistivity at 3% moisture content for specimens prepared with combination of limestone and steel shot aggregates is shown in figure 4.44. Figures 4.45-4.49 show the electrical resistivity plot against moisture content for the mixtures. From figure 4.44, there is a clear trend in the electrical resistivity performance of the specimens in this group. Increasing the quantity of steel shot aggregate decreases the resistance to corrosion initiation of the specimens. However, all the specimens have electrical resistivity values above the threshold for 'low to negligible' probability of corrosion initiation. LSA20-SS80 has the lowest resistivity value of 25 kΩ.cm in this group.

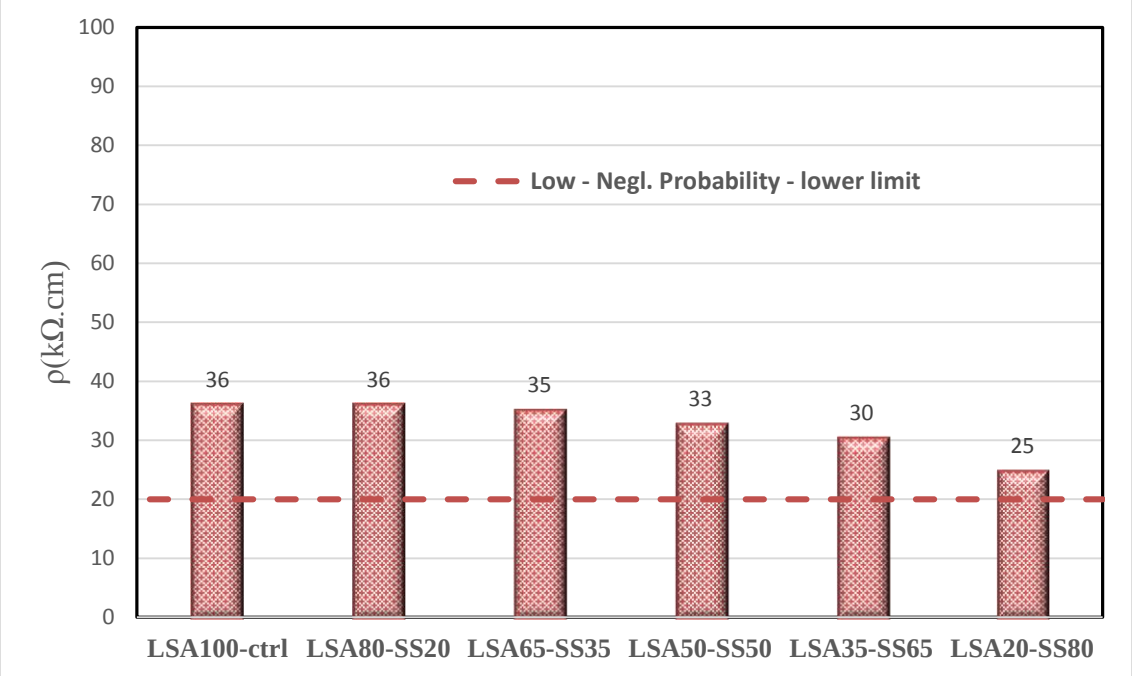

Figure 4.44: Electrical resistivity of HWC with limestone and steel shot aggregates.

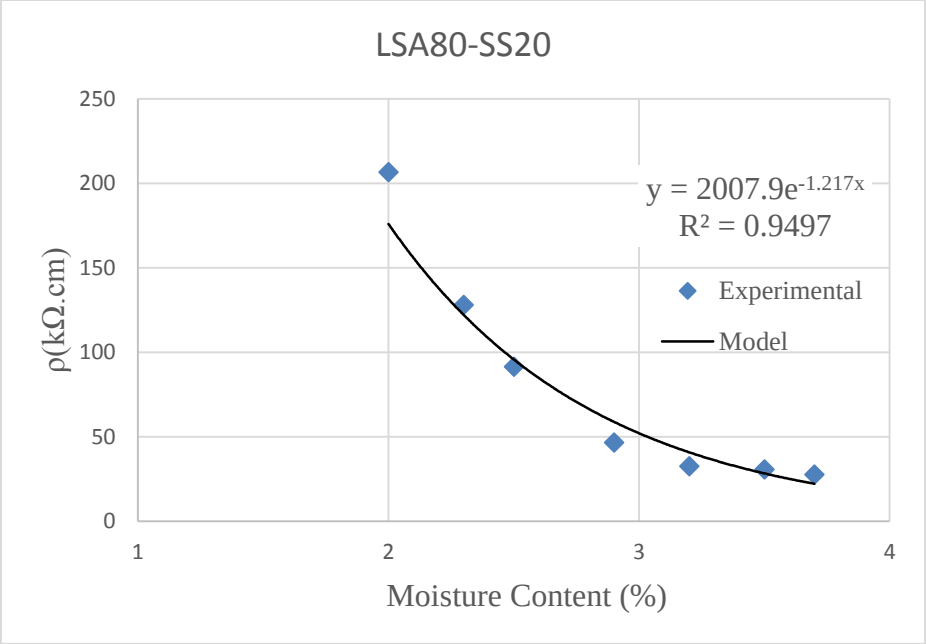

Figure 4.45: Electrical resistivity vs moisture content for LSA80-SS20.

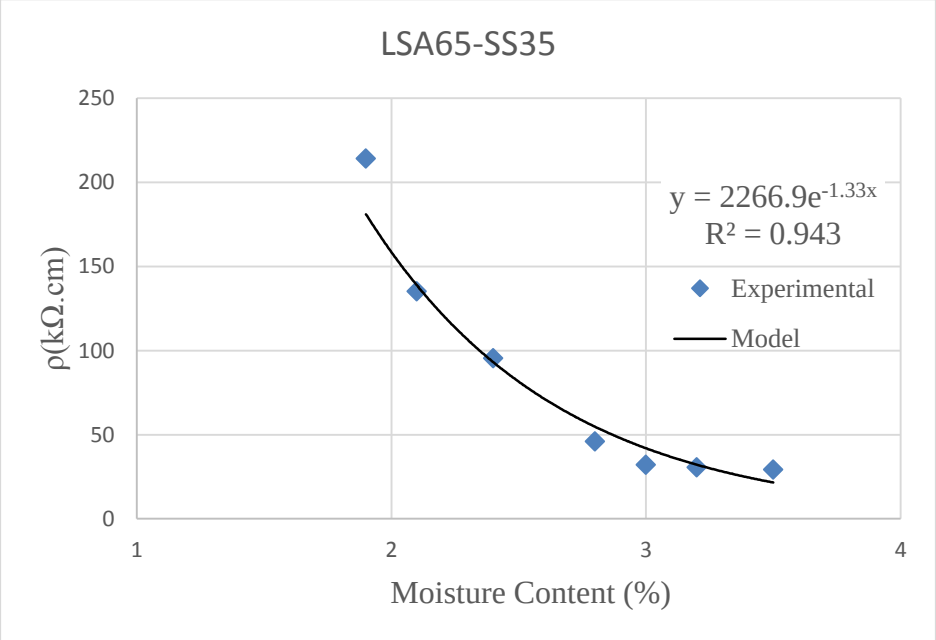

Figure 4.46: Electrical resistivity vs moisture content for LSA65-SS35.

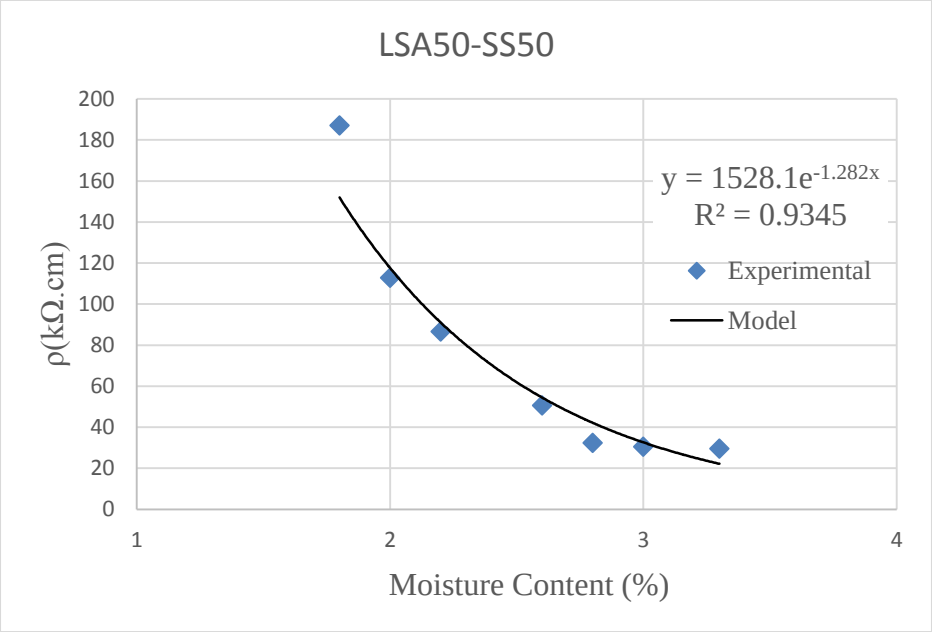

Figure 4.47: Electrical resistivity vs moisture content for LSA50-SS50.

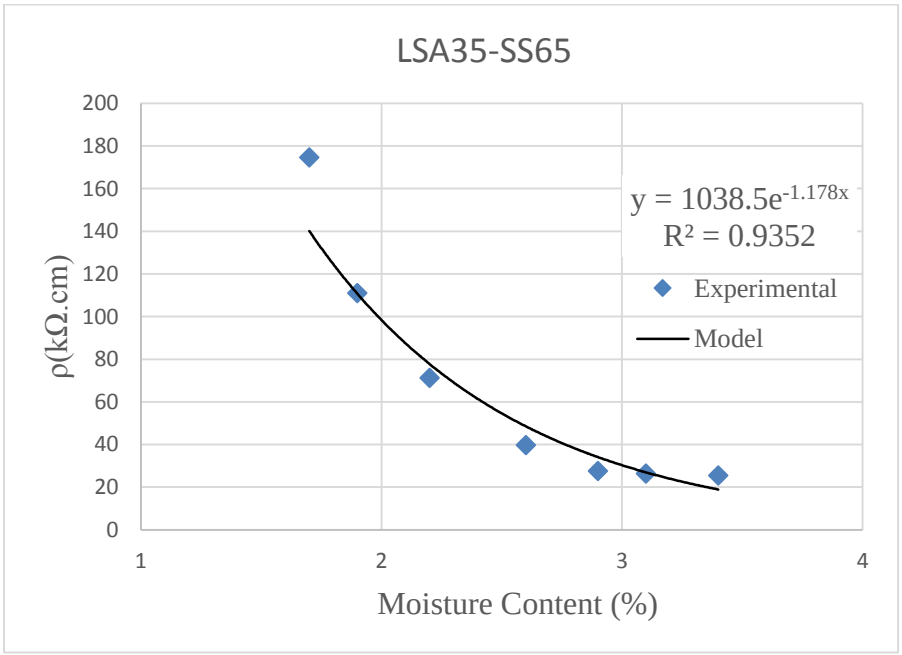

Figure 4.48: Electrical resistivity vs moisture content for LSA35-SS65.

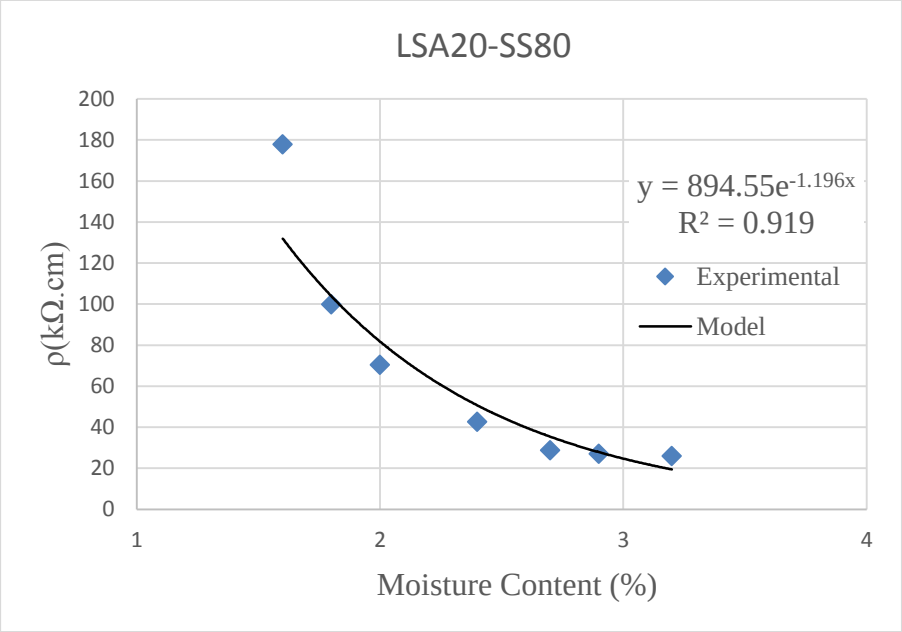

Figure 4.49: Electrical resistivity vs moisture content for LSA20-SS80.

4.7 CHLORIDE DIFFUSION

The results of the chloride diffusion analysis for the HWC mixtures is presented in this section. Figure 4.50 shows a typical plot of measured chloride content percentage by weight of concrete against the specimen depth. The chloride diffusion coefficient, De, is obtained by fitting the Fick's second law equation to the plot. Table 4.8 shows the calculated De values and measure surface concentration, Cs, of all the HWC specimens. The chloride diffusion coefficient for the HWC mixtures ranges from 2.97 x 10^{-8} cm^2/s to 6.48 x 10^{-8} cm^2/s.

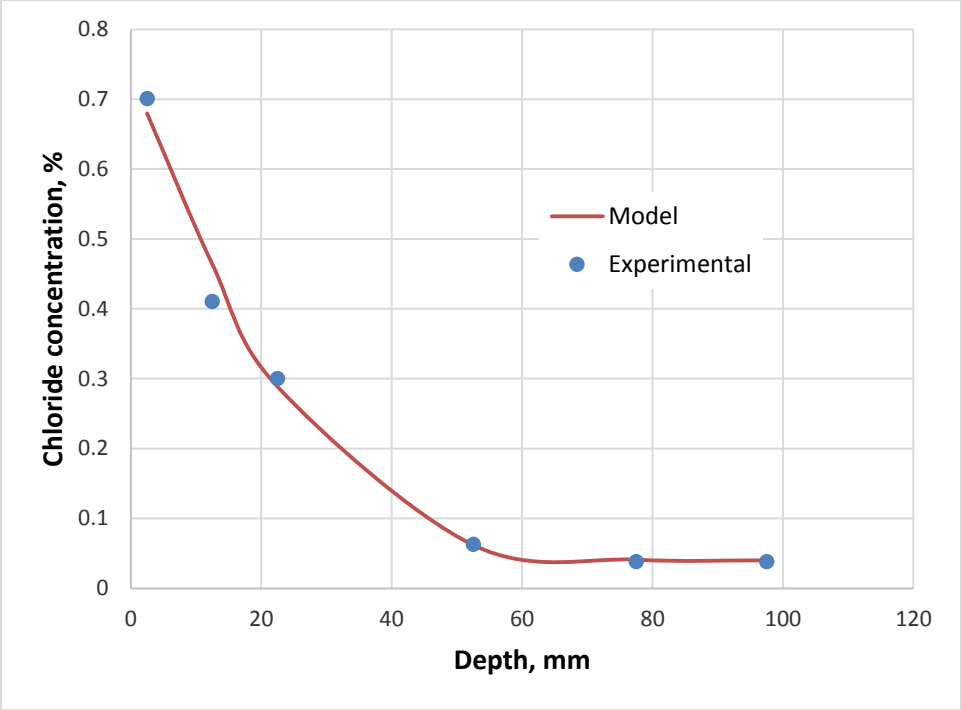

Figure 4.50: Typical chloride concentration against specimen depth.

Table 4.8: Chloride diffusion coefficient, De, and surface concentration, Cs, of HWC specimens.

Mix ID	De, (10^{-8} cm^2/s)	Cs, percent by mass of concrete
LSA100	6.48	0.79
SA100	4.63	0.72
SS100	2.70	0.67
IO100	3.12	0.95
SA80-IO20	4.16	0.60
SA65-IO35	3.48	0.88
SA50-IO50	3.09	0.92
SA35-IO65	2.91	0.76
SA20-IO80	2.88	0.80
SA80-SS20	4.20	0.85
SA65-SS35	3.82	0.64
SA50-SS50	3.46	0.70
SA35-SS65	3.25	0.73
SA20-SS80	3.16	0.68
LSA80-SS20	5.75	0.62
LSA65-SS35	4.88	0.60
LSA50-SS50	3.85	0.58
LSA35-SS65	3.24	0.70
LSA20-SS80	2.97	0.78

4.7.1 Mixtures with 100% coarse aggregate types

The coefficient of chloride diffusion, De for samples prepared with 100% aggregates types is shown in figure 4.51. From the figure, it can be seen that LSA100 has the highest chloride diffusion coefficient, which shows that it is the most permeable in this group. SS100 has the lowest chloride diffusion coefficient of 2.7 x 10^{-8} cm^2/s. The lowest value by SS100 sample may be due to the dense parking of the aggregates since steel shot aggregates have spherical particle size.

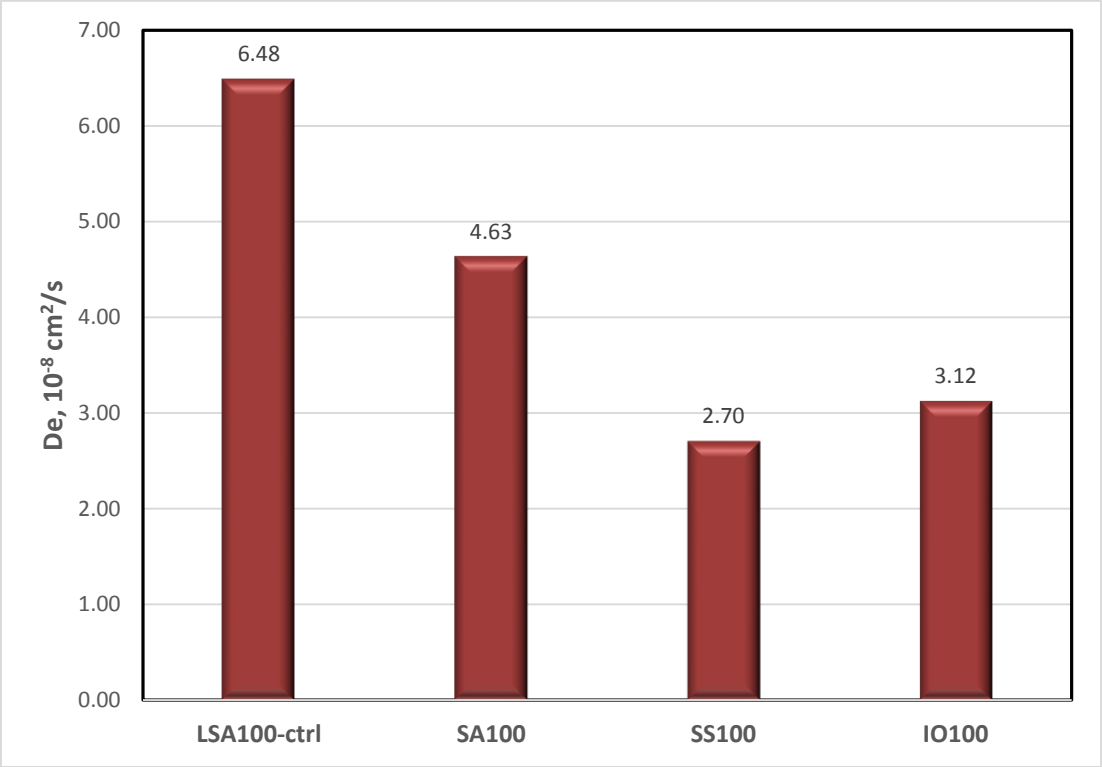

Figure 4.51: Chloride diffusion coefficient, De, of HWC with 100% coarse aggregate types.

4.7.2 Mixtures with steel slag and iron ore as coarse aggregate

Figure 4.52 shows the coefficient of chloride diffusion, De, for samples prepared with combination of steel slag and iron ore aggregates. All the samples have lower diffusion coefficient than the control mix. As the quantity of iron ore aggregates increases, the diffusion coefficient reduces gradually, which indicates that more dense packing is achieved with increasing iron ore aggregate. SA80-IO20 has the highest value while SA20-IO80 has the lowest value in this group.

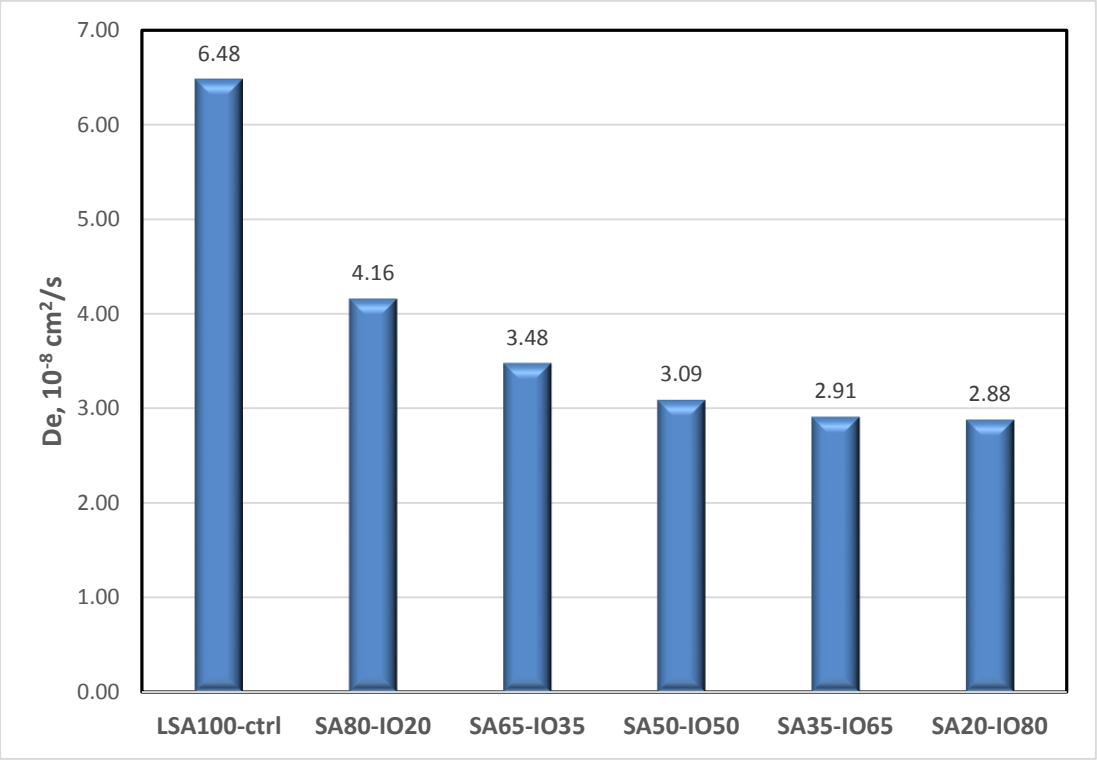

Figure 4.52: Chloride diffusion coefficient, De, of HWC with steel slag and iron ore aggregates.

4.7.3 Mixtures with steel slag and steel shot as coarse aggregate

The coefficient of chloride diffusion, De, for samples prepared with combination of steel slag and steel shot aggregates is shown in figure 4.53. From the figure, it can be seen that all the samples have lower diffusion coefficient than the control mix. The diffusion coefficient reduces as the quantity of steel shot aggregate increase. This shows that samples with higher percentage of steel shot aggregate are less permeable then samples with higher percentage of steel slag aggregates.

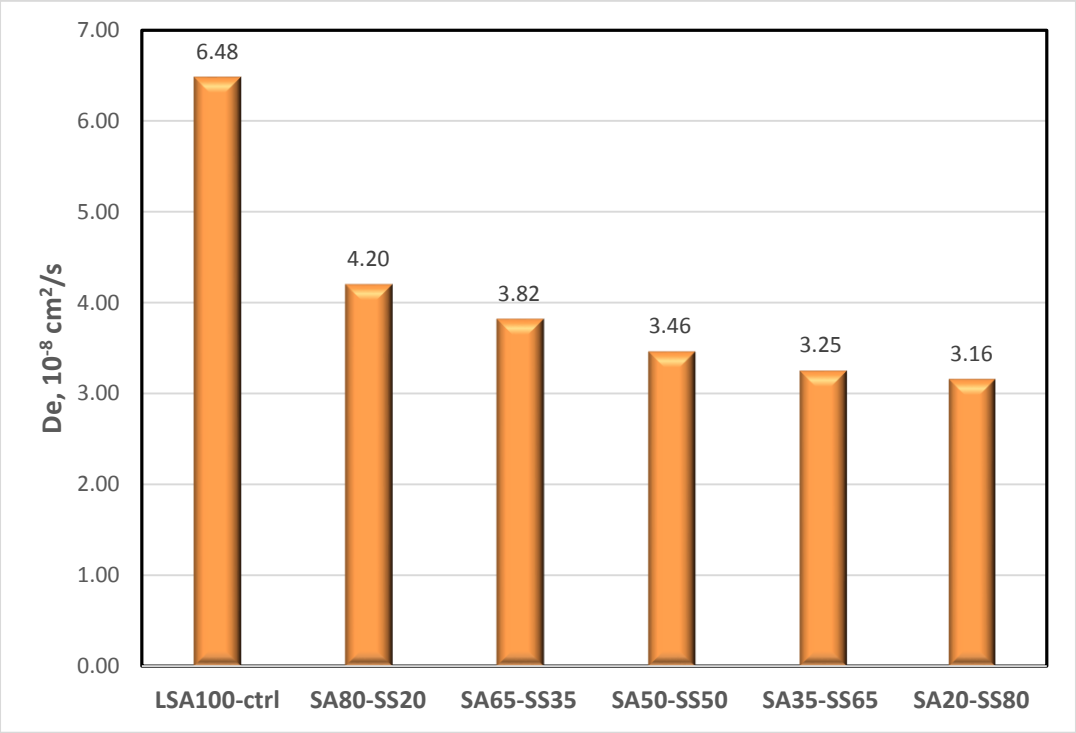

Figure 4.53: Chloride diffusion coefficient, De, of HWC with steel slag and steel shot aggregates.

4.7.4 Mixtures with limestone and steel shot as coarse aggregate

Figure 4.54 shows the coefficient of chloride diffusion, De, for samples prepared with combination of limestone and steel shot aggregates. All the samples in this group have lower diffusion coefficient than the control mix. LSA20-SS80 has the lowest diffusion coefficient of 2.97 x 10^{-8} cm^2/s while LSA80-SS20 has the highest value of 5.75 x 10^{-8} cm^2/s. This general shows that mixtures with higher percentage of steel shot aggregates are less permeable than mixtures with higher percentage of limestone aggregates.

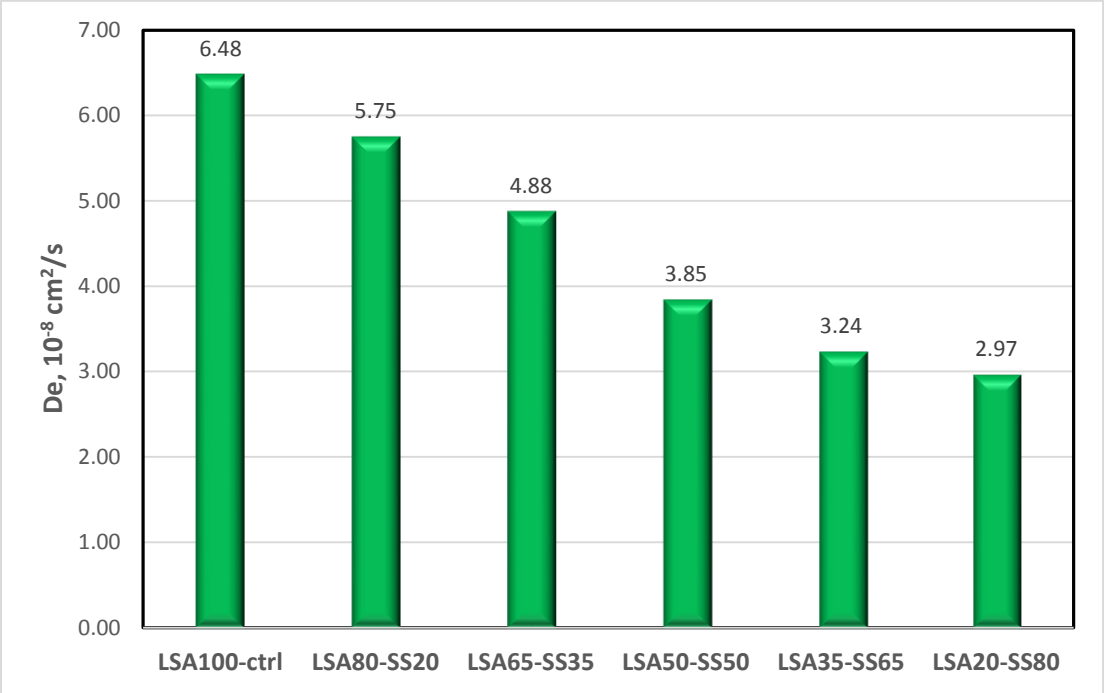

Figure 4.54: Chloride diffusion coefficient, De, of HWC with limestone and steel shot aggregates.

4.7.5 Time to Corrosion Initiation

The essence of coefficient of chloride diffusion of concrete specimens is to evaluate the time to corrosion initiation in that specimen, based on specific chloride content threshold on the surface of embedded reinforcement given by ASTM standard. Table 4.9 shows the chloride limit permissible in different concrete types, as specified by the ASTM standard. Based on the chloride diffusion experimental results, the Fick's equation given in equation (1) can be rearranged to give equation (2) in order to determine the time to corrosion initiation in the HWC specimens. Since water soluble chloride analysis was carried out, 0.15% chloride limit can be taken from Table 4.9 as C_x, concrete cover depth x of 75 mm, while C_s and D_e are the values given in Table 4.8 above.

Table 4.9: Specified chloride content limit for different construction type.

	Chloride limit, percent by mass	
	Test method	
	Acid soluble	Water soluble
Construction type and condition	ASTM C1152	ASTM C1218
Prestressed concrete	0.08	0.06
Reinforced concrete wet in service	0.10	0.08
Reinforced concrete dry in service	0.20	0.15

$$C_x = C_s\left\{1 - erf\left(\frac{x}{2\sqrt{D_e\, t}}\right)\right\} \quad (1)$$

$$t = \frac{x^2}{4\, D_e\left\{InErf\left(1-\frac{C_x}{C_s}\right)\right\}^2} \quad (2)$$

Table 4.10 shows the calculated time to corrosion initiation for all the HWC specimens. SS100 has the highest time to corrosion initiation of 7.7 years among all the mixtures while LSA100 has the lowest value of 3.0 years. This is not surprising because LSA100 has the highest chloride diffusion coefficient, which means that it is the most permeable, and hence, it would require the least time for chloride ion to migrate to the surface of embedded steel.

Table 4.10: Time to corrosion initiation of HWC specimens

Mix ID	Time to corrosion initiation (years)
LSA100	3.0
SA100	4.4
SS100	7.7
IO100	5.9
SA80-IO20	5.4
SA65-IO35	5.6
SA50-IO50	6.1
SA35-IO65	7.2
SA20-IO80	7.5
SA80-SS20	4.6
SA65-SS35	5.6
SA50-SS50	6.0
SA35-SS65	6.3
SA20-SS80	6.7
LSA80-SS20	3.4
LSA65-SS35	4.4
LSA50-SS50	5.8
LSA35-SS65	6.3
LSA20-SS80	6.8

4.8 RADIATION SHIELDING

The radiation shielding capabilities, measured in terms of the attenuated gamma-ray spectra and attenuation coefficients, of each of the 19 HWC mixtures are presented in this section. The attenuated gamma-ray intensity and attenuation coefficient are directly related to the density of the specimens. Specimens with high unit weight possess the optimum radiation shielding characteristics.

Average measurement of three specimens is presented in this section. The gamma-ray spectrum contained a single peak (with 661keV energy) for each measurement and sufficient time was considered in order to obtain good statistics in the area under the peak. The un-attenuated gamma-ray spectrum was first measured to generate a ratio between the attenuated and un-attenuated gamma-ray intensity. The counts under each gamma-ray peak were integrated and fractional attenuation of gamma-ray was calculated using un-attenuated intensity. Table 4.11 shows the integrated transmitted gamma-ray intensity without any sample, Io, transmitted intensity with sample in place, Ix, and the linear effective attenuation coefficient in terms of thickness, μt. SS100 has the highest attenuation coefficient of 2.0 among all the mixtures while LSA100 has the lowest value.

Table 4.11: Integrated gamma-ray intensity and effective attenuation coefficient

	Io = 140509	
Mix ID	**Ix**	**μt**
LSA100	43962	1.2
SA100	35546	1.4
SS100	18273	2.0
IO100	27294	1.6
SA80-IO20	33672	1.4
SA65-IO35	31613	1.4
SA50-IO50	30605	1.5
SA35-IO65	27925	1.6
SA20-IO80	27143	1.6
SA80-SS20	34296	1.4
SA65-SS35	27196	1.6
SA50-SS50	26090	1.6
SA35-SS65	22147	1.8
SA20-SS80	19871	1.9
LSA80-SS20	43225	1.2
LSA65-SS35	37238	1.3
LSA50-SS50	30948	1.5
LSA35-SS65	27520	1.6
LSA20-SS80	24441	1.8

4.8.1 Mixtures with 100% coarse aggregate types

The measured gamma-ray intensity spectra of HWC mixtures prepared with 100% aggregate types are shown in figure 4.55. The figure shows the attenuated gamma-ray spectra of the specimens in this group. Figure 4.56 shows the percentage attenuation of gamma-ray intensity. The percentage attenuation gives a clear indication of the attenuation performance (shielding characteristics) of each specimen. As can be seen in figure 4.55 and 4.56, 100% steel shots specimen, denoted as SS100, exhibited the maximum gamma-ray intensity attenuation, because it gave the maximum fractional percentage attenuation. This is because SS100 has the highest unit weight among all the mixtures. LSA100, with the lowest unit weight in this group exhibited the least gamma-ray intensity attenuation.

The effective linear attenuation coefficient in terms of sample thickness, μt, for the specimens is shown in figure 4.57. As expected, SS100 has the maximum attenuation coefficient of 2.0, which shows that it has the optimum shielding performance in this group. IO100, SA100 and LSA100 has attenuation coefficient of 1.6, 1.4 and 1.2 respectively.

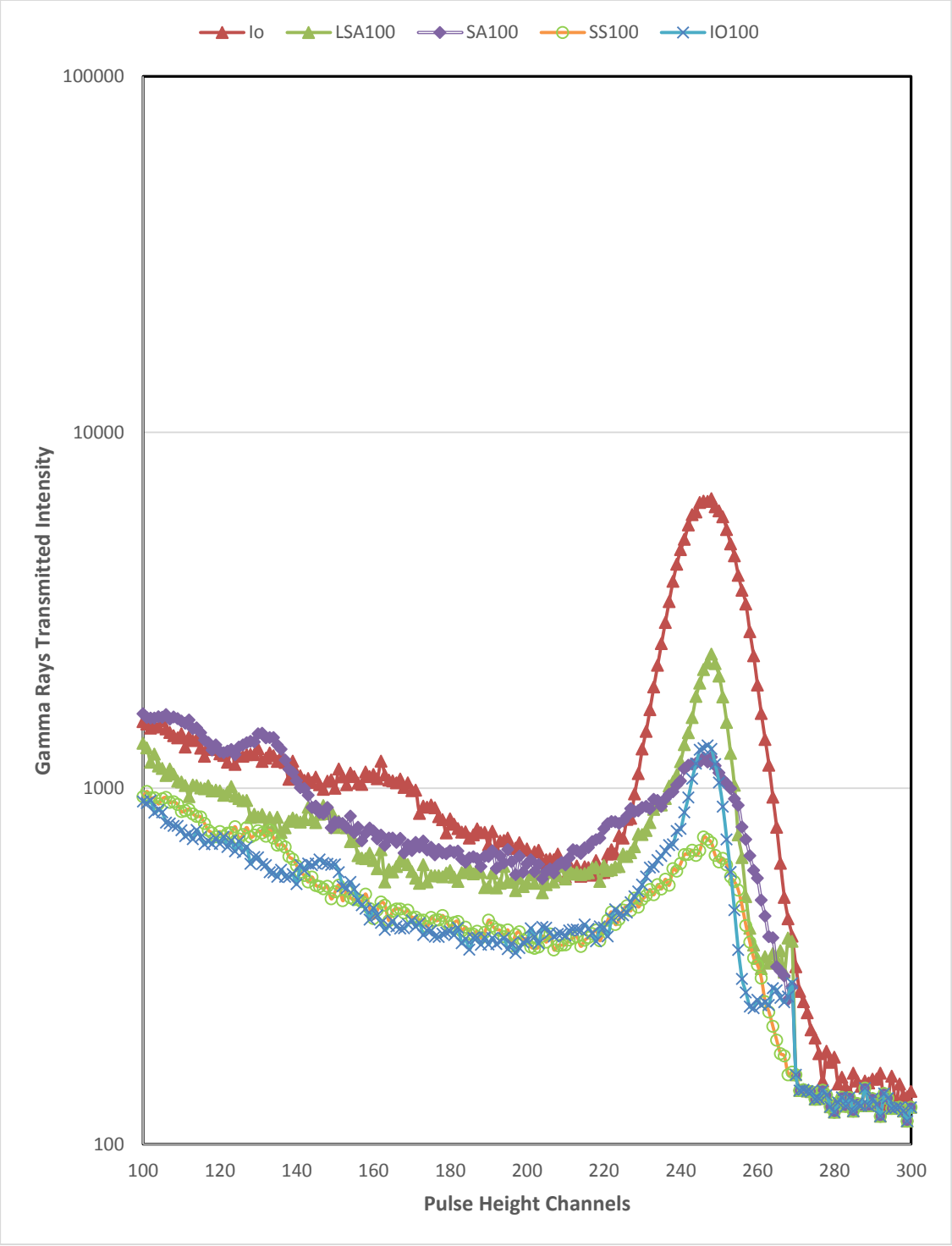

Figure 4.55: Pulse height spectrum for HWC with 100% aggregate types.

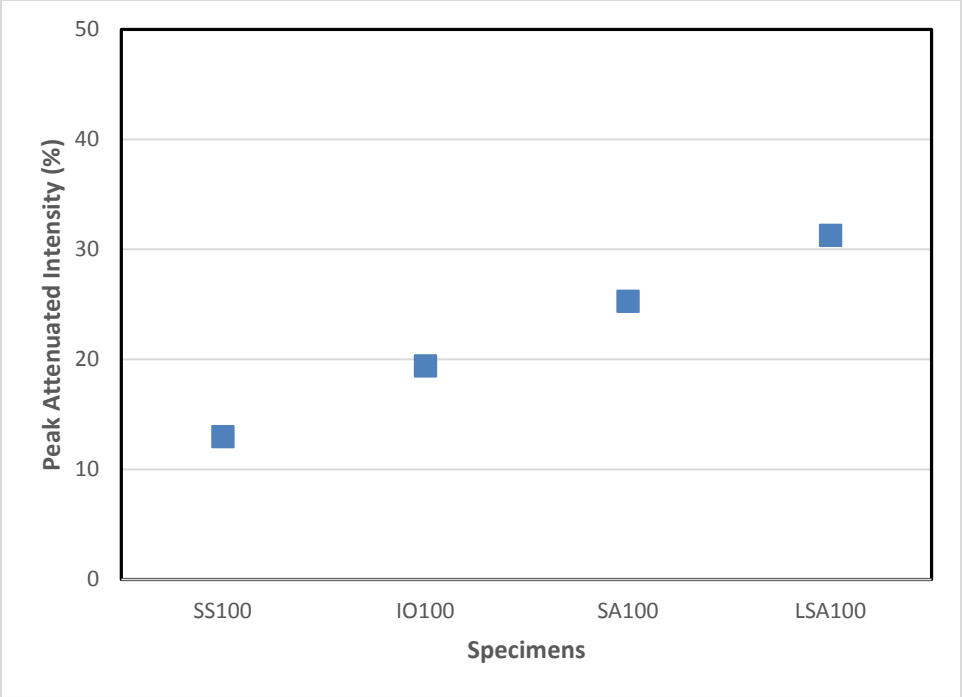

Figure 4.56: Integrated gamma ray transmitted intensity of HWC with 100% aggregate types.

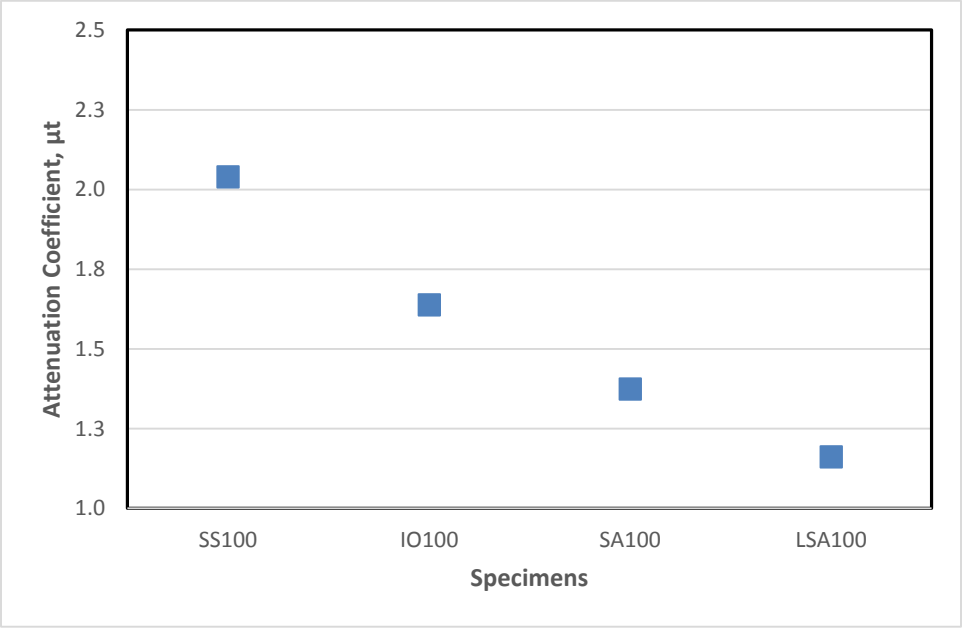

Figure 4.57: Effective linear attenuation coefficient of HWC with 100% aggregate types.

4.8.2 Mixtures with steel slag and iron ore as coarse aggregate

Figure 4.58 shows the gamma-ray intensity spectra of HWC mixtures prepared with combination of steel slag aggregate and iron ore aggregates in varying proportions. Figure 4.59 shows the percentage attenuation of gamma ray intensity. The percentage attenuation gives a clear indication of the shielding characteristics of each specimen. As expected, the heaviest specimen with 20% steel slag aggregate and 80% iron ore aggregate exhibit the optimum attenuation in this group. As the quantity of steel slag in each mixture increases, which depicts decrease in unit weight, the shielding characteristics of the specimens reduces accordingly. This can be clearly seen in figure 4.60, which shows a gradual decrease in the attenuation coefficient of the mixtures. SA20-IO80 has the maximum attenuation coefficient of 1.6, which shows that it has the optimum shielding performance in this group. The smallest attenuation coefficient of 1.4 was recorded for SA80-IO20.

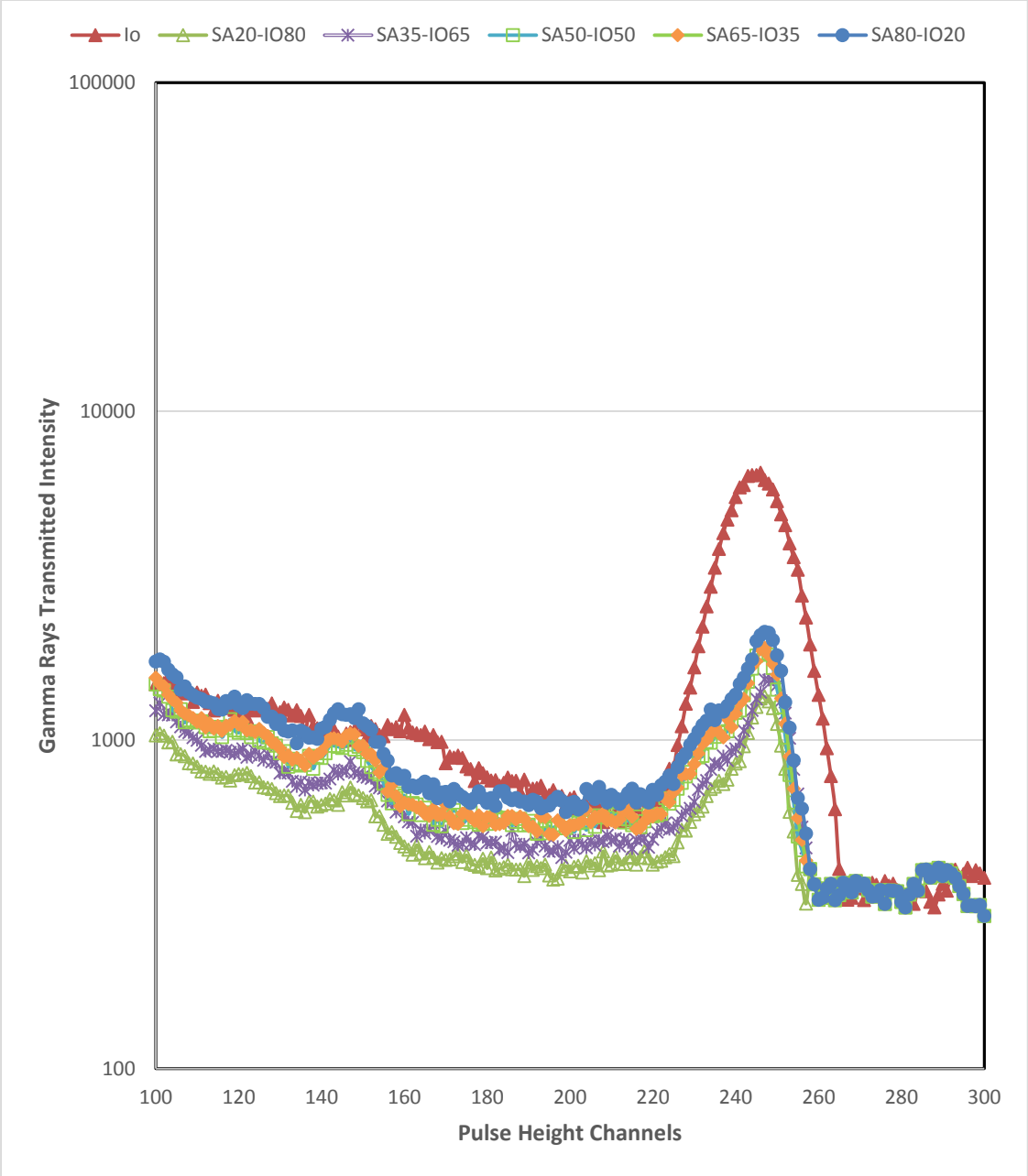

Figure 4.58: Pulse height spectrum for HWC with steel slag and iron ore aggregates.

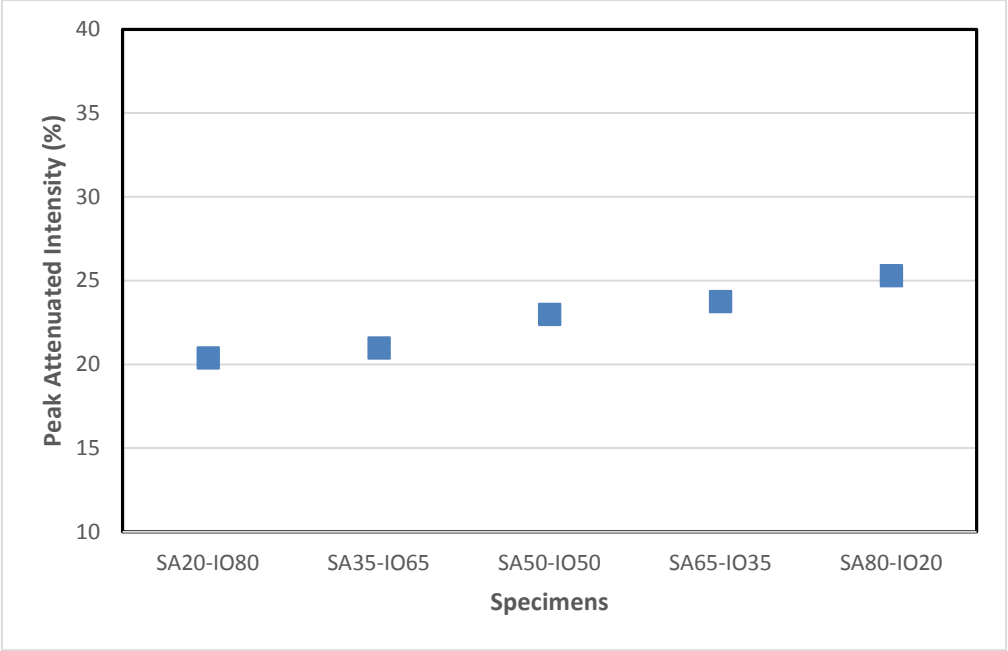

Figure 4.59: Integrated gamma ray transmitted intensity of HWC with steel slag and iron ore aggregates.

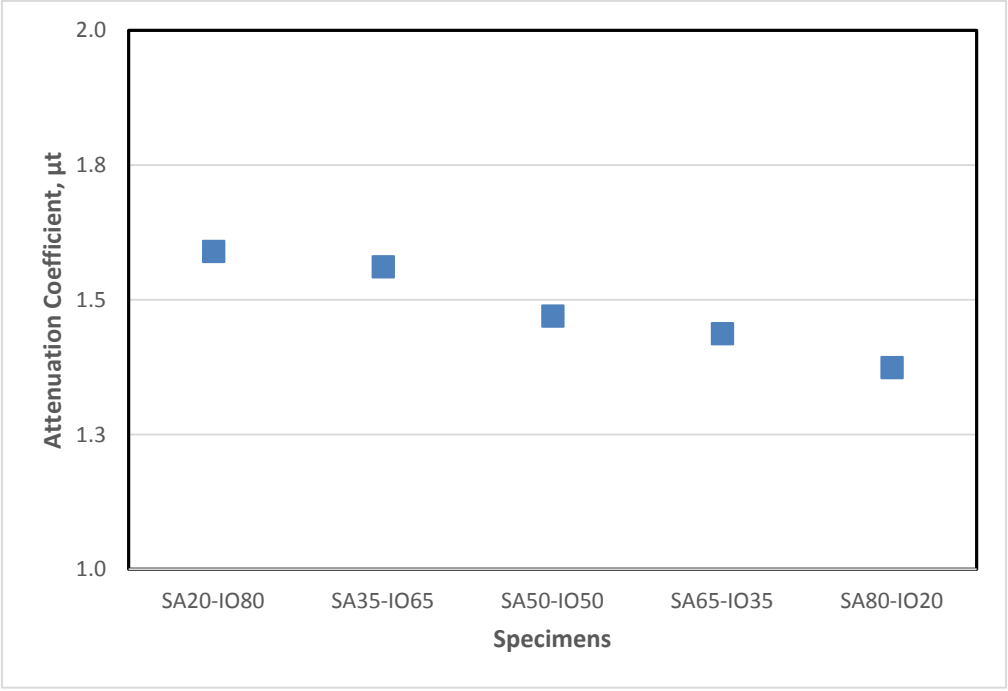

Figure 4.60: Effective linear attenuation coefficient of HWC with steel slag and iron ore aggregates.

4.8.3 Mixtures with steel slag and steel shot as coarse aggregate

Figure 4.61 shows the gamma-ray intensity spectra of HWC mixtures prepared with combination of steel slag aggregate and steel shot aggregates in varying proportions. Figure 4.62 shows the percentage attenuation of gamma ray intensity. The percentage attenuation gives a clear indication of the shielding characteristics of each specimen. SA20-SS80 exhibit the maximum gamma-ray intensity attenuation while SA80-SS20 exhibit the minimum. There is gradual increase in the fractional attenuation percentage as the percentage of steel shot aggregate in the specimens reduces. This implies that better shielding characteristics is achieved as the weight of the specimens increases. Specimens with higher quantity of steel shots has higher unit weight than specimens with lower steel shot percentage, and hence, those specimens possess better shielding characteristics.

The effective linear attenuation coefficient, μt, for the specimens is shown in figure 4.63. As expected, SA20-SS80 has the maximum attenuation coefficient of 1.9, which shows that it has the optimum shielding performance in this group. This value is slightly lower than 2.0 that was obtained for 100% steel shot. This is due to the slight reduction in unit weight of SS100 when 20% steel shot was replaced with steel slag aggregate. SA80-SS20 has the lowest attenuation coefficient of 1.4 in this group

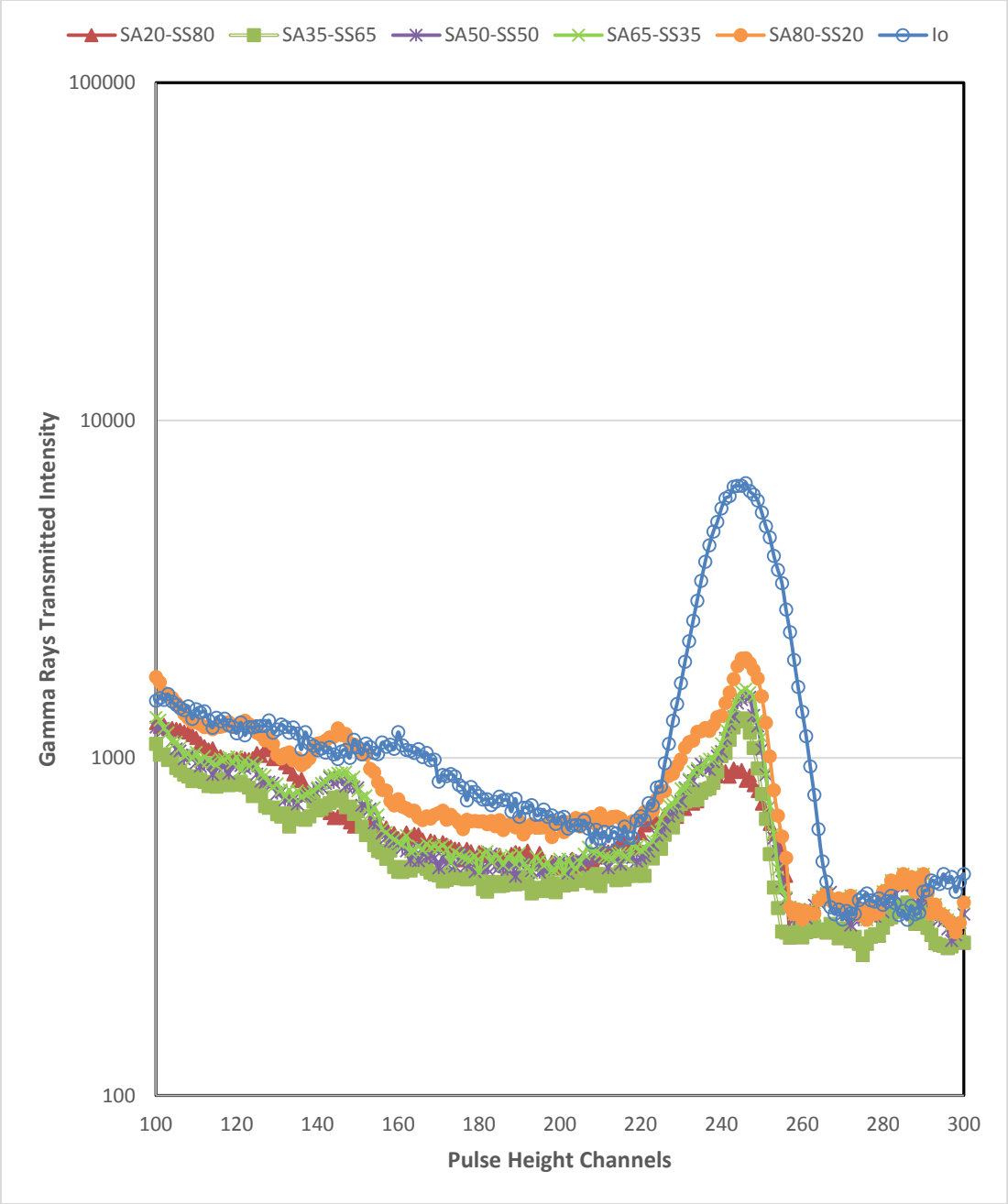

Figure 4.61: Pulse height spectrum for HWC with steel slag and steel shot aggregates.

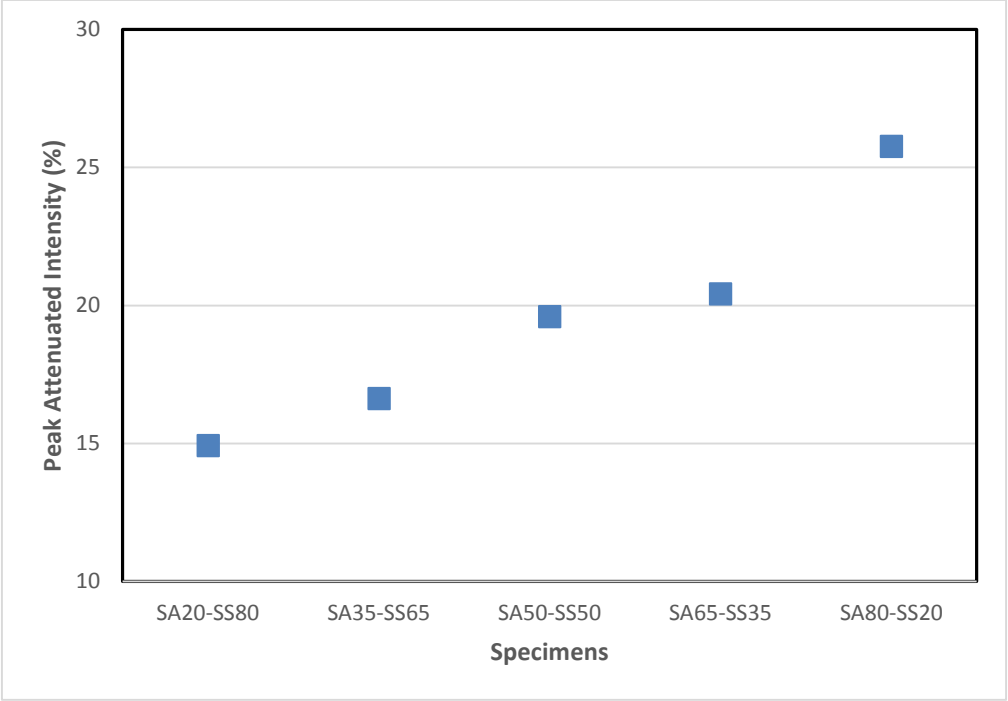

Figure 4.62: Integrated gamma ray transmitted intensity of HWC with steel slag and steel shot aggregates.

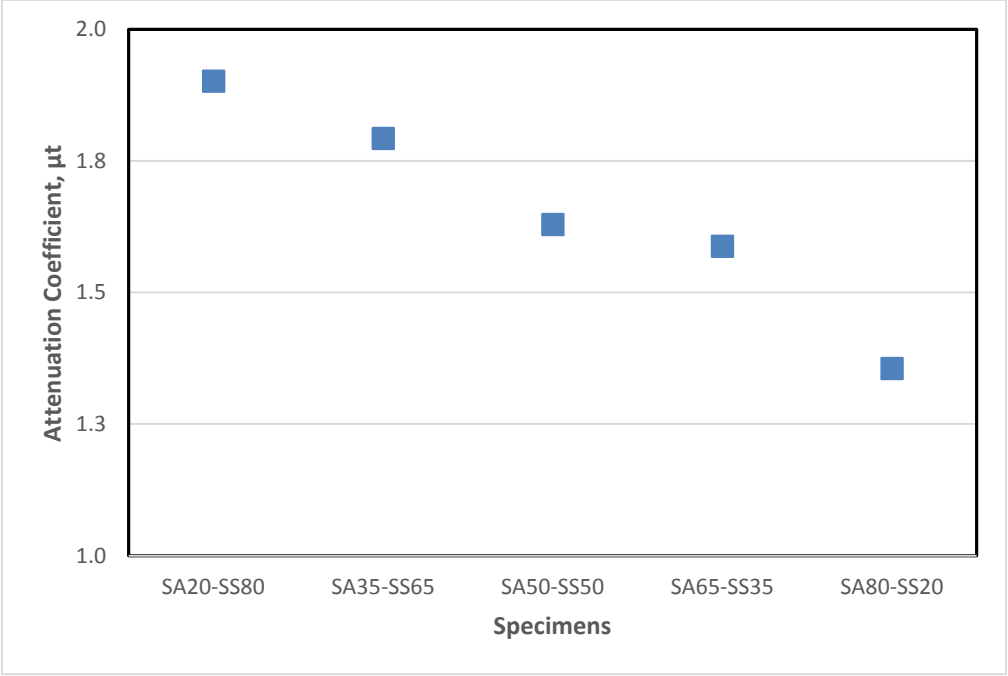

Figure 4.63: Effective linear attenuation coefficient of HWC with steel slag and steel shot aggregates.

4.8.4 Mixtures with limestone and steel shot as coarse aggregate

The measured gamma-ray intensity spectra of HWC mixtures prepared with varying proportions of limestone aggregate and steel shot aggregate are shown in figure 4.64. Figure 4.65 shows the percentage attenuation of gamma ray intensity. The percentage attenuation gives a clear indication of the shielding characteristics of each specimen. As can be seen in figure 4.64 and 4.65, specimen with 20% limestone aggregate and 80% steel shot exhibited the maximum gamma ray shielding. This is because the specimen has the highest unit weight among all the mixtures in this group. The specimen with the least gamma-ray intensity attenuation is LSA80-SS20.

Figure 4.66 shows the effective linear attenuation coefficient, μt, for the specimens. LSA20-SS80 has the maximum attenuation coefficient of 1.8, which further indicate that it has the optimum shielding performance in this group. The smallest attenuation coefficient of 1.2 was recorded for LSA80-SS20 specimen.

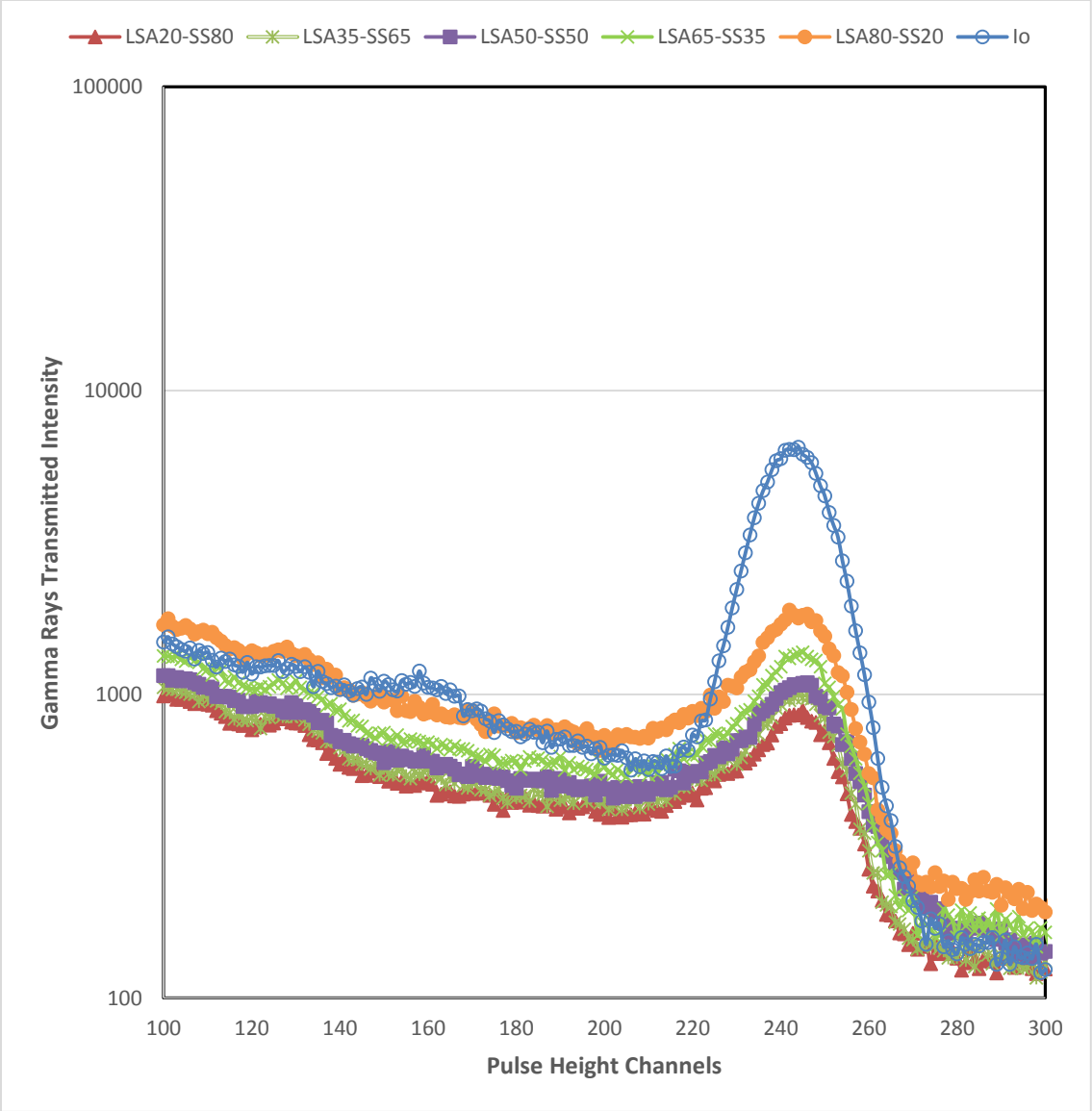

Figure 4.64: Pulse height spectrum for HWC with limestone and steel shot aggregates.

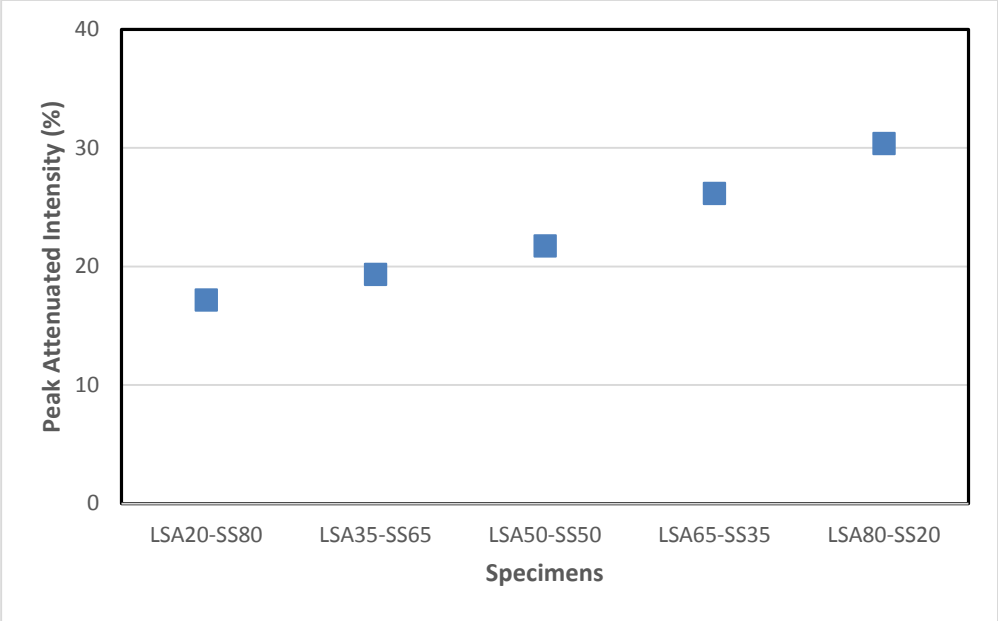

Figure 4.65: Integrated gamma ray transmitted intensity of HWC with limestone and steel shot aggregates.

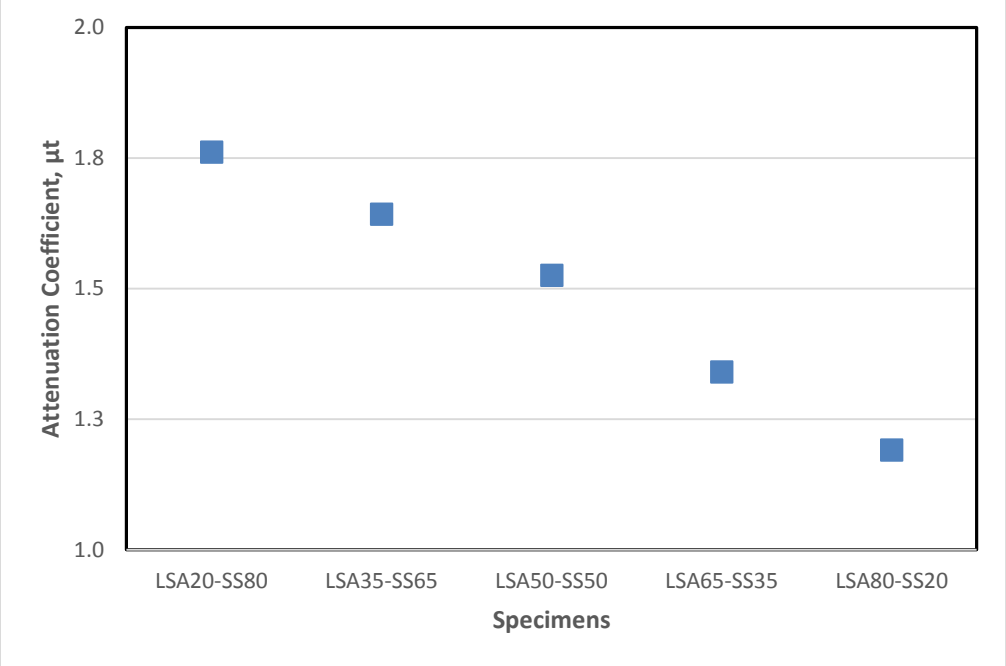

Figure 4.66: Effective linear attenuation coefficient of HWC with limestone and steel shot aggregates.

4.8.5 Optimum thickness of HWC mixtures

Table 4.12 shows the average optimum thickness of each mixture to achieve about 99% gamma-ray attenuation. Figure 4.67 shows a plot of Ix/Io against thickness, using equation (3), for SS100. It can be seen from the figure that the percentage attenuation tends to zero as the specimen thickness increases. However, there should be an optimum thickness to achieve a target percentage attenuation. The optimum thickness was obtained for each mixture by using the mixture with the highest performance, which is SS100, as the reference mixture. 99% target was set because SS100 required 250mm thickness to achieve 99% attenuation. Increasing the thickness further does not improve the attenuation as depicted by figure 4.67.

$$\frac{I_x}{I_o} = e^{-\mu t} \tag{3}$$

For 99% target attenuation, $\frac{I_x}{I_o} = 0.01$, therefore,

$$t = -\frac{\ln(0.01)}{\mu} \tag{4}$$

Since μ is already known for all the specimens, thickness, t, can be calculated.

Based on the values in table 4.12, SS100 has the minimum thickness of 230 mm, while LSA100 has the maximum thickness of 400 mm, for the same 99% attenuation. 100% iron ore specimen, being a major raw materials for HWC commercial production, has thickness of 290 mm, whereas, SA2-IO80, SA65-SS35, SA50-SS20, SA35-SS65, SA20-SS80, LSA35-SS65 and LSA20-SS80 have thickness between 250 to 290mm for the same 99% attenuation.

Table 4.12: Optimum specimen thickness to achieve 99% attenuation

Mix ID	Optimum thickness (mm)
LSA100	400
SA100	340
SS100	230
IO100	290
SA80-IO20	340
SA65-IO35	320
SA50-IO50	310
SA35-IO65	300
SA20-IO80	290
SA80-SS20	340
SA65-SS35	290
SA50-SS50	280
SA35-SS65	260
SA20-SS80	250
LSA80-SS20	390
LSA65-SS35	350
LSA50-SS50	310
LSA35-SS65	290
LSA20-SS80	270

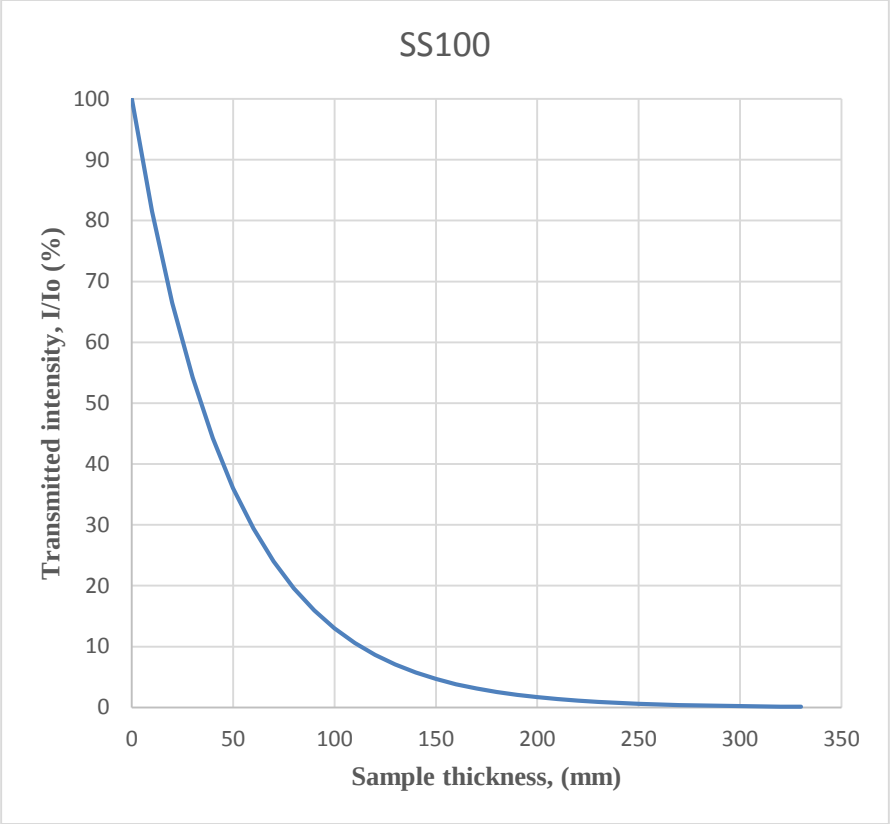

Figure 4.67: Transmitted intensity against thickness of SS100

4.9 COST ANALYSIS

As stated in the introductory part, the cost of production of HWC in the Kingdom of Saudi Arabia is high because the conventional materials for HWC production such steel shot and iron ore aggregates are usually imported. In contrast, the locally available industrial byproduct and limestone aggregate utilized in this study are very cheap, and their combination with the conventional materials enable a significant production cost reduction.

The local unit cost of each materials were collected in order to determine and compare the cost of the developed 19 HWC mixtures in this study. It should be noted that the overall cost of concrete production excludes the costs of transportation, handling, placement and quality control. Table 4.13 through 4.16 show the constituent materials and specimen cost per cubic meter of concrete for HWC mixtures. From the tables, it can be seen that all the mixtures except SA35-SS65, SA20-SS80, LSA35-SS65 and LSA20-SS80 have lower production cost than the two 100% steel shot and iron ore specimens, which are the aggregates normally utilized for commercial production.

Table 4.13: Cost analysis for HWC with 100% aggregate types.

Constituents	Rate, SR/ton(lit)	Rate, SR/kg(lit)	LSA100		SA100		SS100		IO100	
			Quantity	Cost, SR/m3	Quantity	Cost, SR/m3	Quantity	Cost, SR/m3	Quantity	Cost, SR/m3
Cement, kg	**350**	**0.35**	400	140	400	140	400	140	400	140
Water,liter	**0.15**	**0.15**	177	26.55	185	27.75	167	25.05	187	28.05
Limestone, kg	**75**	**0.075**	1128	84.6	0	0	0	0	0	0
Steel slag, kg	**15**	**0.015**	0	0	1331	19.965	0	0	0	0
Steel shot, kg	**2000**	**2**	0	0	0	0	1904	3808	0	0
Iron ore, kg	**1200**	**1.2**	0	0	0	0	0	0	1503	1803.6
Sand, kg	**40**	**0.04**	691	27.64	816	32.64	1167	46.68	921	36.84
SP, liter	**5**	**5**	6	30	6.8	34	9.2	46	7.2	36
Total Cost, SR/m3			308.79		254.36		4065.73		2044.49	

Table 4.14: Cost analysis for HWC with steel slag and iron ore aggregates.

Constituents	Rate, SR/ton(lit)	Rate, SR/kg(lit)	(SA80-IO20)		(SA65-IO35)		(SA50-IO50)		(SA35-IO65)		(SA20-IO80)	
			Quantity	Cost, SR/m3	Quantity	Cost, SR/m3	Quantity	Cost, SR/m3	Quantity	Cost, SR/m3	Quantity	Cost, SR/m3
Cement, kg	**350**	**0.35**	400	140	400	140	400	140	400	140	400	140
Water,liter	**0.15**	**0.15**	185	27.75	185	27.75	186	27.9	186	27.9	186	27.9
Iron Ore, kg	**1200**	**1.2**	273	327.6	485	582	706	847.2	935	1122	1173	1407.6
Steel slag, kg	**15**	**0.015**	1090	16.35	902	13.53	706	10.59	503	7.545	293	4.395
Sand, kg	**40**	**0.04**	835	33.4	850	34	866	34.64	881	35.24	899	35.96
SP, liter	**5**	**5**	6.8	34	6.8	34	6.8	34	7.2	36	7.2	36
Total Cost, SR/m3			579.1		831.28		1094.33		1368.685		1651.855	

Table 4.15: Cost analysis for HWC with steel slag and steel shot aggregates.

Constituents	Rate, SR/ton(lit)	Rate, SR/kg(lit)	(SA80-SS20)		(SA65-SS35)		(SA50-SS50)		(SA35-SS65)		(SA20-SS80)	
			Quantity	Cost, SR/m3	Quantity	Cost, SR/m3	Quantity	Cost, SR/m3	Quantity	Cost, SR/m3	Quantity	Cost, SR/m3
Cement, kg	**350**	**0.35**	400	140	400	140	400	140	400	140	400	140
Water,liter	**0.15**	**0.15**	182	27.3	180	27	178	26.7	175	26.25	172	25.8
Steel shot, kg	**2000**	**2**	283	566	521	1042	784	1568	1075	2150	1402	2804
Steel slag, kg	**15**	**0.015**	1133	16.995	968	14.52	784	11.76	579	8.685	351	5.265
Sand, kg	**40**	**0.04**	868	34.72	912	36.48	961	38.44	1014	40.56	1074	42.96
SP, liter	**5**	**5**	7.2	36	7.2	36	7.6	38	8.4	42	8.8	44
Total Cost, SR/m3			821.015		1296		1822.9		2407.495		3062.025	

Table 4.16: Cost analysis for HWC with limestone and steel shot aggregates.

Constituents	Rate, SR/ton(lit)	Rate, SR/kg(lit)	(LSA80-SS20)		(LSA65-SS35)		(LSA50-SS50)		(LSA35-SS65)		(LSA20-SS80)	
			Quantity	Cost, SR/m3	Quantity	Cost, SR/m3	Quantity	Cost, SR/m3	Quantity	Cost, SR/m3	Quantity	Cost, SR/m3
Cement, kg	**350**	**0.35**	400	140	400	140	400	140	400	140	400	140
Water,liter	**0.15**	**0.15**	175	26.25	174	26.1	173	25.95	172	25.8	170	25.5
Limestone, kg	**75**	**0.075**	981	73.575	854	64.05	707	53.025	537	40.275	335	25.125
Steel shot, kg	**2000**	**2**	245	490	460	920	707	1414	997	1994	1338	2676
Sand, kg	**40**	**0.04**	752	30.08	805	32.2	867	34.68	940	37.6	1025	41
SP, liter	**5**	**5**	7.2	36	7.6	38	8	40	8	40	8.4	42
Total Cost, SR/m3			795.905		1220.35		1707.655		2277.675		2949.625	

CHAPTER 5

CONCLUSION AND RECOMMENDATION

5.1 CONCLUSIONS

This research was conducted to develop heavyweight concrete (HWC) for radiation shielding purpose utilizing indigenous industrial waste materials. The mechanical, durability and radiation shielding characteristics of the developed HWC were investigated. The waste material used were steel slag aggregate in combination with locally available limestone aggregate. Other conventional heavyweight aggregates including steel shot and iron ore aggregates were used. However, both steel shot and iron ore are usually imported into the Kingdom. Based on the data obtained in this study, the following conclusions can be drawn:

5.1.1 Mixtures with 100% coarse aggregate

1. HWC mixtures produced with 100% coarse aggregates had an average 28-day compressive strength ranging from 29.6 MPa to 52.0 MPa. Mixtures prepared with 100% limestone aggregate had the highest 28-day strength of 52.0 MPa while mixtures produced with 100% steel shot aggregate had a compressive strength of 29.6 MPa. Iron ore mixtures produced compressive strength of 40.3 MPa while steel slag mixture had compressive strength of 45.3 MPa.

2. The mixtures in this group had splitting tensile strength between 3.0 MPa – 5.5 MPa. 100% steel slag aggregate concrete had the highest splitting tensile while 100% steel shot concrete had the lowest splitting tensile.
3. Steel shot concrete had relatively high elastic modulus, which is in contrast with its compressive strength. This may be as a result of its stiffness, which tends to improve its deformation performance. The elastic modulus for all the mixtures in this group ranges from 33.0 GPa to 43.9 GPa. In addition, steel shot mixtures exhibited the least shrinkage strain among this group. Iron ore mixtures had the highest shrinkage strain values.
4. In terms of susceptibility to corrosion, LSA mixture was the least susceptible while SS aggregate mixture was the most susceptible. However, all the mixtures have electrical resistivity values above the limit for corrosion initiation probability.
5. Because of high unit weight of SS concrete, it exhibited the best radiation shielding performance among this group. Limestone exhibited the least performance while iron ore and steel slag mixtures are in-between. The radiation shielding performance of the mixture increases with increasing unit weight.

5.1.2 Mixtures with steel slag and iron ore as coarse aggregate

1. Mixtures prepared with combination of steel slag and iron ore (SA-IO mixtures) had compressive strength between 39.0 MPa – 44.0 MPa. The compressive strength reduces as the percentage content of iron ore increases. The average splitting tensile strength of the mixtures ranges from 4.2 MPa to 5.1 MPa. The

splitting tensile strength is in agreement with the compressive strength of the mixtures.

2. Mixture with highest percentage of steel slag aggregate had the highest elastic modulus in this group. The elastic modulus reduces as the quantity of iron ore increases.
3. The lowest shrinkage strain was observed for SA35-IO65 while SA50-IO50 had the highest shrinkage strain in this group.
4. Mixtures with higher percentage of iron ore had the optimum shielding characteristics. The shielding performance reduces with increasing quantity steel slag aggregate.

5.1.3 Mixtures with steel slag and steel shot as coarse aggregate

1. Mixtures prepared with combination of steel slag and steel shot (SA-SS mixtures) had compressive strength between 32.0 MPa – 39.0 MPa. The compressive strength reduces as the percentage content of steel shot increases. The average splitting tensile strength of the mixtures ranges from 3.6 MPa to 4.5 MPa.
2. Specimens produced with high percentage of steel shot aggregate had higher elastic modulus in this group. The elastic modulus ranges from 33.6 GPa to 40.0 GPa, and it increases with increasing steel shot percentage.
3. Mixtures with higher steel shot percentage generally had the least shrinkage strain values throughout the exposure period. SA35-SS65 was the least susceptible to shrinkage while SA80-SS20 had the most shrinkage strain.

4. Mixtures with higher percentage of steel shot had the best shielding characteristics. The shielding performance reduces with increasing quantity of steel slag aggregate.

5.1.4 Mixtures with limestone and steel shot as coarse aggregate

1. Mixtures prepared with combination of limestone and steel shot (LSA-SS mixtures) had compressive strength between 29.1 MPa – 45.0 MPa. The compressive strength reduces as the percentage content of steel shot increases. The average splitting tensile strength of the mixtures ranges from 3.2 MPa to 4.7 MPa. The splitting tensile strengths for the mixtures in this group reduces as the quantity of steel shot increases.
2. The elastic modulus of mixtures in this group are relatively close without much difference in the values. However, higher percentage steel shot mixtures had higher elastic modulus values.
3. LSA20-SS80 had the least shrinkage strain among the mixtures in this group. It was observed that steel shot aggregate concrete generally exhibit the least shrinkage characteristics among all the HWC mixtures prepared.
4. Mixtures with higher percentage of steel shot had the best shielding characteristics in this group. The shielding performance reduces with increasing quantity limestone aggregate.

5.2 RECOMMENDATIONS

Based on the combined mechanical, durability and radiation shielding properties together with cost estimate of the developed heavyweight concrete mixtures, the following mixtures are recommended for use in commercial scale. The mixtures are arranged in increasing order of production cost, which is less than the overall cost of conventional iron ore aggregate specimen.

1. 65% SA + 35% SS (SR 1296)
2. 35% SA + 65% IO (SR 1369)
3. 20% SA + 80% IO (SR 1652)
4. 50% SA50 + 50% SS (SR 1823)

5.3 RECOMMENDATIONS FOR FUTURE WORK

1. Even though it has been reported in some literature that the use of mineral additive does not improve radiation shielding behavior of normal weight concrete, the performance of heavyweight concrete with mineral additive can be investigated.
2. This research was carried out using gamma-ray source for radiation investigation; other radioactive sources can be investigated such as neutron source to evaluate the neutron shielding characteristics of the developed HWCs.
3. Given that this research was carried out on small specimens of 100 mm thickness, further research can look into the possibility of using wall scale model to investigate the radiation shielding properties of the developed HWCs.

4. Assess the radiation shielding characteristics on composite specimens, such as combination of developed HWCs with metallic sheets.

REFERENCES

1. Kaplan, M. F., *Concrete radiation shielding: nuclear physics, concrete properties, design and construction*, 1989. New York: John Wiley & Sons.

2. Maki, Y. and Ohnuma, H., "Application of concrete to the treatment and disposal of radioactive waste in Japan," *Nuclear Engineering and Design*, Dec. 1992., 138(2), pp. 179–188.

3. Kharita, M. H., Takeyeddin, M., Alnassar, M., and Yousef, S., "Development of special radiation shielding concretes using natural local materials and evaluation of their shielding characteristics," *Progress in Nuclear Energy*, Jan. 2008., 50(1), pp. 33–36.

4. Malhotra, V. M. and Mehta, P. K., *Pozzolanic and Cementitious Materials*, 1996. SA: Gordon and Breach Science Publisher.

5. Fillmore, D. L., "Literature Review of the Effects of Radiation and Temperature on the Aging of Concrete," *Idaho National Engineering and Environmental Laboratory*, 2004.

6. Başyigit, C., Akkurt, I., Kilincarslan, S., and Beycioglu, A., "Prediction of compressive strength of heavyweight concrete by ANN and FL models," *Neural Computing and Applications*, Jul. 2009., 19(4), pp. 507–513.

7. Gencel, O., Brostow, W., Ozel, C., and Filiz, M., "Concretes containing hematite for use as shielding barriers," *Medziagotyra*, 2010., 16(3), pp. 249–256.

8. Gencel, O., Brostow, W., Ozel, C., and Filiz, M., "An investigation on the concrete properties containing colemanite," *International Journal of Physical Sciences*, 2010., 5(3), pp. 216–225.

9. Korkut, T., Karabulut, A., Budak, G., Aygün, B., Gencel, O., and Hançerlioğulları, A., "Investigation of neutron shielding properties depending on number of boron atoms for colemanite, ulexite and tincal ores by experiments and FLUKA Monte Carlo simulations.," *Applied radiation and isotopes : including data, instrumentation and methods for use in agriculture, industry and medicine*, Jan. 2012., 70(1), pp. 341–5.

10. Akkurt, I., Basyigit, C., Kilincarslan, S., and Mavi, B., "The shielding of γ-rays by concretes produced with barite," *Progress in Nuclear Energy*, Jan. 2005., 46(1), pp. 1–11.

11. Martínez-Barrera, G., Ureña-Nuñez, F., Gencel, O., and Brostow, W., “Mechanical properties of polypropylene-fiber reinforced concrete after gamma irradiation,” *Composites Part A: Applied Science and Manufacturing*, May 2011., 42(5), pp. 567–572.

12. Sharifi, S., Bagheri, R., and Shirmardi, S. P., “Comparison of shielding properties for ordinary, barite, serpentine and steel–magnetite concretes using MCNP-4C code and available experimental results,” *Annals of Nuclear Energy*, Mar. 2013., 53, pp. 529–534.

13. Kharita, M. H., Yousef, S., and AlNassar, M., “The effect of the initial water to cement ratio on shielding properties of ordinary concrete,” *Progress in Nuclear Energy*, Jul. 2010., 52(5), pp. 491–493.

14. Yılmaz, E., Baltas, H., Kırıs, E., Ustabas, İ., Cevik, U., and El-Khayatt, A. M., “Gamma ray and neutron shielding properties of some concrete materials,” *Annals of Nuclear Energy*, Oct. 2011., 38(10), pp. 2204–2212.

15. Türkmen, İ., Özdemir, Y., Kurudirek, M., Demir, F., Simsek, Ö., and Demirboğa, R., “Calculation of radiation attenuation coefficients in Portland cements mixed with silica fume, blast furnace slag and natural zeolite,” *Annals of Nuclear Energy*, Oct. 2008., 35(10), pp. 1937–1943.

16. Akkurt, I., Akyıldırım, H., Mavi, B., Kilincarslan, S., and Basyigit, C., “Radiation shielding of concrete containing zeolite,” *Radiation Measurements*, Aug. 2010., 45(7), pp. 827–830.

17. Akkurt, I., Altindag, R., Gunoglu, K., and Sarıkaya, H., “Photon attenuation coefficients of concrete including marble aggregates,” *Annals of Nuclear Energy*, May 2012., 43, pp. 56–60.

18. Akkurt, I., Başyiğit, C., Akkaş, A., Kilinçarslan, Ş., Mavi, B., and Günoğlu, K., “Determination of some heavyweight aggregate half value layer thickness used for radiation shielding,” in *Acta Physica Polonica A*, 2012, 121(1), pp. 138–140.

19. Pomaro, B., Salomoni, V. A., Gramegna, F., Prete, G., and Majorana, C. E., “Radiation damage evaluation on concrete shielding for nuclear physics experiments,” *Annals of Solid and Structural Mechanics*, Nov. 2011., 2(2)–(4), pp. 123–142.

20. Gencel, O., Bozkurt, A., Kam, E., and Korkut, T., “Determination and calculation of gamma and neutron shielding characteristics of concretes containing different hematite proportions,” *Annals of Nuclear Energy*, Dec. 2011., 38(12), pp. 2719–2723.

21. Mesbahi, A., Azarpeyvand, A.-A., and Shirazi, A., “Photoneutron production and backscattering in high density concretes used for radiation therapy shielding,” *Annals of Nuclear Energy*, Dec. 2011., 38(12), pp. 2752–2756.

22. Basyigit, C., Uysal, V., Kilinçarslan, S., Mavi, B., Günoğlu, K., Akkurt, I., Akkaş, A., Aslan, M. H., Oral, A. Y., Özer, M., and Çaglar, S. H., “Investigating Radiation Shielding Properties of Different Mineral Origin Heavyweight Concretes,” in *AIP Conference Proceedings*, 2011, 1400(2011), pp. 232–235.

23. Gencel, O., “Physical and mechanical properties of concrete containing hematite as aggregates,” *Science and Engineering of Composite Materials*, Jan. 2011., 18(3), pp. 191–199.

24. Rezaei Ochbelagh, D., AzimKhani, S., and Gasemzadeh Mosavinejad, H., “Effect of gamma and lead as an additive material on the resistance and strength of concrete,” *Nuclear Engineering and Design*, Jun. 2011., 241(6), pp. 2359–2363.

25. Peng, Y.-C. and Hwang, C.-L., “Development of high performance and high strength heavy concrete for radiation shielding structures,” *International Journal of Minerals, Metallurgy, and Materials*, Mar. 2011., 18(1), pp. 89–93.

26. Gallego, E., Lorente, A., and Vega-Carrillo, H. R., “Testing of a high-density concrete as neutron shielding material,” in *Nuclear Technology*, 2009, 168(2), pp. 399–404.

27. Okuno, K., Kawai, M., and Yamada, H., “Development of novel neutron shielding concrete,” in *Nuclear Technology*, 2009, 168(2), pp. 545–552.

28. Sharma, A., Reddy, G. R., Varshney, L., Bharathkumar, H., Vaze, K. K., Ghosh, A. K., Kushwaha, H. S., and Krishnamoorthy, T. S., “Experimental investigations on mechanical and radiation shielding properties of hybrid lead–steel fiber reinforced concrete,” *Nuclear Engineering and Design*, Jul. 2009., 239(7), pp. 1180–1185.

29. Kharita, M. H., Yousef, S., and AlNassar, M., “The effect of carbon powder addition on the properties of hematite radiation shielding concrete,” *Progress in Nuclear Energy*, Mar. 2009., 51(2), pp. 388–392.

30. Awadallah, M. I. and Imran, M. M. A., “Experimental investigation of gamma-ray attenuation in Jordanian building materials using HPGe-spectrometer.,” *Journal of environmental radioactivity*, Jan. 2007., 94(3), pp. 129–36.

31. Akkurt, I., Basyigit, C., Kilincarslan, S., Mavi, B., and Akkurt, a., “Radiation shielding of concretes containing different aggregates,” *Cement and Concrete Composites*, Feb. 2006., 28(2), pp. 153–157.

32. Mahdy, M., Speare, P. R. S., and Abdel-Reheem, A. H., “Shielding properties of heavyweight, high strength concrete,” in *Proceedings, Annual Conference - Canadian Society for Civil Engineering*, 2002, 2002, pp. 925–934.

33. El-Sayed Abdo, A., Kansouh, W. A., and Megahid, R. M., “Investigation of radiation attenuation properties for baryte concrete,” *Japanese Journal of Applied Physics, Part 1: Regular Papers and Short Notes and Review Papers*, 2002., 41(12), pp. 7512–7517.

34. Maslehuddin, M., Naqvi, A. A., Ibrahim, M., and Kalakada, Z., “Radiation shielding properties of concrete with electric arc furnace slag aggregates and steel shots,” *Annals of Nuclear Energy*, Mar. 2013., 53, pp. 192–196.

35. Beushausen, H. and Dittmer, T., “The influence of aggregate type on the strength and elastic modulus of high strength concrete,” *Construction and Building Materials*, Jan. 2015., 74, pp. 132–139.

36. Hong, L., Gu, X., and Lin, F., “Influence of aggregate surface roughness on mechanical properties of interface and concrete,” *Construction and Building Materials*, Aug. 2014., 65, pp. 338–349.

37. Cetin, A. and Carrasquillo, R. L., “High-performance concrete: Influence of coarse aggregates on mechanical properties,” *ACI Materials Journal*, 1998., 95(3), pp. 252–261.

38. Wu, K., Chen, B., and Yao, W., “Study of the influence of aggregate size distribution on mechanical properties of concrete by acoustic emission technique,” *Cement and Concrete Research*, May 2001., 31(6), pp. 919–923.

39. Meddah, M. S., Zitouni, S., and Belâabes, S., “Effect of content and particle size distribution of coarse aggregate on the compressive strength of concrete,” *Construction and Building Materials*, Apr. 2010., 24(4), pp. 505–512.

40. Devi, V. S. and Gnanavel, B. K., “Properties of Concrete Manufactured Using Steel Slag,” *Procedia Engineering*, 2014., 97, pp. 95–104.

41. Zhou, F. P., Lydon, F. D., and Barr, B. I. G., “Effect of coarse aggregate on elastic modulus and compressive strength of high performance concrete,” *Cement and Concrete Research*, Jan. 1995., 25(1), pp. 177–186.

42. Melchers, R. E. and Li, C. Q., “Reinforcement corrosion initiation and activation times in concrete structures exposed to severe marine environments,” *Cement and Concrete Research*, Nov. 2009., 39(11), pp. 1068–1076.

43. Lewis, D. A. and Copenhagen, W. J., “The corrosion of reinforcing steel in concrete in marine atmospheres,” *Corrosion (NACE)*, 1959., 15(7), p. 382t–388t.

44. Wakeman, C. M., Dockweiler, E. V., Stover, H. E., and Whiteneck, L. L., "Use of concrete in marine environments," in *ACI 54 (4)*, 1958, pp. 841–856.

45. Beaton, J. L. and Stratfull, R. F., "Environmental influence on corrosion of reinforcing in concrete bridge subtructures," *Highway Research Record*, 1963., 14, pp. 60–78.

46. Broomfield, J. P., *Corrosion of Steel in Concrete: Understanding, Investigation and Repair.*, 2003. Spoon Press.

47. Ahmad, S., "Reinforcement corrosion in concrete structures, its monitoring and service life prediction - A review," *Cement and Concrete Composites*, May 2003., 25(4)–(5 SPEC), pp. 459–471.

48. Sengul, O., "Use of electrical resistivity as an indicator for durability," *Construction and Building Materials*, Dec. 2014., 73, pp. 434–441.

49. Saleem, M., Shameem, M., Hussain, S. E., and Maslehuddin, M., "Effect of moisture, chloride and sulphate contamination on the electrical resistivity of Portland cement concrete," *Construction and Building Materials*, Apr. 1996., 10(3), pp. 209–214.

50. Presuel-Moreno, F., Wu, Y.-Y., and Liu, Y., "Effect of curing regime on concrete resistivity and aging factor over time," *Construction and Building Materials*, Nov. 2013., 48, pp. 874–882.

51. Ying, J., Xiao, J., and Tam, V. W. Y., "On the variability of chloride diffusion in modelled recycled aggregate concrete," *Construction and Building Materials*, Apr. 2013., 41, pp. 732–741.

52. Dousti, A., Rashetnia, R., Ahmadi, B., and Shekarchi, M., "Influence of exposure temperature on chloride diffusion in concretes incorporating silica fume or natural zeolite," *Construction and Building Materials*, Dec. 2013., 49, pp. 393–399.

53. Farahani, A., Taghaddos, H., and Shekarchi, M., "Prediction of long-term chloride diffusion in silica fume concrete in a marine environment," *Cement and Concrete Composites*, May 2015., 59, pp. 10–17.

54. Hobbs, D. W., "Aggregate influence on chloride ion diffusion into concrete," *Cement and Concrete Research*, Dec. 1999., 29(12), pp. 1995–1998.

55. Liu, X., Chia, K. S., and Zhang, M.-H., "Water absorption, permeability, and resistance to chloride-ion penetration of lightweight aggregate concrete," *Construction and Building Materials*, Jan. 2011., 25(1), pp. 335–343.

56. L'Annunziata, M. F., *Handbook of Radioactivity Analysis*, 2012. Elsevier.

57. Neville, A. M. and Brooks, J. J., *Concrete technology*, 1987. .

58. Aitcin, P. C. and Mehta, P. K., "Effect of coarse-aggregate characteristics on mechanical properties of high-strength concrete," *ACI Materials Journal*, 1990., 87(2), pp. 103–107.

59. Maslehuddin, M., Sharif, A. M., Shameem, M., Ibrahim, M., and Barry, M. ., "Comparison of properties of steel slag and crushed limestone aggregate concretes," *Construction and Building Materials*, Mar. 2003., 17(2), pp. 105–112.

60. Aquino, C., Inoue, M., Miura, H., Mizuta, M., and Okamoto, T., "The effects of limestone aggregate on concrete properties," *Construction and Building Materials*, Dec. 2010., 24(12), pp. 2363–2368.

61. Yaşar, E., Erdoğan, Y., and Kılıç, A., "Effect of limestone aggregate type and water–cement ratio on concrete strength," *Materials Letters*, Feb. 2004., 58(5), pp. 772–777.

62. Poitevin, P., "Limestone aggregate concrete, usefulness and durability," *Cement and Concrete Composites*, Apr. 1999., 21(2), pp. 89–97.

63. Elices, M. and Rocco, C. G., "Effect of aggregate size on the fracture and mechanical properties of a simple concrete," *Engineering Fracture Mechanics*, Sep. 2008., 75(13), pp. 3839–3851.

64. Tasong, W. ., Lynsdale, C. ., and Cripps, J. ., "Aggregate-cement paste interface. ii: influence of aggregate physical properties," *Cement and Concrete Research*, Oct. 1998., 28(10), pp. 1453–1465.

65. Rao, G. A. and Prasad, B. K. R., "Influence of the roughness of aggregate surface on the interface bond strength," *Cement and Concrete Research*, Feb. 2002., 32(2), pp. 253–257.

66. Alexander, M. G., "Two experimental techniques for studying the effects of the interfacial zone between cement paste and rock," *Cement and Concrete Research*, May 1993., 23(3), pp. 567–575.

67. Beshr, H., Almusallam, A. ., and Maslehuddin, M., "Effect of coarse aggregate quality on the mechanical properties of high strength concrete," *Construction and Building Materials*, Mar. 2003., 17(2), pp. 97–103.

68. Brooks, J. J., *Concrete and Masonry Movements*, 2015. Elsevier.

69. Saito, M., Kawamura, M., and Arakawa, S., "Role of aggregate in the shrinkage of ordinary portland and expansive cement concrete," *Cement and Concrete Composites*, Jan. 1991., 13(2), pp. 115–121.

70. Bungey, J. H., *The Testing of Concrete in Structures.*, 1989. London: Surrey University Press.

Vitae

Name :AZEEZ Mukhtar Oluwaseun

Nationality :Nigerian

Date of Birth :12/5/1985

Email :mukhtar_world@yahoo.com

Address :No 10, Koba ope area, Hospital Road, Iwo, Osun State, Nigeria

Academic Background :Mr. Mukhtar Azeez obtained his BSc. in Civil Engineering from Obafemi Awolowo University, Nigeria in November 2008. He joined Civil and Environmental Engineering department, KFUPM with the Saudi Arabia Ministry of Education scholarship to purse his MS (Structures & Materials) degree in August 2012.

Publications:

1. **Azeez, M. O.**, Al-Dulaijan S., Maslehuddin M., Naqvi A.A., Al-Amoudi O.S.B., Ahmad, S., "Experimental investigation of gamma-ray attenuation of concrete containing different heavyweight aggregates". In progress.
2. **Azeez, M. O.**, Al-Dulaijan S., Maslehuddin M., Naqvi A.A., Al-Amoudi O.S.B., Ahmad, S., "Mechanical, durability and radiation shielding properties of concrete containing iron ore and steel slag aggregates". In progress.